Structures of three MORN repeat proteins and a re-evaluation of the proposed lipid-binding properties of MORN repeats.

Sara Sajko*[,1], Irina Grishkovskaya*[,1], Julius Kostan*[,1], Melissa Graewert[2], Kim Setiawan[3], Linda Trübestein[1], Korbinian Niedermüller[3], Charlotte Gehin[4,5], Antonio Sponga[1], Martin Puchinger[1], Anne-Claude Gavin[4,6], Thomas Leonard[1], Dimitri Svergun[2], Terry K. Smith[7], Brooke Morriswood[3,$], Kristina Djinovic-Carugo[1,8,$]

* Equal contribution

$ Authors for correspondence:
Brooke Morriswood (brooke.morriswood@uni-wuerzburg.de)
Kristina Djinovic-Carugo (kristina.djinovic@univie.ac.at)

Affiliations:
[1]Department of Structural and Computational Biology, Max Perutz Labs, University of Vienna, Campus Vienna Biocenter 5, A-1030 Vienna, Austria

[2]European Molecular Biology Laboratory, Hamburg Unit, c/o DESY, Notkestrasse 85, 22607 Hamburg, Germany

[3]Department of Cell and Developmental Biology, Biocenter, University of Würzburg, 97074 Würzburg, Germany

[4]European Molecular Biology Laboratory, Heidelberg Unit, Meyerhofstraße 1, 69117 Heidelberg, Germany

[5]Institute of Bioengineering, Laboratory of Lipid Cell Biology, École polytechnique fédérale de Lausanne (EPFL) CH-1015 Lausanne, Switzerland

[6]Department for Cell Physiology and Metabolism, University of Geneva, Centre Medical Universitaire, Rue Michel-Servet 1, CH-1211 Geneva 4, Switzerland

[7]School of Biology, BSRC, University of St. Andrews, North Haugh, St. Andrews, Fife KY16 9ST, UK

[8]Department of Biochemistry, Faculty of Chemistry and Chemical Technology, University of Ljubljana, Večna pot 113, SI-1000 Ljubljana, Slovenia

Keywords: MORN repeat, MORN1, structure, phospholipids, *Trypanosoma,* Apicomplexa.

ABSTRACT

MORN (Membrane Occupation and Recognition Nexus) repeat proteins have a wide taxonomic distribution, being found in both prokaryotes and eukaryotes. Despite this ubiquity, they remain poorly characterised at both a structural and a functional level compared to other common repeats. In functional terms, they are often assumed to be lipid-binding modules that mediate membrane targeting. We addressed this putative activity by focusing on a protein composed solely of MORN repeats - *Trypanosoma brucei* MORN1. Surprisingly, no evidence for binding to membranes or lipid vesicles by TbMORN1 could be obtained either in vivo or in vitro. Conversely, TbMORN1 did interact with individual phospholipids. High- and low-resolution structures of the MORN1 protein from *Trypanosoma brucei* and homologous proteins from the parasites *Toxoplasma gondii* and *Plasmodium falciparum* were obtained using a combination of macromolecular crystallography, small-angle X-ray scattering, and electron microscopy. This enabled a first structure-based definition of the MORN repeat itself. Furthermore, all three structures dimerised via their C-termini in an antiparallel configuration. The dimers could form extended or V-shaped quaternary structures depending on the presence of specific interface residues. This work provides a new perspective on MORN repeats, showing that they are protein-protein interaction modules capable of mediating both dimerisation and oligomerisation.

INTRODUCTION

MORN (Membrane Occupation and Recognition Nexus) repeats were first discovered in 2000, as a result of a screen for proteins present in the triad junctions of skeletal muscle (Takeshima et al., 2000). The junctophilins, the protein family identified in this screen, were observed to have 8 repeats present in their N-terminal regions. The repeats were given the name MORN based on a proposed role in mediating plasma membrane association of the N-terminal domain of the junctophilins. The MORN repeats were initially classified as being 14 amino acids in length, with an approximate consensus sequence of YEGEWxNGKxHGYG (Takeshima et al., 2000). A bioinformatics analysis at the time indicated that assemblies of 8 consecutive MORN repeats were also present in a putative junctophilin orthologue in a nematode (*Caenorhabditis elegans*), a family of plant (*Arabidopsis thaliana*) lipid kinases, and a bacterial (*Cyanobacterium*) protein (Takeshima et al., 2000). Later genome-era bioinformatics has shown that MORN repeat proteins are in fact found ubiquitously, being present in both eukaryotes and prokaryotes (El-Gebali et al., 2019).

The number of MORN repeats in any given protein can vary greatly, from 2 to over 20, and they are found in combination with a wide range of other domains. Most published work now favours a 23-amino acid length for a single MORN repeat, with the highly-conserved GxG motif at residues 12-14 (Gubbels et al., 2006, Hu et al., 2006, Im et al., 2007). A 14-amino acid length is still favoured by some groups, however (Bennett et al., 2013, Habicht et al., 2015). Notable mammalian MORN repeat proteins besides the junctophilins include ALS2/alsin, at least two radial spoke proteins (RSPH10B, RSPH1/meichroacidin), the histone methyltransferase SETD7, and MORN4/retinophilin (Tsuchida et al., 1998, Wilson et al., 2002, Otomo et al., 2003, Mecklenburg, 2007).

MORN repeats are generally assumed to be lipid-binding modules, but direct evidence for this function is actually lacking. In junctophilins, there is good evidence that the N-terminal region containing the MORN repeats mediates plasma membrane targeting (Takeshima et al., 2000, Nakada et al., 2018, Rossi et al., 2019). It has not been demonstrated whether the MORN repeats or the other sequences in the N-terminal region are responsible for this targeting activity. In addition, the targeting activity itself may be due to either protein-lipid or protein-protein interactions.

In addition, although there is good evidence that the N-terminal region (amino acids 1-452), of junctophilin-2 can directly bind lipids, it has not specifically been shown that the MORN repeats are responsible (Bennett et al., 2013). This is because the N-terminal region consists of 6 MORN repeats, a 140 amino acids long joining region, 2 additional MORN repeats, and an alpha-helical region. Binding could therefore be mediated by other nearby sequences, especially the run of over 100 amino acids that occurs between repeats 6 and 7. Work on the family of plant phosphatidylinositol(4)phosphate 5-kinases (PIPKs) that contain MORN repeats has led to suggestions that the repeats might regulate the activity of the kinase domain, bind to phospholipids, or mediate protein-protein interactions (Ma et al., 2006, Im et al., 2007, Camacho et al., 2009). Another recent report on junctophilin-2 showed that upon cleavage by an endogenous protease, the N-terminal region translocates to the nucleus via a nuclear localisation signal and functions there as a transcription factor (Guo et al., 2018). It

112 therefore remains unclear what role(s) this ubiquitous class of repeat actually have (Mikami
113 et al., 2010).
114
115 Coupled to this lack of unambiguous functional data is a lack of high-resolution structural
116 information, exemplified by the ongoing lack of consensus as to whether a single repeat is
117 composed of 14 or 23 amino acids. This contrasts sharply with the considerable amount of
118 information available on other classes of protein repeats such as ankyrin repeats, leucine-
119 rich repeats, or WD40 repeats (Andrade et al., 2001, Kajava, 2012). Until very recently, the
120 structure of the histone methyltransferase SETD7 was the sole representative of the MORN
121 repeat protein family (Jacobs et al., 2002, Wilson et al., 2002, Xiao et al., 2003). Even here,
122 the structure of the N-terminal domain containing the MORN repeats is incomplete, and the
123 level of sequence similarity of the repeats to those of junctophilins and other MORN repeat-
124 containing proteins makes assignment difficult. Each repeat appears to form a β-hairpin with
125 an acidic surface, but it remains unclear if this is a general property of MORN repeats. The
126 SETD7 structure has not been analysed in this context, with more focus applied to its
127 catalytic methyltransferase domain. In particular, a structure-based definition of the repeat
128 class itself is currently lacking.
129
130 To address this, and additionally to tackle the question of putative lipid binding, it would
131 obviously be advantageous to utilise a protein that is composed solely of MORN repeats. In
132 this way, the contribution of other sequences or domains could be discounted. The MORN1
133 protein from the early-branching eukaryote *Trypanosoma brucei* is an ideal candidate in this
134 regard, and has the advantage of also being well-characterised at a cell biology level
135 (Morriswood et al., 2009, Esson et al., 2012, Morriswood et al., 2013, Morriswood & Schmidt,
136 2015).
137
138 TbMORN1 consists of 15 consecutive 23-amino acid MORN repeats, with barely any
139 intervening sequence (Fig. 1A). In *T. brucei*, TbMORN1 is localised to an ~2 μm long
140 cytoskeleton-associated structure (the hook complex) that is found just below the inner leaflet
141 of the plasma membrane. The hook complex encircles the neck of a small invagination of the
142 plasma membrane that contains the root of the cell's single flagellum (Lacomble et al., 2009).
143 This invagination, termed the flagellar pocket, is the sole site of endo- and exocytosis in
144 trypanosomes and is thought to be analogous to the ciliary pocket that is found at the base
145 of some mammalian primary cilia (Grunfelder et al., 2003, Engstler et al., 2004, Molla-Herman
146 et al., 2010).
147
148 Previous work on TbMORN1 demonstrated by fluorescence recovery after photobleaching
149 (FRAP) that it is a stable component of the hook complex, and a list of its binding partners
150 and near neighbours has been obtained using proximity-dependent biotin identification
151 (BioID) (Esson et al., 2012, Morriswood et al., 2013). In functional terms, depletion of
152 TbMORN1 by RNAi in the mammalian-infective (bloodstream) form of the parasite resulted in
153 a lethal phenotype (Morriswood et al., 2009). Functional analysis indicated that the protein
154 might be involved in endocytosis, as well as regulating the flow of macromolecular cargo
155 through the neck of the flagellar pocket (Morriswood & Schmidt, 2015).
156

In order to investigate the putative lipid-binding capacity of TbMORN1 and its three-dimensional structure, a detailed biochemical, structural, and functional analysis of the TbMORN1 protein was carried out. A truncated form missing the first MORN repeat that was best suited for in vitro work was found not to bind to phospholipid vesicles under any conditions, but was able to associate with individual lipid molecules. High-resolution crystal structures and biophysical analyses of a truncated form of the TbMORN1 protein and its homologues from the parasites *Toxoplasma gondii* (TgMORN1) and *Plasmodium falciparum* (PfMORN1) enabled, for the first time, a structure-based definition of the MORN repeat. All three structures are antiparallel dimers joined via their C-termini, and, when possessed of the correct key residues, can adopt extended or V-shaped quaternary structures. This provides a new insight into MORN repeats, showing that they are capable of mediating homotypic interactions.

RESULTS

TbMORN1 forms tail-to-tail dimers *via* its C-terminus

TbMORN1 is composed of 15 consecutive 23-amino acid MORN repeats, with a 5-amino acid extension after the 6th repeat (Fig. 1A). An alignment of the repeats in TbMORN1 revealed several highly conserved glycine residues, with a rough consensus of $YxGEWx_2Gx_3GxGx_3Yx_2Gx_2$ (Fig. 1A, sequence logo). Bioinformatic analysis of TbMORN1 predicted an all-β secondary structure, with each repeat expected to form a β-hairpin (strand-loop-strand) pattern (Fig. 1A).

Limited proteolysis showed progressive digestion occurring from the N-terminus, while the C-terminus was fairly stable (Fig. S1A, B). Consequently, a panel of different truncations was cloned according to the MORN repeat boundaries predicted by the alignment (Fig. 1A). These truncations were named according to the number of repeats (1-15) they contained. These constructs were expressed in bacteria and purified using a two-step protocol combining affinity purification and size exclusion chromatography (Fig. S1C).

The yields of TbMORN1(1-15) were always very low due to aggregation in the first purification step, making this construct not generally suitable for molecular biophysics assays. Size exclusion chromatography coupled to multi-angle light scattering (SEC-MALS) analysis of purified TbMORN1(1-15) elution profiles suggested the formation of higher-order assemblies (Fig. 1B). By contrast, TbMORN1(2-15) displayed a well-defined monodisperse peak in SEC-MALS, with a molecular weight corresponding to a dimer (Fig. 1B). This strongly suggested that the first MORN repeat mediated oligomerisation. Further successive truncations from the N-terminus (TbMORN1(7-15) and TbMORN1(10-15)) also eluted as monodisperse dimers, suggesting that dimerisation of TbMORN1 is mediated by the C-terminus (Fig. S1D). Consistent with this conclusion, removal of the last MORN repeat in the construct TbMORN1(1-14) resulted in the elution of a mixture of monomers, dimers, and higher-order

structures (Fig. 1B). This demonstrated that the C-terminal repeats play an important role in dimer stabilisation.

Circular dichroism (CD) measurements taken of TbMORN1(1-15), TbMORN1(2-15), and TbMORN1(7-15) indicated >30% antiparallel β-strand content for each construct (Fig. S1E), and were in good agreement with a priori bioinformatic predictions (Fig. 1A). Thermostability measurements of TbMORN1(1-15), TbMORN1(2-15) and TbMORN1(7-15) using CD returned values in °C of 45.6 +/- 0.1, 43.5+/-0.1, and 42.2+/-0.1 respectively, showing an expected incremental contribution of MORN repeats to the overall stability of the protein.

To map which residues were likely mediating dimerisation, cross-linking mass spectrometry (XL-MS) was used to analyse TbMORN1(1-15). Two different chemical cross-linkers were used: EDC (1-ethyl-3-(3-dimethylaminopropyl)carbodiimide), which has a zero-length spacer arm, and BS^3 (bis(sulphosuccinimidyl)suberate), which has an 11.4 Å spacer arm. For both chemicals, most cross-links were observed to form between repeats 13, 14, and 15, especially via repeat 14 (Table S1). These data were consistent with those obtained by SEC-MALS (Fig. 1B, Fig. S1D), suggesting that TbMORN1 forms tail-to-tail dimers via their C-termini. It remained unclear whether the polypeptide chains in dimers were in a parallel or antiparallel orientation, however.

TbMORN1 can bind lipid side chains but not phospholipid liposomes

To identify candidate phospholipids that interacted with TbMORN1, we initially used PIP strips. These resulted in the identification of a number of candidates, of which $PI(4,5)P_2$ was the most interesting due to its well-established role as an endocytic cofactor. We subsequently used fluorescence anisotropy (FA) to quantify binding of TbMORN1 to $PI(4,5)P_2$, but these results could subsequently not be validated in liposome binding assays (Fig. S2). We carried out additional controls modifying liposome curvatures and concentrating $PI(4,5)P_2$ in microdomains by addition of cholesterol, but this did not result in binding (Fig. S4A). Through sequence analysis we identified putative binding sites in repeats 13 and 14 and mutagenised selected Arg and Lys residues to Ala. The mutagenesis did not affect secondary structure content or lipid binding as assessed by FA, but when both sites were mutated simultaneously, the protein became monomeric (Fig. S4B-D). Subsequent assays showed that the positive results of the FA experiments were principally due to an interaction with longer aliphatic chains rather than the lipid headgroup (Fig. S5).

TbMORN1 co-purifies with PE but does not bind to lipid vesicles in vitro

A caveat to the previous conclusion was that the purified recombinant TbMORN1 was obtained via mechanical lysis of bacterial cells in the absence of detergent (see Materials and Methods). It was therefore possible that bacterial lipids might be occupying the lipid binding sites on TbMORN1.

To test this, purified recombinant TbMORN1(1-15) and TbMORN1(10-15) were treated according to a de-lipidation protocol, and the resulting supernatants were analysed by mass

246 spectrometry. Interestingly, large amounts of phosphatidylethanolamine (PE) were found to
247 have been bound to TbMORN1(1-15) (Fig. 2A). The co-purifying PE displayed a remarkably
248 narrow window of molecular moieties differing in the length of the aliphatic chain (30:0, 33:1,
249 34:1, 36:2). No significant PE presence was detected in supernatants obtained following de-
250 lipidation of TbMORN1(10-15) (Fig 2B). Given that TbMORN1(10-15) showed robust binding
251 to PI(4,5)P_2 with a longer 16-carbon aliphatic chain (Fig. S2C), this suggested that PE was
252 not occluding the binding site.
253
254 To remove co-purifying lipids, recombinant TbMORN1(1-15) was purified using hydrophobic
255 interaction chromatography - in this regime, almost no lipids were detected in the elutions.
256 Triton X-100 treatment was also found to efficiently remove bound lipids.
257
258 Co-purification of PE with TbMORN1(1-15) is not evidence of physiological interaction, as PE
259 is highly abundant in bacteria and carries a net neutral charge (Cronan, 2003). As such, PE
260 might simply have associated with the recombinant protein following lysis of the bacteria
261 prior to purification. To investigate this, mass spectrometry analysis of whole-cell lipid
262 extracts from bacteria expressing recombinant TbMORN1(1-15) or TbMORN1(10-15) was
263 carried out. Curiously, bacterial cells expressing TbMORN1(1-15) showed elevated levels of
264 PE (Fig. 2C). This effect was not seen in bacterial cells expressing TbMORN1(10-15), which
265 had approximately wild-type levels of PE (Fig. 2D).
266
267 In summary, TbMORN1(1-15) but not TbMORN1(10-15) was found to have co-purifying PE,
268 and bacterial cells expressing TbMORN1(1-15) appeared to have elevated levels of PE. This
269 suggested that PE might be a plausible candidate for a physiological interaction partner of
270 TbMORN1, and that it requires MORN repeats 1-9 for binding.
271
272 To test the possibility of PE binding, and also to check whether the presence of co-purifying
273 PE was affecting possible PI(4,5)P_2 binding, pelleting assays using sucrose-loaded vesicles
274 (SLVs) were carried out. No association with liposomes was seen regardless if the protein
275 was treated with Triton X-100 beforehand (Fig. S6A-C).
276
277 Finally, in an unbiased and high-throughput approach, TbMORN1 was tested in a liposome
278 microarray assay (LiMA). The EGFP-TbMORN1(2-15) protein showed no significant
279 preference or affinity for liposomes across the whole range of conditions tested (Fig. S6D, E).
280
281 Taken together, these data suggest that TbMORN1 requires long aliphatic chains of the lipid
282 for binding, which would explain the negative results in the liposome-based assays.
283
284

285 TbMORN1 does not associate with membranes *in vivo*

286
287 At this point, the only remaining positive indicators of an interaction of TbMORN1 with lipids
288 came from the PIP strips (Fig. S2A), and the bacterial mass spectrometry data (Fig. 2A, C).
289 Both these positive pieces of evidence related to TbMORN1(1-15), which was polydisperse
290 in vitro and formed large oligomers (Fig. 1B). It was not possible to test the membrane-

binding activity of these polydisperse oligomers in vitro however, as the purification yields of TbMORN1(1-15) were always low. As an alternative, the possible membrane association of TbMORN1(1-15) was examined in vivo.

For these experiments, cell lines of bloodstream form *T. brucei* were generated that inducibly expressed TbMORN1(1-15) with an N-terminal Ty1 epitope tag. Induction of Ty1-TbMORN1(1-15) overexpression using tetracycline (Tet) produced a strong growth defect in all three *T. brucei* clones tested (Fig. 3A). A rise in the number of so-called "BigEye" cells with grossly enlarged flagellar pockets was seen in the same 96-hour time window (Fig. 3B). Such a phenotype had previously been seen following depletion of TbMORN1 (Morriswood & Schmidt, 2015). The BigEye phenotype is thought to result from perturbations to membrane traffic, especially endocytosis (Allen et al., 2003).

Immunoblotting with anti-TbMORN1 antibodies confirmed tight and inducible expression of the ectopic Ty1-TbMORN1 protein (Fig. 3C, left panel). The presence of the Ty1 epitope tag in the ectopic protein was confirmed by blotting with anti-Ty1 antibodies (Fig. 3C, right panel). Quantification of the immunoblots indicated only around 2-fold overexpression of Ty1-TbMORN1 relative to endogenous TbMORN1 protein (Fig. 3D).

The strong growth defect and the production of BigEye cells were unexpected, and could potentially be due either to the overexpression of the TbMORN1 protein, or to the presence of the Ty1 tag. To check whether overexpression alone could drive a negative outcome, cells that inducibly expressed untagged TbMORN1 from an ectopic locus were generated. Overexpression of untagged TbMORN1 from the ectopic locus was detected by immunoblotting (Fig. S7A). Quantification of overexpression indicated that approximately 7 times more TbMORN1 protein was present in induced cells relative to controls (Fig. S7B). Cells overexpressing untagged TbMORN1 exhibited a very strong growth defect and the BigEye phenotype, stronger than that seen for overexpression of Ty1-TbMORN1 (Fig. S7C). Therefore, TbMORN1 protein levels alone were capable of producing a negative effect on growth in the absence of the Ty1 tag. It was however not possible to obtain cells that solely expressed Ty1-TbMORN1 by endogenous replacement, despite repeated attempts. This indicated that Ty1-TbMORN1 cannot functionally compensate for the loss of the untagged endogenous protein.

The localisation of the overexpressed Ty1-TbMORN1 was assessed using immunofluorescence microscopy. Uninduced cells labelled with anti-TbMORN1 antibodies showed the expected localisation of endogenous TbMORN1 at the hook complex. Conversely, the Ty1-TbMORN1-overexpressing cells displayed a whole-cell labelling pattern (Fig. 3E, left panels). In these cells no sign of protein aggregation was observed, but the different distribution compared to the controls suggested that the Ty1-TbMORN1 protein might not localise correctly. Immunofluorescence microscopy analysis of detergent-extracted cytoskeleton fractions labelled using anti-Ty1 antibodies confirmed that Ty1-TbMORN1 was able to target correctly to the hook complex; as expected, no labelling was seen in uninduced controls. (Fig. 3E, right panels).

336 To confirm the immunofluorescence microscopy observations, one-step biochemical
337 fractionation using the non-ionic detergent IGEPAL was used. The detergent-soluble
338 cytoplasmic fraction (supernatant, SN) was separated from the detergent-insoluble
339 cytoskeleton (pellet, P) by centrifugation (Fig. 3F). In control cells, endogenous TbMORN1
340 associated almost entirely with the cytoskeletal (P) fraction (Fig. 3G). Blotting fractions from
341 Ty1-TbMORN1-overexpressing cells with anti-TbMORN1 antibodies showed that the
342 overexpressed Ty1-TbMORN1 was mostly detergent-soluble and therefore present in the
343 cytoplasmic fraction (Fig. 3G, arrow 1). However, a small amount of the Ty1-TbMORN1
344 protein associated with the cytoskeleton (P) fraction. This association was accompanied by
345 a displacement of some of the endogenous protein into the cytoplasmic SN fraction (Fig. 3G,
346 arrows 2).
347
348 Quantification of fractionation data supported the qualitative analysis (Fig. 3H). Summing the
349 signals of Ty1-TbMORN1 and TbMORN1 present in the cytoskeletal (P) fraction in
350 overexpressing cells indicated that the total amount of cytoskeleton-associated protein was
351 approximately the same as in controls (Fig. 3H, grey bar). This suggested that there are a
352 finite number of Ty1-TbMORN1 molecules that can associate with the cytoskeleton. As the
353 total amount of endogenous and ectopic TbMORN1 associated with the cytoskeleton is
354 roughly the same in both overexpressing cells and controls, this suggested also that the
355 dominant negative cellular effects are primarily due to the endogenous and ectopic
356 TbMORN1 in the cytoplasmic (SN) fraction.
357
358 To determine if the cytoplasmic fraction of endogenous and ectopic TbMORN1 in the
359 overexpressing cells was organelle-associated or cytosolic, two-step fractionations were
360 carried out (Fig. 4A). These assays involved a first extraction with digitonin to generate a
361 cytosolic fraction (SN1), then a second extraction with IGEPAL to generate an organelle-
362 associated fraction (SN2). Digitonin has an affinity for cholesterol and other lipids enriched in
363 the plasma membrane, so at the right concentration it should enable the extraction of cytosol
364 while leaving organelle membranes relatively intact (Adam et al., 1990).
365
366 The conditions for digitonin extraction were optimised using a cell line expressing cytosolic
367 GFP as a marker (Fig. S8) (Batram et al., 2014). A two-step extraction using first digitonin and
368 then IGEPAL was carried out on Ty1-TbMORN1 overexpressing cells, with the cells
369 expressing cytosolic GFP spiked in alongside them (Fig. 4A). The digitonin supernatant (SN1)
370 was enriched for cytosol, as shown by the presence of the GFP marker. The organelle-
371 associated fraction, tracked by immunoblotting for the ER lumenal chaperone BiP, was
372 present in the pellet (P1). The P1 fraction was subsequently extracted using IGEPAL and the
373 BiP marker was observed to predominantly partition into SN2 (Fig. 4B). Analysing equal
374 fractions by immunoblotting showed that the Ty1-TbMORN1 and TbMORN1 proteins not
375 associated with the cytoskeleton were predominantly cytosolic and partitioned with the GFP
376 marker into the SN1 fraction (Fig. 4B, arrows 1).
377
378 The Ty1-TbMORN1 and TbMORN1 in the P1 fraction (Fig. 4A) were not strongly extracted by
379 IGEPAL and therefore barely present in the second supernatant (SN2), while the ER marker
380 BiP was (Fig. 4B, arrows 2). Almost all the Ty1-TbMORN1 and TbMORN1 present in P1

381 partitioned into the second pellet, P2. Quantification of multiple independent experiments
382 using the three separate clones produced results consistent with the exemplary blot shown
383 (Fig. 4C, D). The presence of the overexpressed Ty1-TbMORN1 and displaced endogenous
384 TbMORN1 in the digitonin supernatant (SN1) indicated that they are predominantly cytosolic.
385
386 In conclusion, the extensive studies conducted on TbMORN1 here provide no evidence that
387 its MORN repeats are able to associate with phospholipid membranes in vivo, or directly
388 interact with phospholipid vesicles in vitro.
389
390

391 High-resolution crystal structures of three MORN repeat proteins

392
393 If MORN repeats do not bind membranes, then this raises the question of what they really
394 do, and whether this other function might unify the various observations made about MORN
395 repeat proteins to date. ALS2 has been suggested to use its MORN repeats to form an
396 antiparallel dimer (Kunita et al., 2004), and the evidence obtained here showed that
397 TbMORN1 molecules also formed tail-to-tail dimers via their C-termini (Figs. 1, S1).
398 Mammalian PI(4)P 5-kinases are also dimers, implying that the MORN repeats found at the
399 N-termini of the family of plant PIPKs might function to mediate homotypic interactions (Rao
400 et al., 1998). To investigate the molecular basis of TbMORN1 dimerisation, high-resolution
401 structural studies were used.
402
403 Crystallisation trials were initially performed with TbMORN1(2-15) and TbMORN1(7-15).
404 Diffraction data were obtained for TbMORN1(7-15) in two different crystal forms ($P2_1$ and C2),
405 but attempts to solve the phase problem using experimental phasing approaches (multiple
406 isomorphous replacement, multiple anomalous scattering exploiting selenium and sulphur
407 atom signals) and molecular replacement failed due to low reproducibility of crystals,
408 anisotropy of diffraction data, and absence of sufficient homology of TbMORN1 to other
409 MORN repeat-containing proteins of known structure. At that point, the only MORN repeat-
410 containing protein for which the crystal structure was solved was SETD7, a histone
411 methyltransferase. SETD7 is predicted by the TRUST algorithm to contain up to 6 MORN
412 repeats at its N-terminus (Szklarczyk & Heringa, 2004). However, the repeats display low
413 sequence homology to both the MORN repeats of TbMORN1 and the consensus MORN
414 repeat sequence obtained by Pfam (El-Gebali et al., 2019). This prevented successful use of
415 molecular replacement as an approach.
416
417 As a new tactic, the MORN1 proteins from the apicomplexan parasites *Plasmodium*
418 *falciparum* (PfMORN1) and *Toxoplasma gondii* (TgMORN1) were targeted for structure
419 determination. Despite their evolutionary distance, they share high (57% and 54%,
420 respectively) sequence identity with TbMORN1 (Fig. S9A, B). CD measurements of purified
421 recombinant protein indicated that TgMORN1, TgMORN1(7-15), PfMORN1, PfMORN1(2-15)
422 and PfMORN1(7-15) all had an overall β-structure (Fig. S9C, D). This agrees with
423 bioinformatic predictions and is consistent with the data obtained for TbMORN1 (Fig. S1E).
424

425 Diffracting crystals of selenomethionine-labelled PfMORN1(7-15) were obtained and its
426 crystal structure was determined to 2.14 Å resolution using the single-wavelength anomalous
427 dispersion (SAD) method. The structures of TgMORN1(7-15) and both $P2_1$ and C2 crystal
428 forms of TbMORN1(7-15) were subsequently determined to 2.90, 2.35 and 2.53 Å resolution,
429 respectively, with the PfMORN1(7-15) structure used as a search model for the molecular
430 replacement (Fig. 5A-C). The structures of PfMORN1(7-15), TgMORN1(7-15), and both $P2_1$
431 and C2 forms of TbMORN1(7-15) were refined to an R_{work}/R_{free} of 23.0%/26.4%,
432 28.3%/32.2%, 23.2%/25.6% and 22.5%/28.2%, respectively (Table 1). TbMORN1(7-15) $P2_1$
433 (Fig. 5A), C2 (Fig. S10A) and TgMORN1(7-15) (Fig. 5B) crystallised with one dimer in the
434 asymmetric unit, while PfMORN1(7-15) (Fig. 5C) crystallised with one subunit in the
435 asymmetric unit, and the functional dimer was formed via crystallographic symmetry axis.
436
437 All MORN1(7-15) crystal structures show subunit interactions via the C-terminal regions to
438 form antiparallel tail-to-tail dimers, with variable inter-subunit angles and dimerisation
439 interfaces (Fig. 5A-C, Fig. S10A). The two subunits in the TbMORN1(7-15) C2 crystal form
440 and the TgMORN1(7-15) dimer make a rather straight assembly, while in the $P2_1$ form they
441 display a bend of about 30° (Fig. S10A), leading to a rod-shaped particle appearance. This
442 dimer architecture is consistent with the limited proteolysis data, which had indicated that
443 the N-terminal regions of the molecule are more susceptible to limited proteolysis (Fig. S1A,
444 B). Interestingly, PfMORN1(7-15) displays a V-shaped dimer with an inter-subunit angle of
445 about 45°, and incorporates a structural Zn^{2+} ion at the dimer interface (Fig. 5C). One crystal
446 form of TgMORN1(7-15) also adopts the same V-shape seen for PfMORN1(7-15) (Fig. S12B).
447 Here too, a Zn^{2+} ion is found at the dimer interface.
448
449 Superimposing the TbMORN1(7-15) $P2_1$ subunit with the structures of the TgMORN1(7-15)
450 and PfMORN1(7-15) subunits over 202 C_α atoms yielded rmsd values of 1.0 and 1.1 Å,
451 respectively, revealing high structural similarity between the three proteins. The common
452 structural feature of all three subunits is an elongated and twisted β-sheet. The curved shape
453 of each constituent MORN repeat forms a groove laterally delimited by a rim. An individual
454 MORN1(7-15) subunit is approximately 80 Å in length and displays a longitudinal groove of
455 about 16 Å in depth (Fig. 5A).
456
457 Comparison of a single TbMORN1(7-15) subunit with known three-dimensional structures
458 was carried out using the DALI server (Holm & Rosenstrom, 2010, Holm & Laakso, 2016).
459 This revealed closest similarity with the G-box domain at the C-terminus of the human CPAP
460 protein. CPAP is a centriolar protein essential for microtubule recruitment. The G-box
461 comprises a single elongated β-sheet with all residues being solvent-exposed, and is capable
462 of forming supramolecular assemblies [PDB entry 4LZF, (Hatzopoulos et al., 2013)]. Despite
463 the low sequence identity (10%) between TbMORN1(7-15) and CPAP, the Z-score calculated
464 by DALI suggested a significant similarity between the two structures (rmsd over 155
465 superimposed C_α atoms = 3.9 Å, Z-score = 12).
466

467 ## A structure-based redefinition of the MORN repeat

468

469 The crystal structures confirmed that each 23-amino acid MORN repeat is composed of a β-
470 hairpin followed by a 6-residue loop that connects to the next MORN repeat. Each β-hairpin
471 is composed of two 6-residue β-strands connected by a 5-residue loop. The MORN repeats
472 from TbMORN1(7-15) could be readily superimposed, showing a high level of structural
473 conservation (Fig. 5D). Based on this high level of conservation, a revised sequence
474 alignment of the TbMORN1 repeats was constructed that better reflects the structural
475 architecture of the protein (Fig. 5E, compare with Fig. 1A). The alignment of repeats 7-15 was
476 obtained directly from structural superpositions and used to bootstrap the alignment of the
477 repeats 1-6.
478
479 The new consensus MORN repeat sequence displays three highly-conserved features: a GxG
480 motif at the start, a conserved glycine (G) at position 10, and a YEGEW motif at positions 13-
481 17 (Fig. 5E). A slightly less conserved LxY motif is at positions 5-7. The GxG motif is at the
482 beginning of the first β-strand, while the YEGEW motif comprises most of the second β-
483 strand.
484
485 The glycine residues at position 10 are in a β-hairpin of type I, where the most commonly-
486 observed residue at this position is a glycine (Hutchinson & Thornton, 1994). The GxG motif
487 is strictly conserved because the first G residue adopts a main chain conformation mapping
488 to the lower right corner of the Ramachandran plot, which is exclusively allowed for glycines.
489 The conformation of this glycine is stabilised via a main-chain hydrogen bond with the
490 tryptophan (W) residue of the YEGEW motif (Fig. 5F). The high conservation of the second
491 glycine residue in the GxG motif is to accommodate the highly conserved neighbouring
492 aromatic residues from the YEGEW and LxY motifs, as any larger side chain would create
493 steric clashes. The tyrosine and tryptophan side chains of the YEGEW and LxY motifs provide
494 a textbook example of aromatic stacking, filling up the groove and stabilising the tertiary
495 structure of the TbMORN1 subunit (Fig. 5F, G). The highly conserved tyrosine of the YEGEW
496 motif is sandwiched in a T-shaped π-stacking interaction between two tryptophan residues,
497 one from its own motif and the second from the following YEGEW motif (Fig. 5F). The tyrosine
498 of the LxY motif is stabilised via hydrophobic and/or aromatic stacking interactions with the
499 leucine residues in its own and the subsequent LxY motif.
500
501 Three MORN repeats of SETD7 display similar general features, but differ in details, and can
502 be aligned with TbMORN1 repeat 7 over 22-23 aligned C_α atoms with an rmsd of 2.3, 1.5 and
503 1.9 Å respectively (Fig. S10B). The first glycine residue in the SETD7 MORN repeats is
504 conserved with that in TbMORN1, while tyrosine, phenylalanine, and valine replace the
505 tryptophan of the YEGEW motif (Fig. S10C).
506
507
508

509 TbMORN1 forms an extended antiparallel dimer with overall negative charge

510
511 The TbMORN1(7-15) antiparallel dimer displays a two-fold symmetry perpendicular to the
512 longitudinal axis of the assembly (Fig. 5A). Analysis of amino acid conservation derived from
513 a sequence alignment of representative MORN repeat-containing proteins showed a well

514 conserved stretch of residues in the groove (Fig. S11A). Due to the twofold symmetric nature
515 of the quaternary structure assembly, structural and surface properties are displayed on
516 opposite sides of the elongated dimeric particle and perpetuated symmetrically along the
517 rims (Fig. S11).
518
519 The TbMORN1 dimer displays an overall negative electrostatic potential with a central
520 positively-charged pocket (Fig. S11B). The overall negative charge of TbMORN1(7-15) and
521 the lack of pronounced positive patches that could serve as binding sites for negatively-
522 charged phospholipid polar heads is consistent with the negative binding data for lipid
523 membranes (Fig. S11B, C).
524
525 TbMORN1(7-15) formed an extended antiparallel dimer in both crystal lattices, while
526 TgMORN1(7-15) adopted this architecture in one crystal form. The extended dimer interface
527 is built from residues in MORN repeats 12-15, which connect the two subunits in an
528 antiparallel, tail-to-tail orientation (Fig. 5A-C). In both crystal forms of TbMORN1(7-15), the
529 central core of the dimer interface is broadly similar (Fig. 6A, Fig. S12A). Due to the twofold
530 symmetry, the majority of the stabilising interactions are duplicated and build up an extended
531 dimer interface.
532
533 The tightest overlap between the two subunits occurs through MORN repeats 14 and 15. A
534 series of hydrophobic and aromatic π-stacking interactions between residues from repeats
535 14 and 15, together with hydrogen bonds across the edges, stabilise the dimer (Fig. 6A, Fig.
536 S12A). Furthermore, the very negatively-charged C-terminal region of one TbMORN1 subunit
537 forms an arch above the positively-charged platform contributed by Lys316 and Arg293 (Fig.
538 S11B). Two residues from MORN repeat 14 - Lys325 (subunit A) and Asp326 (subunit B) -
539 form a salt bridge, which further stabilises the dimer interface.
540
541 In the $P2_1$ and C2 TbMORN1(7-15) crystal forms, the dimer interfaces occupy surface areas
542 of 747 $Å^2$ and 966 $Å^2$, respectively. Calculations of gain in solvation free energy (Δ^iG) upon
543 dimer formation for TbMORN1(7-15) C2 and $P2_1$ performed with the PDBePISA package
544 (Krissinel & Henrick, 2007) yielded values of -20.1 kcal/mol and -11.3 kcal/mol, respectively,
545 with corresponding p-values of interface specificity 0.01 and 0.08. Δ^iG values lower than -10
546 to -15 kcal/mol and p-values lower than 0.5 are significant for stable protein dimers,
547 indicating highly specific dimerisation interfaces (Krissinel & Henrick, 2007).
548
549 In the C2 crystal form, the dimer is additionally stabilised by two disulphide bridges formed
550 between Cys351 at the C-terminus of repeat 15, and Cys282 from the β-hairpin loop of repeat
551 12 (Fig. S12A). In the $P2_1$ crystal structure, the position of the loop differs from that in the C2
552 dimer, and keeps the C_α atoms of Cys351 and Cys282 at a distance of 11.7 Å, preventing
553 disulphide bond formation. Here, the side chain of Cys351 is engaged in a polar interaction
554 with Asp303 (Fig. 6A, Fig. S12A).
555
556 In comparison to the TbMORN1(7-15) C2 crystal form, the extended TgMORN1(7-15)
557 structure has an approximately 1.5-times smaller dimer interface (601 $Å^2$), which is
558 contributed by residues from MORN repeats 13-15 only (Fig. 5B, Fig. S12C). This is closer in

size to the 747 Å^2 interface of the P2$_1$ crystal form of TbMORN1(7-15). The final C-terminal part of the protein seems to be flexible and does not engage in the stabilisation of the dimer. In comparison to TbMORN1(7-15), the dimer interface of TgMORN1(7-15) is not built around aromatic stacking, but instead employs hydrophobic interactions between Phe350 and neighbouring small hydrophobic residues, such as Leu335 and Leu327 (Fig. S12C).

A retroactive validation of the dimer interface came from the earlier PI(4,5)P$_2$-binding work. Mutagenesis of repeat 14 had produced a mixture of monomers and dimers, while the simultaneous mutagenesis of two candidate sites in repeats 13 and 14 had resulted in a pure monomer population (Fig. S4B). Analysis of the interaction and electrostatic maps of TbMORN1(7-15) and its mutagenised variants clearly showed that Arg293 and Lys316, residing in repeats 13 and 14 respectively, are crucial for maintaining TbMORN1 in a stable dimeric state through electrostatic interactions (Fig. 6C). Lys315 (in MORN repeat 14) does not appear to be directly involved in the dimerisation interface, but could peripherally contribute to the stabilisation of the C-terminal region of TbMORN1 through its electrostatic potential. Residues Arg292, Lys296 (both in MORN repeat 13), and Arg321, Lys325 (both in MORN repeat 14) were mapped to the outer surface of the dimer and therefore do not take part in the dimerisation interface (Fig. 6A, Fig. S12A).

The transition of TbMORN1(2-15)^{Mut14} from a dimeric to a mixed monomer/dimer population is therefore a direct consequence of the single point mutation K316A, whereas the complete abrogation of dimerisation observed for the TbMORN1(2-15)$^{Mut13+14}$ double mutant can be attributed to a synergistic effect of both R293A and K316A point mutations (Fig. 6C, Fig. S4B), thereby verifying their contribution to dimer formation.

The V-shaped and extended dimer forms of apicomplexan MORN1 proteins

Unlike the extended dimers of TbMORN1(7-15) and TgMORN1(7-15), the V-shaped PfMORN1(7-15) is mainly stabilised by a single Zn^{2+} ion incorporated into the core of its dimer interface, spanning over 665 Å^2 (Fig. 5C, Fig 6B). The Cys306 and Asp309 residues from each subunit tetrahedrally coordinate the Zn^{2+} at expected distances (2.32 Å for Zn^{2+}-S and 1.94 Å for Zn^{2+}-O). In addition, residues from repeats 13-15 are involved in stabilising the dimer via a combination of hydrophobic, polar, and electrostatic interactions across the subunits.

Although TgMORN1(7-15) was predominantly found as an extended dimer (Fig. 5B), a V-shaped form similar to that of PfMORN1(7-15) was also observed in the crystal lattice (Fig. S12B). The two V-shaped dimers share the same coordination sphere of a Zn^{2+} ion, which in TgMORN1(7-15) is provided by the Cys305 and Asp308 residues (Fig. S12D). The latter residue in turn interacts with the Ser310 from the other subunit. While the salt bridge and anion π-interactions are also conserved between the two V-shaped dimers, the aromatic stacking present in the core of the PfMORN1(7-15) dimer interface is functionally replaced in the TgMORN1(7-15) V-shaped dimer by a series of aromatic stacking interactions at its vertex.

604 Although Asp residues 303 (TbMORN1), 308 (TgMORN1) and 309 (PfMORN1) are conserved
605 in all the three proteins, the coordination of a Zn^{2+} ion clearly demands the presence of both
606 cysteine and aspartate residues. Such pairs are present in PfMORN1 and TgMORN1, but not
607 in TbMORN1, where the cysteine residue at the corresponding position is replaced by
608 Leu301. The coordination residues map to the β-hairpin of MORN repeat 13, which in
609 TgMORN1 and PfMORN1, but not TbMORN1, contains an insertion of a glutamate residue -
610 Glu307 and Glu308, respectively. Taking part in an anion π-interaction with a phenylalanine
611 residue (Phe303 and Phe304, respectively), the resulting Glu-Phe pairs effectively stabilise
612 the TgMORN1 and PfMORN1 dimers in their V-shaped form. Moreover, these very same
613 glutamate residues further stabilise the two V-shaped dimers by being involved in a salt
614 bridge with lysine residues (Lys321 in TgMORN1 and Lys322 in PfMORN1). At the equivalent
615 position in TbMORN1, Lys316 does not participate in a salt bridge, but rather points towards
616 the negative patch at the C-terminal part of the other subunit and stabilises the extended
617 dimer via electrostatic interactions.
618
619 To see whether it was possible to predict if a MORN repeat protein forms either extended or
620 V-shaped dimers, or both, a comparative sequence analysis was carried out. The sequences
621 of 15 selected MORN repeat proteins from various protist lineages were aligned with the C-
622 terminal parts of TbMORN1, TgMORN1 and PfMORN1 encompassing repeats 12-15 (Fig.
623 S13). The residues in the crystal structures of TgMORN1(7-15) and PfMORN1(7-15) forming
624 the Zn^{2+}-coordination sphere and anion π-interaction were taken as a fingerprint for a V-
625 shaped dimer. All sequences of MORN repeat proteins from kinetoplastids contain a leucine
626 residue (Leu301 in the case of *T. brucei*) at the position of the coordinating Cys residue. They
627 additionally lack the Phe-Glu pair that flank the coordinating Cys residue and form the anion
628 π-interaction. As these residues are essential for V-shape dimerisation, the kinetoplastid
629 proteins should form extended dimers only. Conversely, all protein sequences in the dataset
630 from apicomplexans (*Toxoplasma gondii, Plasmodium falciparum, Gregarina niphandrode*s,
631 *Babesia microti*, *Cryptosporidium parvum, Eimeria acervuline, Theileria equi*) contained these
632 cysteine, phenylalanine, and glutamate residues. This suggests that all these apicomplexan
633 proteins can adopt both extended and V-shaped forms. In addition, the sequences from the
634 alveolates *Symbiodinium microadriaticum* and *Perkinsus marinus*, and the stramenopile
635 *Aureococcus anophagefferens* also contain these three residues, implying that they too
636 should adopt both extended and V-shaped conformations. Apicomplexans belong to the
637 Alveolata clade, and both alveolates and stramenopiles are in the SAR supergroup (Adl et al.,
638 2019). This suggests that the ability to adopt two conformations might have arisen within this
639 specific clade, and possibly explains its absence from the kinetoplastid sequences, as
640 kinetoplastids are excavates. The functional implications of this built-in structural plasticity
641 seemingly modulated by the presence of zinc ions remain intriguing.
642

643 MORN1 proteins adopt extended conformations in solution

644
645 The crystal structures were all consistent with the earlier results of the cross-linking mass
646 spectrometry experiments carried out on TbMORN1 in solution, which had indicated close
647 proximity between repeats 13-15 (Table S1). To investigate the presence of V-shaped and
648 extended dimers in solution, all three MORN1 proteins were structurally analysed using small-

649 angle X-ray scattering (SAXS). SAXS analysis of TbMORN1(7-15) and TgMORN1(7-15)
650 indicated an extended dimer in solution, and the crystal structures could be docked into the
651 calculated molecular envelopes without difficulty (Fig. 7A, B, Fig. S12E). The SAXS analysis
652 of PfMORN1(7-15) indicated an extended structure, similar to that seen for TbMORN1(7-15)
653 and TgMORN1(7-15) (Fig. 7C, Fig. S12E). This supports the prediction that TgMORN1 and
654 PfMORN1 are capable of adopting two different conformations. Subsequent SAXS
655 experiments produced a molecular envelope for TbMORN1(2-15) into which an extrapolated
656 version of the model of TbMORN1(7-15) could be docked as an extended dimer (Fig. 7D, Fig.
657 S12E).
658
659 Rotary shadowing EM on TbMORN1(2-15) produced results consistent with the SAXS
660 analysis, showing small kinked rods approximately 25 nm in length (Fig. 7E). The population
661 was homogeneous, consistent with the monodispersity of this sample observed by SEC-
662 MALS (Fig. 1B). Comparison of the maximal dimer dimension (D_{max}) for TbMORN1(2-15)
663 obtained from SAXS and EM showed a very good agreement between the two values of 250-
664 260 Å. Rotary shadowing EM was also carried out on the small amount of TbMORN1(1-15)
665 that eluted from the SEC column (Fig. 7F, G). Full-length TbMORN1 was far more
666 heterogeneous than TbMORN1(2-15), consistent with the polydispersity observed by SEC-
667 MALS (Fig. 1B). In addition to single kinked rods, longer filamentous assemblies of varying
668 length were occasionally observed (Fig. 7F). Rarely, much larger meshlike assemblies of full-
669 length TbMORN1 could be observed (Fig. 7G), offering a tantalising clue into the higher-order
670 assembly properties of the protein. These properties will be investigated in future work.
671

672 # DISCUSSION

673
674 MORN repeats were first named almost 20 years ago, in a paper identifying the junctophilin
675 protein family (Takeshima et al., 2000). While there is abundant evidence that junctophilins
676 associate with the plasma membrane, and that the MORN repeat-containing region is likely
677 to mediate this, there is to the authors' knowledge no report demonstrating that the
678 junctophilin MORN repeats directly interact with lipids (Takeshima et al., 2000, Munro et al.,
679 2016, Woo et al., 2016, Perni et al., 2017, Jayasinghe et al., 2018, Nakada et al., 2018, Rossi
680 et al., 2019).
681
682 This evidence that the MORN repeat-containing region of junctophilins mediates plasma
683 membrane targeting has been repeatedly cited as showing that MORN repeats directly bind
684 lipids. Warnings that the function of MORN repeats has not really been elucidated, and that
685 extant data are frequently contradictory, have been largely overlooked (Mikami et al., 2010).
686 We therefore set out to test the lipid-binding hypothesis by using a protein composed
687 exclusively of MORN repeats, TbMORN1.
688
689 Early experiments utilising isolated lipids in PIP strips and fluorescence anisotropy assays
690 suggested an ability of TbMORN1 to bind specific phospholipids. These results could never
691 be confirmed in liposome pelleting assays however, and the quantitative molecular
692 biophysics data strongly suggest that the observed binding was to the aliphatic chains of the
693 isolated lipids.

694
695 Given that TbMORN1 is a cytoskeleton-associated protein, it is hard to imagine how it would
696 be able to access the hydrophobic chains of membrane-embedded phospholipids in vivo,
697 although it is localised directly under the cytoplasmic leaflet of the plasma membrane. The
698 electrostatic profile of TbMORN1(7-15) is also not suggestive of membrane binding, with a
699 strong overall negative charge profile (Fig. S11B).
700
701 Unexpectedly, purified recombinant TbMORN1(1-15) was found to co-purify with PE.
702 Bacteria expressing TbMORN1(1-15) showed elevated levels of PE, which might suggest that
703 TbMORN1 was binding and sequestering the lipid, requiring them to upregulate synthesis
704 (Fig. 2A, C). Almost no PE was found to co-purify with TbMORN1(10-15), and none was
705 detected with the apicomplexan MORN1 proteins. This suggests that the first 9 MORN
706 repeats of TbMORN1 might be a major interaction area for PE.
707
708 No co-purification of PE was seen with the apicomplexan MORN1 proteins despite >50%
709 identity at an amino acid level. This lipid-binding activity therefore seems specific to
710 TbMORN1. The elevation of PE levels seen in bacteria expressing TbMORN1(1-15) is highly
711 unusual, and the authors do not currently have a good explanation apart from invoking lipid
712 sequestration and transport to specific sites (Chung et al., 2015, Moser von Filseck et al.,
713 2015). If the PE co-purifying with recombinant TbMORN1(1-15) was just carry-over, then the
714 lipid profile should resemble that of total bacterial cellular lipids, which is not the case.
715 Furthermore, the bound PE moieties display a narrow range of aliphatic chains, suggesting
716 specificity of binding/recognition.
717
718 Lipids in trypanosomes have, in general, much longer aliphatic chains than those in bacteria.
719 In *T. brucei*, PE accounts for around 10-20% of total lipid, with aliphatic chains of 36:0 being
720 the dominant isoform (Richmond et al., 2010). In *E. coli*, PE is the predominant zwitterionic
721 lipid and accounts for around 80% of total lipid (Epand & Epand, 2009). As the length of the
722 side chains in bacterial lipids is predominantly 14 and 16 carbon atoms (Pramanik & Keasling,
723 1997), PE molecules with 16 carbon atoms chains are the most common. Notably,
724 TbMORN1(1-15) overexpressed in *E. coli* co-purified with PE species of much greater length
725 (30:0 – 36:2) (Fig. 2A), which was also reflected in increased production of these PE species
726 in overexpressing bacteria (Fig. 2C). Taken together, these data strongly suggest the
727 specificity of TbMORN1(1-15) towards PE species with aliphatic chains of a length
728 characteristic for *T. brucei*.
729
730 Neither PE nor any other lipids were observed in the crystal structure of TbMORN1(7-15).
731 This might be due to the fact that TbMORN1(7-15) does not contain the N-terminal part of
732 the molecule. Alternatively, the lysine methylation step used to enhance crystallisation might
733 have prevented electrostatic interactions with lipid molecules due to the loss of positive
734 charge.
735
736 Due to the twofold symmetry of both extended and V-shaped MORN1 dimers, the dimeric
737 particle displays the conserved groove on opposite sides, therefore excluding this region for
738 interaction with the membranes and leaving as an option the rims lining the groove. In the

739 extended dimers, the two rims display a concave and a convex curvature (Fig. S11),
740 suggestive of membrane sculpting BAR domain proteins which interact with membranes
741 mainly via non-specific electrostatic interactions (Salzer et al., 2017, Carman & Dominguez,
742 2018). These curved surfaces in MORN1 dimers nevertheless do not display a pronounced
743 positive charge, nor the typical membrane insertion motifs characteristic for BAR domain
744 proteins, thus refuting the hypothesis for membrane binding. In conclusion, the quaternary
745 structure architecture together with surface properties of the MORN1 dimers do not support
746 membrane binding.
747
748 It is important to note that phospholipid binding and membrane binding are two separate
749 things. Not interacting with membranes might not preclude the TbMORN1 proteins extracting
750 PE or other phospholipids out of membranes without stably interacting with the membranes
751 themselves. A similar hypothesis would be that TbMORN1 functions as a carrier/transporter
752 of lipids with aliphatic chains within a certain length, as for example found for non-vesicular
753 phosphatidylserine transport by oxysterol-binding proteins from the site of synthesis to the
754 site of biological activity (Maeda et al., 2013). What would be the corresponding physiological
755 role in the context of the flagellar pocket in trypanosomes is difficult to envisage at present.
756 For now, the simplest interpretation remains that there is no interaction of TbMORN1 with
757 lipid membranes, and consequently no physiological interaction with membrane-embedded
758 phospholipids either. These data have clear implications for other MORN repeat proteins.
759 Junctophilins do appear to bind lipids, but it is not clear if their MORN repeats are mediating
760 this or are merely within the region/domain involved (Bennett et al., 2013, Jiang et al., 2019).
761
762 Based on the data presented in this study, the presence of MORN repeats in a protein should
763 not be taken as indicative of lipid binding or lipid membrane binding without experimental
764 evidence. Equally, evidence of binding from PIP strips alone should be interpreted with
765 caution.
766
767 If MORN repeats are not lipid binding modules by default, this raises the question of what
768 they might actually be doing. The structural studies presented here make a case that one
769 conserved function of MORN repeats is in homotypic interactions, and possibly also in
770 higher-order assembly. The role of MORN repeats in heterotypic interactions has recently
771 been demonstrated at a structural level (Li et al., 2019). In the case of TbMORN1, previous
772 work using proximity-dependent labelling (BioID) has already established that it has a number
773 of direct and indirect binding partners in vivo (Morriswood et al., 2013).
774
775 All three MORN1 proteins analysed here formed tail-to-tail dimers via their C-termini with the
776 subunits aligned in an antiparallel arrangement. The all-β structure of the proteins folds in a
777 twisting elongated shape, with a groove lined with aromatic side chains running longitudinally
778 through it. While this manuscript was in preparation, Li et al. published a high-resolution
779 structure of the MORN4/retinophilin protein in complex with the myosin 3a tail. Binding was
780 mediated by this central groove, showing that it can be engaged in very high-affinity protein-
781 protein interactions (Li et al., 2019).
782

783 The three high-resolution structures described in this work are amongst the first canonical
784 MORN repeat proteins to be detailed. Given that the structures are from representatives of
785 two of the five eukaryotic supergroups - the excavates, and the SAR (stramenopiles,
786 alveolates, Rhizaria) clade - this demonstrates how the fundamental structure of the MORN
787 repeat has been conserved over evolutionary time.
788
789 The crystal structures in extended conformations were consistent with the lower-resolution
790 SAXS data obtained on the same proteins in solution (Fig. 7A-C, Fig. S12E, Table S1). Based
791 on the crystallographic data, the apicomplexan MORN1 proteins appear capable of forming
792 both extended and V-shaped conformations. The key residues mediating the dimer interface
793 in the V-shaped form were defined, and shown to be conserved throughout the Apicomplexa.
794 It thus seems possible that all apicomplexan MORN1 proteins can adopt these two
795 conformations.
796
797 MORN1 proteins in Apicomplexa have been shown to be a key component of the basal
798 complex, which undergoes a constriction event at the end of the cell division cycle (Gubbels
799 et al., 2006, Hu, 2008). It is therefore tempting to speculate that these extended (Zn-free) and
800 V-shaped (Zn-bound) conformations represent the pre- and post-constriction states of the
801 MORN1 proteins in the basal complex. If so, this would constitute a remarkable
802 rearrangement of the subunits in the dimer, which would move through about 145°
803 (Supplementary Video 1). It is interesting in this context to note that high levels of Zn ions are
804 required to support the growth of the blood-stage *P. falciparum* parasite (Marvin et al., 2012).
805
806 The high-resolution structures also enabled a new structure-based consensus sequence for
807 a MORN repeat to be defined (Fig. 5E). A single MORN repeat forms a β-hairpin, one of the
808 conserved building blocks of structural biology, followed by a long tail. The structural basis
809 for the conservation of individual residues within the MORN repeat has been defined (Fig. 5E,
810 F). These structures strongly argue that an individual MORN repeat is longer than 14 amino
811 acids. Despite the lower level of sequence conservation in the tail following the hairpin, a 23-
812 amino acid length seems the most parsimonious definition from a structural perspective.
813
814 One interesting consequence of this redefinition of the repeat is that it suggests that full-
815 length TbMORN1 begins with an incomplete repeat, a feature also noted in the
816 MORN4/retinophilin structure (Li et al., 2019). The (M)IYSEGE residues at the very N-terminus
817 are predicted to form only a single β-strand rather than a complete hairpin (Fig. 5E). Li et al.
818 suggested that this incomplete repeat could function as a capping element, but given that
819 the first repeat in MORN1 is critical for oligomerisation leading to formation of filamentous
820 structures, an alternative explanation is possible: the N-terminus of a second TbMORN1
821 molecule (itself encoding a single β-strand) could complete this hairpin through
822 intermolecular interactions. Oligomerisation would thus be driven by a "split-MORN repeat"
823 mechanism where a complete hairpin is formed by the interaction of the N-termini of two
824 proteins. Further work will be needed to test this hypothesis. The concluding data presented
825 here suggest that TbMORN1 utilises this oligomerisation capacity to build mesh-like
826 assemblies, which can reach considerable size in vitro (Fig. 7G). These mesh-like assemblies
827 may reflect the endogenous organisation of the protein in vivo, where a number of binding

828 partners have already been identified (Morriswood et al., 2013). The biophysical properties of
829 these meshworks, as well as their protein-protein interactions and possible lipid-carrying
830 roles, are likely to be fruitful avenues of investigation.
831
832
833

834 MATERIALS AND METHODS:

835

836 **Antibodies and other reagents**

837 All custom antibodies have been described previously. The rabbit anti-TbMORN1 were made
838 for a previous project (Morriswood et al., 2013). The mouse monoclonal anti-Ty1 (BB2)
839 antibodies were a gift from Cynthia He (University of Singapore) (Bastin et al., 1996). The
840 mouse monoclonal anti-PFR1,2 antibodies (L13D6) were a gift from Keith Gull (University of
841 Oxford) (Kohl et al., 1999). The anti-BiP antibodies were a gift from Jay Bangs (University at
842 Buffalo) (Bangs et al., 1993). The rabbit anti-GFP antibodies were a gift from Graham Warren
843 (MRC Laboratory for Molecular Cell Biology) (Pelletier et al., 2002). The following antibodies
844 were obtained from commercial sources: anti-strep tag StrepMAB-Classic (IBA Biosciences),
845 HRP-conjugated anti-mouse (ThermoFisher Scientific), anti-GST (Santa Cruz Biotechnology).
846 Defatted BSA was purchased from Sigma-Aldrich.
847
848

849 **Cloning and mutagenesis of expression constructs**

850 The 1077 bp TbMORN1 open reading frame (ORF) (UniProt accession no. Q587D3;
851 TriTrypDB database accession no. Tb927.6.4670) was amplified by PCR from genomic DNA
852 obtained from *Trypanosoma brucei brucei* strain Lister 427 and ligated into vector pETM-13
853 encoding a Strep-tag at the 3' end of the insert. TbMORN1 truncations were generated using
854 this construct as a template by ligase-independent cloning (Doyle, 2005). The sequences for
855 TbMORN1(2-15) and TbMORN1(1-14) were additionally ligated into the pCoofy12 vector
856 encoding a 3C protease-cleavable N-terminal Twin-Strep-tag (Scholz et al., 2013) by
857 sequence and ligation-independent cloning (Li & Elledge, 2012). Mutagenesis constructs
858 were generated by standard methods using the pre-existing pCoofy12_TbMORN1(2-15)
859 construct as the template (Hemsley et al., 1989). All primer sequences are available upon
860 request. For LiMA experiments, the construct encoding the EGFP-TbMORN1(2-15) was
861 cloned in a two-step procedure by sequence and ligation-independent cloning followed by
862 Gibson assembly using pCoofy12_TbMORN1(2-15) and the pEGFP-C1 vector (Gibson et al.,
863 2009). The 1092 bp TgMORN1 (UniProt accession no. Q3S2E8) and 1095 bp PfMORN1
864 (UniProt accession no. Q8IJ93) ORFs were amplified by PCR from genomic DNA. Truncations
865 of the TgMORN1 and PfMORN1 constructs were generated using ligase-independent
866 cloning. The TgMORN1 constructs were additionally ligated into the pET14 vector encoding
867 a 3C protease-cleavable N-terminal His10-tag. The PfMORN1 constructs were additionally
868 ligated into the pCoofy32 encoding a 3C protease-cleavable N-terminal His10-tag and C-
869 terminal OneStrep-tag.
870
871

872 **Recombinant protein expression and purification**
873 Rosetta 2 (DE3)pLysS bacterial cells transformed with the required expression plasmids were
874 grown at 37 °C with shaking in the presence of the appropriate antibiotics. Large scale
875 expression was carried out either in Luria-Broth or in auto-induction (ZY) medium (Studier,
876 2005), with 500 ml media being inoculated with 3-5 ml of pre-cultured cells. Cells in Luria-
877 Broth were grown to an OD_{600} ~ 0.8 – 1.0, after which 50 µM IPTG was added to induce
878 recombinant protein expression. The cells were then incubated at lower temperature
879 (overnight, 20 °C). The cells were then harvested by centrifugation (5000 x g, 30 min), and
880 either lysed immediately or stored at -80 °C. For purification, the cells were resuspended in
881 lysis buffer (50 mM Tris-HCl pH 8.5, 200 mM NaCl, 5% (w/v) glycerol, 1 mM DTT, protease
882 inhibitor cocktail, benzonase). The pellet emulsions were first homogenised by mixing on ice
883 using a T 10 basic Ultra-Turrax dispersing instrument (IKA), and lysis was accomplished using
884 a single cycle in a cell disruptor (Constant systems Ltd), with the pressure set to 1.35 kPa.
885 Lysates were clarified by centrifugation (18,000 x g, 45 min, 4 °C), and a two-step fast protein
886 liquid chromatography (FPLC) purification protocol using an ÄKTA Protein Purification
887 System (GE Healthcare Life Sciences) at 8 °C was then followed to obtain the recombinant
888 protein. The supernatants were applied to two connected Strep-Trap HP 5 ml columns
889 packed with Strep-Tactin ligand immobilized in an agarose matrix (GE Healthcare Life
890 Sciences) previously equilibrated with equilibration buffer (50 mM Tris-HCl pH 8.5, 200 mM
891 NaCl, 2% (w/v) glycerol, 1 mM DTT). Flow speed was adjusted to 2.5 ml/min. When 100%
892 step gradient of elution buffer (equilibration buffer plus 2.5 mM D-desthiobiotin) was applied,
893 the bound proteins were eluted in a single chromatographic peak. Selected peak fractions
894 were examined by SDS-PAGE for protein content and purity, pooled accordingly, and
895 concentrated in Amicon Ultra centrifugal filter units (MerckMillipore, various pore sizes)
896 according to the manufacturer's instructions. These affinity-purified protein concentrates
897 were then applied to a previously equilibrated HiLoad 16/600 Superdex 200 pg column (GE
898 Healthcare Life Sciences) packed with dextran covalently bound to highly cross-linked
899 agarose, enabling separation of proteins with MW in the range of 10 – 600 kDa. Flow speed
900 was adjusted to 1 ml/min and fractions of 1.5 ml were collected. Fractions corresponding to
901 the targeted chromatographic peak were examined for protein content by SDS-PAGE,
902 pooled accordingly to their purity, concentrated, and stored at -80 °C until use.
903
904 **Limited proteolysis**
905 Purified recombinant His-TbMORN1(1-15) at 1 mg/ml was separately incubated with three
906 proteases with different cleavage specificities (α-chymotrypsin, trypsin, and proteinase K) in
907 20 mM Tris-HCl pH 8.5, 200 mM NaCl, 2% glycerol, 0.2 mM $CaCl_2$ (15 min, RT). The
908 proteases were used at dilutions of 1:100 - 1:2000. The reactions were stopped by the
909 addition of SDS-Coomassie sample loading buffer for analysis by gel electrophoresis. The
910 indicated protein bands were extracted from the gel and subjected to mass spectrometry
911 analysis.
912
913
914 **Size-exclusion chromatography coupled to multi-angle light scattering (SEC-MALS)**
915 The MW and oligomeric state of purified proteins were verified by size exclusion
916 chromatography (SEC) coupled to multi-angle light scattering (MALS), using a Superdex 200

917 Increase 10/300 GL column (GE Healthcare Life Sciences). Up to five protein samples of 100
918 µl were dialysed against 2x 1 L of freshly-prepared, degassed gel filtration buffer (20 mM Tris-
919 HCl pH 8.5, 200 mM NaCl, 2% (w/v) glycerol, 0.5 mM DTT) (overnight, 4 °C). Gel filtration
920 buffer was also used for overnight equilibration of the column and in the subsequent
921 measurements. Protein samples were clarified by centrifugation using a TLA-55 rotor in an
922 Optima MAX-XP table top ultracentrifuge (Beckman Coulter) (90,720 x g, 30 min, 4 °C). 100
923 µl of 2 – 4 mg/ml protein samples were applied to a column using the 1260 Infinity HPLC
924 system (Agilent Technologies) coupled to a MiniDawn Treos detector (Wyatt Technologies)
925 with a laser emitting at 690 nm. An RI-101 detector (Shodex) was used for refractive index
926 determination and the Astra 7 software package (Wyatt Technologies) for data analysis. No
927 correction of the refractive index was necessary due to the 2% (w/v) glycerol content in the
928 buffer.
929
930
931 **Circular dichroism (CD)**
932 Far-UV CD was used both for measurement of secondary structure and for validation of the
933 thermostability of TbMORN1 constructs. To avoid the absorption of Tris and NaCl below 180
934 nm (Kelly et al., 2005), three protein samples of 100 µl were first dialysed against 2x 1 L of
935 dialysis buffer (20 mM NaH_2PO_4, 20 mM Na_2HPO_4, 200 mM NaF) (overnight, 4 °C). The pH
936 8.0 was adjusted by mixing the mono- and dibasic sodium phosphate solutions. The dialysed
937 proteins were clarified by centrifugation in an Optima MAX-XP tabletop ultracentrifuge
938 (Beckman Coulter Life Sciences) (90,720 x g, 30 min, 4 °C). The concentration of protein
939 samples was adjusted to 0.25 mg/ml. CD measurements were carried out in a quartz cuvette
940 with an optical path length of 0.5 mm (Stana Scientific Ltd) using a Chirascan Plus
941 spectrophotometer (Applied Photophysics) equipped with the Chirascan-plus DMS software
942 package. The CD profiles for secondary structure calculations were obtained at RT in the
943 range of 190 – 260 nm. Further analysis was carried out using the BeStSel server, which is
944 specialised in the analysis of CD data from proteins rich in β-strands (Micsonai et al., 2015,
945 Micsonai et al., 2018). Data were converted to Δε ($M^{-1}cm^{-1}$) and uploaded to the BeStSel
946 online server. Melting experiments were performed in the range of 190 – 260 nm, 20 – 80 °C,
947 with a temperature ramp of 0.8 °C/min. Data were analysed with Global 3 software package.
948
949
950
951 **Chemical cross-linking coupled to mass spectrometry (XL-MS)**
952 For chemical cross-linking with EDC (1-ethyl-3-(3-dimethylaminopropyl)carbodiimide
953 hydrochloride) or BS^3 (bis(sulfosuccinimidyl)suberate), 200-300 µl of approximately 30 µM
954 TbMORN1 sample was dialysed twice against 1 L of EDC buffer (20 mM MES-NaOH pH 6.8,
955 200 mM NaCl) or BS^3 buffer (20 mM HEPES-NaOH pH 8.0, 200 mM NaCl) (overnight, 4 °C).
956 Following dialysis, the protein was clarified by centrifugation (90,720 x g, 30 min, 4 °C) using
957 a TLA-55 rotor in an Optima MAX-XP tabletop ultracentrifuge (Beckman Coulter Life
958 Sciences). EDC (ThermoFischer Scientific) was first equilibrated to RT and then a stock
959 solution in EDC buffer was prepared. 1.3 µM TbMORN1 previously dialysed in EDC buffer
960 was mixed with 0, 200, and 400 µM EDC (all final concentrations) in a total volume of 40 µl.
961 After a 30 min incubation at RT, 10 µl of SDS loading buffer was added and the mixtures

962 were further denatured by heating (95 °C, 10 min). The experiments with BS^3 were carried
963 out identically except that BS^3 buffer and 3.4 µM TbMORN1 were used, and the incubation
964 time was 120 min. Samples were separated by SDS-PAGE, stained with Coomassie dye, and
965 selected bands corresponding to monomers and dimers cross-linked with 400 µM cross-
966 linker were excised and subjected to enzymatic digestion and subsequent mass
967 spectrometry analysis. Coomassie Brilliant Blue-stained excised bands were destained with
968 a mixture of acetonitrile and 50 mM ammonium bicarbonate (ambic), in two consecutive steps
969 (each 10 min, RT). The proteins were reduced using 10 mM DTT in 50 mM ambic for (30 min,
970 56 °C), alkylated with 50 mM iodoacetamide in 30 mM ambic in the dark (30 min, RT), and
971 digested with trypsin (Promega, mass spectroscopy grade) (overnight, 37 °C). The reaction
972 was stopped using 10% (v/v) formic acid and extracted peptides were desalted using C18
973 Stagetips (Rappsilber et al., 2007). Peptides were analysed on an UltiMate 3000 HPLC
974 RSLCnano system coupled to a Q Exactive HF mass spectrometer, equipped with a
975 Nanospray Flex ion source (all Thermo Fisher Scientific). Peptides were loaded onto a trap
976 PepMap 300 C18 column of dimensions 5 mm x 300 µm i.d., packed with 5 µm particles with
977 a pore size of 100 Å (Thermo Fisher Scientific) and separated on an analytical C18 100 column
978 of dimensions 500 mm x 75 µm i.d., packed with 2 µm particles with a pore size of 100 Å
979 (Thermo Fisher Scientific), applying a linear gradient from 2% to 40% solvent B (80%
980 acetonitrile, 0.1% formic acid) at a flow rate of 230 nl/min over 120 min. The mass
981 spectrometer was operated in a data-dependent mode at high resolution of both MS1 and
982 MS2 level. Peptides with a charge of +1, +2 or of a higher than +7, were excluded from
983 fragmentation. To identify cross-linked peptides, the spectra were searched using pLink
984 software v1.23 (Yang et al., 2012). Q Exactive HF raw-files were pre-processed and
985 converted to mgf-files using pParse (Yuan et al., 2012). The MaxQuant database (Tyanova et
986 al., 2016) was used to search the spectra for the most abundant protein hits.
987 Carbamidomethylation of cysteine and oxidation of methionine residues were set as variable
988 modifications. Trypsin was set as an enzyme specificity, and EDC or BS^3 was set as a cross-
989 linking chemistry. In case of EDC, aspartic and glutamic acid residues, as well as C-termini
990 of proteins, were allowed to be linked with lysine residues. In the case of BS^3, lysine residues
991 and N-termini of proteins were allowed to be linked with lysine residues, N-termini of proteins,
992 as well as to serine, threonine and tyrosine residues. Search results were filtered for 1% FDR
993 (false discovery rate) on the PSM (number of peptide-spectrum matches) level and a
994 maximum allowed precursor mass deviation of 5 ppm. To remove low quality PSMs, an
995 additional e-Value cutoff of < 0.001 was applied. In order to distinguish intra- from inter-
996 molecular chemical cross-links, results from monomers and dimers were compared. A
997 potential inter-molecular cross-link must have shown the following criteria: (1) minimally 3
998 peptide PSMs in dimer and (2) minimally 3-times more PSMs in dimer than in monomer.
999
1000
1001 **Protein-lipid overlay assays (PIP strips)**
1002 PIP strips were purchased from Echelon Biosciences. PBS-T (PBS, 0.1% TWEEN-20) was
1003 used as a general buffer. Purified recombinant TbMORN1(1-15) was clarified by
1004 centrifugation (20,817 x g, 20 min, 4 °C) prior to use. The PIP strips were blocked using
1005 blocking buffer (3% (w/v) defatted BSA, PBS-T) (60 min, RT) and then incubated with 5 µg/ml
1006 of TbMORN1 in 10 ml of blocking solution (60 min, RT). After three washes with PBS-T, the

1007 membranes were overlaid with anti-strep antibodies diluted in blocking solution (60 min, RT).
1008 After a further three PBS-T washes, the membranes were overlaid with HRP-conjugated
1009 secondary antibodies (60 min, RT). The membranes were then washed three times with PBS-
1010 T and visualised by ECL (Western Blotting substrate, Thermo Fisher) using a Fusion FX
1011 imager (Vilber Lourmat). All binding and wash steps were carried out with gentle agitation of
1012 the membranes. For the positive control, the PIP strip was overlaid with GST-tagged PLC-δ1
1013 PH domain (Echelon Biosciences) and mouse monoclonal anti-GST antibodies (Santa Cruz
1014 Biotechnology) were used.
1015
1016
1017 **Fluorescence anisotropy**
1018 Stocks of BODIPY TMR-labelled PI C6, PI(4)P C6, PI(3,4)P_2 C6, PI(3,5)P_2 C6, PI(4,5)P_2 C6 and
1019 PI(4,5)P_2 C16 were sonicated (5 min, RT) in a sonication bath, and in parallel with purified
1020 recombinant TbMORN1(2-15), TbMORN1(7-15), TbMORN1(10-15), were clarified by
1021 centrifugation (20,817 x g, 20 min, 4 °C). The concentrations of lipid stocks were determined
1022 with a Hitachi U-3501 UV-VIS spectrophotometer, using quartz absorbance cuvettes and an
1023 optical path length of 10 mm (Hellma Analytics). For this purpose, the maximum absorbance
1024 of BODIPY TMR dye at λ = 544 nm was measured; its extinction coefficient ε = 60,000 $cm^{-1}M^{-1}$.
1025
1026 The total volume of each respective sample in a cuvette was 110 µl, which consisted
1027 of a lipid stock and a protein in gel filtration buffer (20 mM Tris-HCl pH 8.5, 200 mM NaCl,
1028 2% (w/v) glycerol, 0.5 mM DTT). The concentration of selected TbMORN1 constructs was
1029 varied from 0 to 35 µM (or more), while the concentration of added lipid was kept constant
1030 at 0.1 µM. Measurements were performed on a Perkin Elmer LS50B fluorimeter in quartz
1031 cuvettes with an optical path length of 10 x 2 mm (Hellma Analytics). To ensure a constant
1032 temperature of 20 °C in the measured sample, the measurement cell was connected to a
1033 water bath. The parameters for fluorescence anisotropy (r) measurements were: λ_{ex} = 544 nm
1034 and aperture of excitation slit = 15 nm; λ_{em} = 574 nm and aperture of emission wavelength =
1035 20 nm; time of integration = 1 s and T = 20 °C. The grating factor (G factor), which provides
1036 grating correction for the optical system, was determined on samples with exclusively 0.1 µM
1037 lipid and kept constant during measurement of each concentration series. Triplicates of each
1038 protein concentration point were measured and afterwards averaged using Excel software.
1039 Graphs were drawn and fitted in SigmaPlot ver. 13.0. The equation used for fitting was a four
1040 parameters logistic curve where:

1041 $$y = + \frac{(-min)}{1+(\frac{x}{EC50})^{-Hillslope}} ,$$

1042
1043 options were set to default; initial parameters values, as well as parameters min, max, EC50,
1044 Hillslope, were selected automatically, parameter constraints were max > min and EC50 > 0,
1045 number of iterations was 200, and tolerance was kept at $1e^{-10}$. The reduced chi-square
1046 method was used to compute parameters' standard errors. Experimental r values of
1047 respective 0.1 µM BODIPY TMR-lipid and protein-TMR BODIPY-lipid mixtures were
1048 compared with theoretical values obtained by Perrin equation.
1049
1050

1051 **Mass spectrometry analysis of extracted lipids**
1052 Lipid extractions from purified recombinant full length and truncated TbMORN1 were
1053 achieved by three successive vigorous extractions with ethanol (90% v/v) according to a
1054 published protocol (Fyffe et al., 2006). The pooled extracts were dried using N_2 gas in a glass
1055 vial and re-extracted using a modified Bligh and Dyer method (Richmond et al., 2010). For
1056 whole *E. coli* lipid extracts, cells were washed with PBS and extracted following the modified
1057 Bligh and Dyer method. All extracts were dried under N_2 gas in glass vials and stored at 4 °C.
1058 Extracts were dissolved in 15 µl of $CHCl_3$:CH_3OH (1:2) and 15 µl of acetonitrile:propan-2-
1059 ol:water (6:7:2) and analysed with an Absceix 4000 QTrap, a triple quadrupole mass
1060 spectrometer equipped with a nano-electrospray source. Samples were delivered using a
1061 Nanomate interface in direct infusion mode (~125 nl/min). Lipid extracts were analysed in
1062 both positive and negative ion modes using a capillary voltage of 1.25 kV. MS/MS scanning
1063 (daughter, precursor and neutral loss scans) were performed using nitrogen as the collision
1064 gas with collision energies between 35-90 V, allowing lipid structure assignments.
1065
1066
1067 **Preparation of liposomes and liposome sedimentation assay**
1068 The preparation of liposomes has been described previously (Zens et al., 2015). Liposomes
1069 were prepared from $CHCl_3$ stocks of 10 mg/ml of 1-palmitoyl-2-oleoyl-sn-glycero-3-
1070 phosphocholine, POPC, 16:0-18:1 (Avanti Polar Lipids) and 1 mg/ml of porcine brain L-α-
1071 phosphatidylinositol 4,5-bisphosphate, PI(4,5)P_2 (Avanti Polar Lipids). Lipid mixtures of 0-
1072 20% of PI(4,5)P_2 and 80-100% of POPC were first dried under a stream of nitrogen, and then
1073 vacuum dried for at least one hour. Dried lipid mixtures were hydrated in gel filtration buffer,
1074 incubated for 10 min at RT, gently mixed, further incubated for 20 min and sonicated for 2
1075 min at RT in a water bath, followed by 5 freeze-thaw cycles. Using a mini-extruder (Avanti
1076 Polar Lipids), vesicles were then extruded through polycarbonate filters with 0.4 µm and 0.1
1077 µm pore sizes. TbMORN1(2-15) and Doc2B, a positive control for PI(4,5)P_2 binding, were
1078 clarified by centrifugation in a TLA-55 rotor for 30 min at 90,720 x g, 4 °C, using an Optima
1079 MAX-XP tabletop ultracentrifuge (Beckman Coulter Life Sciences), prior to the liposome
1080 sedimentation assay. For the assay, proteins and liposomes were mixed in polycarbonate
1081 tubes (Beckman Coulter) and incubated for 30 min at RT. The final concentrations of
1082 liposomes and proteins were 0.5 mg/ml and 10 µM, respectively. The liposomes were
1083 pelleted by centrifugation in an ultracentrifuge for 40 min at 180,743 x g, 20 °C, using a TLA-
1084 100 rotor (Beckman Coulter). Supernatants and pellets were separated and mixed with 5x
1085 and 1x SDS-PAGE loading dye, respectively. Two independent experiments were performed.
1086 Samples were separated on 15% acrylamide gels by SDS-PAGE and after electrophoresis,
1087 gels were stained with Coomassie Brilliant Blue staining solution and scanned. The amounts
1088 of proteins in supernatants and pellets were quantified with QuantiScan 32 software.
1089
1090
1091 **Preparation of sucrose-loaded vesicles (SLVs) and pelleting assay**
1092 To generate synthetic SLVs, lipids reconstituted in $CHCl_3$ were mixed in the following ratio:
1093 30% DOPC; 35% DOPE; 15% DOPS; 20% cholesterol. 5 mol % PI(4,5)P_2 was added in place
1094 of 5 mol% DOPE in the PI(4,5)P_2-containing liposomes. Lipids were extracted from
1095 bloodstream form *T. brucei* according to an established protocol (Bligh & Dyer, 1959). Briefly,

1096 mid-log phase cells were harvested by centrifugation (750 x g, 10 min, RT), washed once
1097 with PBS, then resuspended in 100 µl PBS and transferred to a glass tube. 375 µl of 1:2 (v/v)
1098 $CHCl_3$:MeOH was added and the mixture was vortexed (20 s) and then incubated with
1099 continuous agitation (15 min, RT). A further 125 µl $CHCl_3$ was then added to make the mixture
1100 biphasic, and following brief vortexing 125 µl ddH_2O was added. The mixture was vortexed
1101 again and then separated by centrifugation (1000 x g, 5 min, RT). The lower organic layer was
1102 then transferred to a new glass vial, dried under a nitrogen stream, and kept at 4 °C until use.
1103 For the preparation of SLVs from trypanosomal lipids the lyophilized lipids (extract from $8x10^7$
1104 cell equivalents) were reconstituted in 50 µl $CHCl_3$. 6 µM Rhodamine B dihexadecanoyl
1105 phosphoethanolamine (Rh-DHPE) was added to all lipid mixtures to facilitate the visualisation
1106 of the SLVs. The lipid mixtures were dried under a nitrogen stream, and the lipid films
1107 hydrated in 20 mM HEPES pH 7.4, 0.3 M sucrose. The lipid mixtures were subjected to 4
1108 cycles of freezing in liquid nitrogen followed by thawing in a sonicating water bath at RT. The
1109 vesicles were pelleted by centrifugation (250,000 x g, 30 min, RT) and resuspended in 20 mM
1110 HEPES pH 7.4, 100 mM KCl to a total lipid concentration of 1 mM. SLVs were incubated with
1111 1.5 µM purified TbMORN1(2-15) in gel filtration buffer (20 mM Tris-HCl pH 8.5, 200 mM NaCl,
1112 2% glycerol, 1 mM DTT) at a 1:1 ratio (30 min, RT). To separate soluble and SLV-bound
1113 TbMORN1(2-15), the vesicles were pelleted by centrifugation (8,700 x g, 30 min, RT), and
1114 equal volumes of supernatant and resuspended pellet were separated by SDS-PAGE and
1115 analysed by Coomassie staining.
1116
1117
1118 **Liposome microarray assay (LiMA)**
1119 LiMA (Saliba et al., 2014) was performed according to the standard protocol (Saliba et al.,
1120 2016). TbMORN1(2-15) tagged N-terminally with EGFP and two positive controls, PLCδ1-PH
1121 and Lactadherin-C2, both fused to superfolder GFP (sfGFP), were applied to microarrays
1122 printed with different signalling lipids. In brief, lipids of interest were combined with the carrier
1123 lipid DOPC, PEGylated PE, and PE labelled with Atto 647 dye (PE-Atto 647, 0.1 mol%). Lipid
1124 mixtures containing 2, 5, and 10 mol% of the signalling lipid were spotted onto a thin agarose
1125 layer (TAL). The agarose layers were hydrated using buffer A (20 mM Tris-HCl pH 8.5, 200
1126 mM NaCl) and vesicles formed spontaneously. Efficiency of liposome formation was verified
1127 by fluorescence microscopy. The protein was diluted to 7 µM in buffer A and 40 µl was
1128 applied to each array. Microarrays were incubated (20 min, RT) and subsequently washed
1129 three times with 40 µl of buffer A. Chips were analysed by automated fluorescence
1130 microscopy. Positions of liposomes were determined by tracking the fluorescence of PE-Atto
1131 647 and images were taken for 3 ms and 5 ms exposure times. In parallel, the fluorescence
1132 of EGFP was determined for 1, 5, 10, 30, 75, 100, 200 and 300 ms exposures. Images were
1133 processed using CellProfiler and CPAnalyst. Only EGFP signals that overlapped with Atto
1134 647 signals were taken into account. Normalised binding intensity (NBI) was calculated as
1135 the ratio between EGFP and Atto 647 fluorescence, normalised by exposure time. Three
1136 microarrays were examined, carrying liposomes with the following signalling lipids; PIP-chip:
1137 DOPA, DOPE, DOPI, DOPS, DODAG, cardiolipin, BMP, DOPI(4,5)P_2, DOPG; GLP-chip:
1138 ceramide C16, ceramide(1)P C16, ceramide(1)P C18, S(1)P, S, SM, DOPI(4,5)P_2, DOPS; SL-
1139 chip: DOPI(3)P, brain PI(4)P, DOPI(5)P, DOPI(3,4)P_2, DOPI(3,5)P_2, brain PI(4,5)P_2,
1140 DOPI(3,4,5)P_3, DOPS and cholesterol. Each microarray was performed in triplicate.

1141
1142 **Cell culture and cell line generation**
1143 Bloodstream form *T. brucei* cells were maintained in HMI-9 media supplemented with 10%
1144 foetal bovine serum (Sigma-Aldrich, St. Louis, USA) at 37 °C and 5% CO_2 in cell culture flasks
1145 with filter lids (Greiner). For overexpression studies, 427 strain "single marker" cells - which
1146 express T7 RNA polymerase and the Tetracycline repressor protein, both maintained under
1147 2.5 µg/ml G418 selection - were used (Wirtz et al., 1999). For optimisation of digitonin
1148 extraction conditions, the GFP^{ESPro}-221^{ES}.121^{tet} cell line, which constitutively expresses GFP
1149 from the VSG expression site, was used (Batram et al., 2014). Constructs for overexpression
1150 of Ty1-tagged TbMORN1 and untagged TbMORN1 were obtained by cloning the required
1151 ORFs into the pLEW100v5-HYG plasmid; the identity of the inserts was verified by DNA
1152 sequencing followed by BLAST analysis against the TbMORN1 ORF (Tb927.6.4670). The
1153 plasmids were linearised by NotI digestion, and plasmid DNA was purified by ethanol
1154 precipitation. Linearisation was verified using agarose gel electrophoresis. Stable cell lines
1155 were generated by using 20 µg of the linearised plasmids to transfect ~$3x10^7$ "single marker"
1156 cells in transfection buffer (90 mM Na_2PO_4, 5 mM KCl, 0.15 mM $CaCl_2$, 50 mM HEPES pH
1157 7.3) using the X-001 program of an Amaxa Nucleofector II (Lonza, Switzerland) (Burkard et
1158 al., 2007, Schumann Burkard et al., 2011). Clones were obtained from the transfected cells
1159 by limiting dilution under 5 µg/ml hygromycin selection. The presence of the transgene in the
1160 genomic DNA of isolated clones was verified by PCR.
1161
1162
1163 **Growth curves and BigEye cell counts**
1164 22 ml cells at a defined starting concentration were divided into two flasks of 10 ml each, and
1165 overexpression of the ectopic transgene was initiated in one flask by the addition of
1166 tetracycline to a final concentration of 1 µg/ml. For overexpression of Ty1-TbMORN1, a
1167 starting concentration of $1x10^4$ cells/ml was used, and the cells were split and reseeded at
1168 this concentration after 48 h. For overexpression of untagged TbMORN1, a starting
1169 concentration of $1x10^3$ cells/ml was used with no reseeding. Tetracycline was refreshed every
1170 24 h in both cases. Population density was measured using a Z2 Coulter Counter (Beckman
1171 Coulter, Krefeld, Germany) at the indicated timepoints. For quantification of BigEye cell
1172 incidence at the indicated timepoints, the cultures were briefly agitated to mix the cells, which
1173 were then allowed to settle for 30 min. The culture flasks were then examined directly using
1174 an inverted phase contrast microscope (Leitz Labovert) and a 10x objective lens. Three fields
1175 of view were chosen at random for each flask and the number of normal and BigEye cells
1176 manually quantified, using higher magnification where necessary. Given the low
1177 magnification used, the numbers presented are likely to be underestimates of the true
1178 incidence.
1179
1180
1181 **Immunoblotting**
1182 To obtain whole cell lysates, cell concentration was measured using a Z2 Coulter Counter,
1183 and a defined volume was then transferred to 15 ml Falcon tubes. The cells were pelleted by
1184 centrifugation (750 x g, 10 min, RT), resuspended in 1 ml PBS, and transferred to microfuge
1185 tubes. The cells were again pelleted (1800 x g, 2 min, RT), and the cell pellet then directly

1186 resuspended in SDS loading buffer to a final concentration of 2 x 10^5 cells/µl. The lysates
1187 were heated (95 °C, 10 min) before use. Lysates were separated by SDS-PAGE (1.4x10^6
1188 cells/lane in a 15-well gel of 1.0 mm thickness), and the proteins then transferred to
1189 nitrocellulose membranes. The membranes were blocked in blocking buffer (10% milk, PBS,
1190 0.3% TWEEN-20) (30 min, RT), and then incubated with the indicated primary antibodies in
1191 blocking buffer (1 h, RT). The membranes were washed three times in PBS-T (PBS, 0.3%
1192 TWEEN-20), and were then incubated with IRDye-conjugated secondary antibodies in PBS-
1193 T (1 h, RT). After a further three washes in PBS-T the membranes were briefly dried between
1194 sheets of filter paper and then imaged using an Odyssey CLx (LI-COR Biosciences, Bad
1195 Homberg, Germany). Processing and quantification was carried out using ImageStudioLite
1196 software (LI-COR Biosciences).
1197
1198
1199 **Immunofluorescence microscopy**
1200 Cell concentration was measured using a Z2 Coulter Counter, and 10^6 cells per coverslip
1201 were taken. The cells were transferred to 15 ml Falcon tubes, and fixed directly in media by
1202 the addition of paraformaldehyde solution to a final concentration of 4% (37 °C, 20 min). 10
1203 ml trypanosome dilution buffer (TDB; 20 mM Na_2HPO_4, 2 mM NaH_2PO_4, 5 mM KCl, 80 mM
1204 NaCl, 1 mM $MgSO_4$, 20 mM glucose) was then added, and the cells were pelleted by
1205 centrifugation (750 x g, 10 min, RT). The supernatant was removed, the cell pellet was
1206 resuspended in 500 µl TDB, and the cells were transferred to poly-L-lysine-coated coverslips
1207 in a 24-well plate. The cells were attached to the coverslips by centrifugation (750 x g, 4 min,
1208 RT), and the cells were permeabilised using a solution of 0.25% TritonX-100 in PBS (5 min,
1209 RT). The cells were washed with PBS, blocked using a solution of 3% BSA in PBS (30 min,
1210 RT), and sequentially incubated with primary and secondary antibodies diluted in PBS (1 h,
1211 RT for each) with three PBS wash steps after each incubation. After the final wash, the
1212 coverslips were rinsed in ddH_2O, excess fluid removed by wicking, and mounted on glass
1213 slides using Fluoromount-DAPI (Southern Biotech). For analysis of detergent-extracted
1214 cytoskeletons, cells were washed using TDB and attached to poly-L-lysine coverslips as
1215 described above. The cells were incubated in extraction buffer (0.5% IGEPAL, 0.1 M PIPES-
1216 NaOH pH 6.9, 2 mM EGTA, 1 mM $MgSO_4$, 0.1 mM EDTA, cOmplete protease inhibitors
1217 [Roche]) (5 min, RT), washed three times with extraction buffer, and then fixed with ice-cold
1218 MeOH (-20 °C, 30 min). Blocking, antibody incubation steps, and mounting were as
1219 described above. All liquid handling was carried out using a P1000 micropipette, and
1220 pipetting was done as gently as possible to minimise shear forces. The coverslips were
1221 imaged using a Leica DMI6000B inverted microscope equipped with a Leica DFC365 camera
1222 and a 100x oil objective lens (NA1.4) and running Leica Application Suite X software. The
1223 same exposure times were used for acquisition of +/-Tet samples, and 40 z-slices of 0.21
1224 µm thickness were taken per field of view. Image processing was carried out using ImageJ.
1225 Maximum intensity z-projections are shown.
1226
1227
1228 **Fractionation**
1229 Cell concentration was measured using a Z2 Coulter Counter, and an equal number of cells
1230 (~2.5x10^7 per experiment) was taken from the control (-Tet) and overexpression (+Tet)

1231 samples and transferred to 50 ml Falcon tubes. The cells were pelleted by centrifugation (750
1232 x g, 10 min, 4 °C), and the cell pellets then resuspended in 1 ml TDB and transferred to
1233 microfuge tubes. The cells were pelleted by centrifugation (1800 x g, 2 min, 4 °C), and then
1234 resuspended in 200 µl extraction buffer (see Immunofluorescence microscopy section for
1235 composition). After a short incubation (15 min, RT, orbital mixer), a 5% (10 µl) input sample
1236 was taken, and the mixtures separated by centrifugation (3400 x g, 2 min, 4 °C) into
1237 detergent-soluble (cytoplasmic) supernatant and detergent-insoluble (cytoskeleton) pellet
1238 fractions. The supernatant was transferred to a fresh microfuge tube, its exact volume noted,
1239 and a 5% sample taken. The tube containing the pellet was centrifuged a second time (3400
1240 x g, 2 min, 4 °C) in order to bring down material sticking to the tube wall; this second
1241 supernatant was discarded. The pellet was resuspended in 200 µl extraction buffer and a 5%
1242 sample (10 µl) taken. SDS loading buffer was added to the input, supernatant, and pellet
1243 samples to a final volume of 20 µl, and denaturation assisted by heating (95 °C, 10 min).
1244 Equal fractions were loaded onto polyacrylamide gels, separated by SDS-PAGE, and
1245 analysed by immunoblotting. In the exemplary blot shown (Fig. 5G), each sample is a 4.5%
1246 fraction, equivalent to ~10^6 cells in the Input fraction. For optimisation of extraction conditions
1247 using digitonin, essentially the same protocol was followed except that ultra-pure digitonin
1248 (Calbiochem) in TDB buffer was used and incubations were carried out at 24 °C in a heating
1249 block. For the two-step digitonin/IGEPAL fractionations (Fig. 8), cells were pelleted by
1250 centrifugation (750 x g, 10 min, RT), resuspended in 1 ml TDB, transferred to microfuge tubes,
1251 and pelleted again (750 x g, 3 min, RT). The cell pellet was resuspended in 400 µl of 40 µg/ml
1252 digitonin in TDB and extracted (25 min, 24 °C), after which a 5% input sample was taken.
1253 The mixture was then separated by centrifugation (750 x g, 5 min, RT) and 320 µl of the
1254 cytosolic fraction (SN1) transferred to a fresh tube and a 5% sample was taken. The cell pellet
1255 was then resuspended with 1 ml TDB and the extracted cells again pelleted by centrifugation
1256 (750 x g, 5 min, RT). The extracted cells were then resuspended in 400 µl extraction buffer
1257 (see Immunofluorescence section above for composition) and incubated (24 °C, 15 min,
1258 heating block with shaker). After the incubation, a 5% sample (P1) was taken, and the
1259 extracted cells pelleted by centrifugation (3400 x g, 2 min, RT). 320 µl of the supernatant
1260 (SN2) was transferred to a fresh microfuge tube and a 5% sample was taken. The pellet was
1261 resuspended in 1 ml TDB and centrifuged again (750 x g, 5 min, RT). The pellet (P2) was then
1262 resuspended in 400 µl extraction buffer. SDS loading buffer was added to the 5% samples
1263 (I, SN1, SN2, P1, P2) to a final volume of 40 µl. Samples were analysed by immunoblotting
1264 as detailed above.
1265
1266
1267 **Crystallisation**
1268 Crystallisation of TbMORN1(7-15) (with a C-terminal Strep tag), TgMORN1(7-15) and
1269 PfMORN1(7-15) (both with affinity tags removed) was performed at 22 °C using a sitting-drop
1270 vapour diffusion technique and micro-dispensing liquid handling robots (Phoenix RE (Art
1271 Robbins Instruments) and Mosquito (TTP labtech)). In the case of TbMORN1(7-15), crystals
1272 only appeared from reductively methylated protein, using a standard protocol (Walter et al.,
1273 2006). The best diffracting crystals of TbMORN1(7-15) were grown at a protein concentration
1274 of 3.5 mg/ml in the following conditions: 0.166 M Tris-HCl pH 8.8, 0.15 M $MgCl_2$, 0.45 M KI,
1275 24% PEG 2000 MME, and 4% glycerol. The tetragonal crystals of TgMORN1(7-15) were

obtained at a protein concentration of 10 mg/ml in the following conditions: 0.1 M Tris-HCl pH 8.2, 15% PEG 3350, 0.2 M NaCl. The diffracting crystals of both selenomethionine-containing crystals and native crystals of PfMORN1(7-15) were obtained at a protein concentration of 8 mg/ml in the conditions "B11" from the Morpheus II crystallisation screen (Molecular Dimensions): 2 mM divalents mix (0.5 mM $MnCl_3$, 0.5 mM $CoCl_2$, 0.5 mM $NiCl_2$, 0.5 mM $Zn(OAc)_2$, 0.1 M Buffer System 6, pH 8.5 (Gly-Gly, AMPD), and 50% precipitation Mix 7 (20 % PEG 8000, 40% 1,5-Pentanediol). The crystals were flash cooled in liquid nitrogen prior to data collection.

X-ray diffraction data collection and crystal structure determination

Initially, the structure of PfMORN1(7-15) was determined using the single-wavelength anomalous diffraction (SAD) method. The selenomethionine dataset was collected at the beamline ID29 (ESRF, Grenoble) at 100K at the peak of selenium using a wavelength of 0.979 Å. The data frames were processed using the XDS package (Kabsch, 2010), and converted to mtz format with the program AIMLESS (Winn et al., 2011). The apo-PfMORN1(7-15) structure was solved using single anomalous diffraction with AUTOSOL software from the PHENIX package. The structures of TgMORN1(7-15) and TbMORN1(7-15) were then solved using the molecular replacement program PHASER (McCoy et al., 2007) with the atomic coordinates of PfMORN1(7-15) as a search model. The structures were then refined with REFMAC and Phenix Refine and rebuilt using Coot (Murshudov et al., 1997, Emsley & Cowtan, 2004, Adams et al., 2010). The structures were validated and corrected using the PDB_REDO server (Joosten et al., 2014). The figures were produced using Pymol (Schrödinger, LLC.) and Chimera software (Pettersen et al., 2004). Coordinates have been deposited in the protein data bank (accession codes 6T4D, 6T4R, 6T68, 6T69, 6T6Q). Data collection and refinement statistics are reported in Table 1.

Small angle X-ray scattering (SAXS)

Synchrotron radiation X-ray scattering from various MORN constructs in solution were collected at different synchrotron facilities (Table S3). TgMORN1(7-15), TbMORN1(7-15) as well as PfMORN1(7-15) were collected at the EMBL P12 beamline of the storage ring PETRA III (DESY, Hamburg, Germany) (Blanchet et al., 2015). Images were recorded using a photon counting Pilatus-2M detector at a sample to detector distance of 3.1 m and a wavelength (λ) of 1.2 Å covering the range of momentum transfer $0.01 < s < 0.5$ Å^{-1}; with $s = 4\pi\sin\theta/\lambda$, where 2θ is the scattering angle. To obtain data from a monodisperse sample from TgMORN1(7-15) and TbMORN1(7-15), a size exclusion chromatography column directly coupled to the scattering experiment (SEC-SAXS) was employed. The parallel collection of UV and light scattering data allowed the protein to be monitored while it eluted from the column (Graewert et al., 2015). Throughout the complete chromatography process, 1 s sample exposures were recorded. As mobile phase, the various buffers were used; TbMORN1(7-15): 20mM Tris-HCl pH 8.5, 200 mM NaCl, 2% (v/v) glycerol, 1 mM DTT; TgMORN1(7-15): 20 mM Tris-HCl pH 7.5, 100 mM NaCl. 100 µl of purified sample (3.8 mg/mL TbMORN1(7-15) and 2.6 mg/ml TgMORN1(7-15)) were injected onto a Superdex 200 10/300 (GE Healthcare) column and the flow rate was set to 0.5 ml/min. SAXS data were recorded from macromolecular free fractions

corresponding to the matched solvent blank. PfMORN1(7-15) was measured in batch mode from a concentration series spanning 1-8 mg/ml. 20 mM Tris-HCl pH 7.5, 100 mM NaCl buffer was measured for background subtraction. As a concentration dependent increase in size was detectable further analysis were based solely on the data collected at 1 mg/ml. In a similar manner as described above, TbMORN1(2-15) data were collected at ESRF BM29 beamline (Pernot et al., 2013) in SEC-SAXS mode with the setup described in by Brennich et al. (Brennich et al., 2017). SAXS data from the run were collected at a wavelength of 0.99Å using a sample-to-detector (PILATUS 1 M, DECTRIS) distance of 2.867m. Here too, a Superdex 200 10/300 (GE Healthcare) column was used as well as 20mM Tris-HCl pH 8.5, 200 mM NaCl, 2% (v/v) glycerol, 1 mM DTT as mobile phase. 100 µl of 5.8 mg/ml TbMORN1(2-15) were injected. Data reduction to produce final scattering profiles of dimeric MORN1 constructs were performed using standard methods. Briefly, 2D-to-1D radial averaging was performed using the SASFLOW pipeline (Franke et al., 2017). For data collected at ESRF EDNA pipeline (Brennich et al., 2016) was used. CHROMIXS was used for the visualisation and reduction of the SEC-SAXS datasets (Panjkovich & Svergun, 2018). Aided by the integrated prediction algorithms in CHROMIXS the optimal frames within the elution peak and the buffer regions were selected. Single buffer frames were then subtracted from sample frames one by one, scaled and averaged to produce the final subtracted curve. The indirect inverse Fourier transform of the SAXS data and the corresponding probable real space-scattering pair distance distribution (p(r) versus r profile) of the various MORN1 constructs were calculated using GNOM (Svergun, 1992), from which the R_g and D_{max} were determined. The p(r) versus r profile were also used for *ab initio* bead modelling of selected MORN1 constructs. For this, 20 independent runs of DAMMIF (Franke & Svergun, 2009) in the case of TbMORN1(2-15) and DAMMIN (Svergun, 1999) in case of the shorter MORN1(7-15) constructs were performed. From these the most probable models were selected by DAMAVER (Volkov & Svergun, 2003). The ab initio modelling was performed with and without symmetry constraints (p2 symmetry to reflect the dimeric state of the protein). Comparison with theoretical curves calculated from the X-tal structures described here was performed with Crysol (Svergun et al., 1995). Due to the elongated nature of the molecules, fits were improved by increasing LM (maximum order of harmonics) to 50. The molecular mass (MM) was evaluated based on concentration independent methods according to Porod (Porod, 1951) and as implemented in the ATSAS package. Dimensionless Kratky plots were constructed according to (Receveur-Brechot & Durand, 2012) and the reference point for globular proteins at √3, 1.1 indicated. Graphical representation was produced using Pymol Molecular Graphics System (Schrödinger, LLC.). The SAXS data (Table S3) and ab initio bead models as well as fits to the crystal structures described within this work have been deposited into the Small-Angle Scattering Biological Data Bank (SASBDB) (Valentini et al., 2015) under the accession codes SASDG97, SASDGA7, SASDGB7, SASDGC7.

Transmission electron microscopy (EM) with rotary shadowing

TbMORN1 and TbMORN1(2-15) were purified according to the two-step procedure detailed above. They were then diluted in spraying buffer (100 mM $NH_4CH_3CO_2$-NaOH pH 8.5, 30% (v/v) glycerol) to a final concentration of 50 – 100 µg/ml. Diluted samples were sprayed onto freshly cleaved mica chips (Christine Gröpl) and immediately transferred into a MED020 high

vacuum evaporator (BAL-TEC) equipped with electron guns. While rotating, samples were coated with 0.6 nm of Platinum (BALTIC) at an angle of 4°, followed by 6 nm of Carbon (Oerlicon) at 90°. The obtained replicas were floated off the mica chips, transferred to 400 mesh Cu/Pd grids (Agar Scientific), and examined using a Morgagni 268D transmission electron microscope (FEI) operated at 80 kV. Images were acquired using an 11 megapixel Morada CCD camera (Olympus-SIS).

ACKNOWLEDGEMENTS

Financial support was from Austrian Science Fund (FWF) grants P22265-B12 FWF (to Graham Warren) P27016-B21 (to Brooke Morriswood and Kristina Djinovic-Carugo), P28135 and P30584 (both to Tom Leonard). Kristina Djinovic-Carugo's research was additionally supported by Austrian Science Fund (FWF) Projects I525 and I1593, P22276, P19060 and W1221, Federal Ministry of Economy, Family and Youth through the initiative “Laura Bassi Centres of Expertise”, funding the Centre of Optimized Structural Studies, N°253275, by the Wellcome Trust Collaborative Award (201543/Z/16), COST action BM1405 - Non-globular proteins - from sequence to structure, function and application in molecular physiopathology (NGP-NET), WWTF (Vienna Science and Technology Fund) Chemical Biology project LS17-008, and by the University of Vienna. Anne-Claude Gavin acknowledges the financial support of the Louis-Jeantet Foundation. Funding also came from Medical Research Council grant MR/Mo20118/1 (to Terry Smith). We are indebted to Graham Warren (MRC Laboratory for Molecular Cell Biology, University College London), for comments and support. We are grateful to Sonja Lorenz (University of Würzburg) for critical reading of the manuscript. Valeria Stefania carried out the SAXS measurements. The Martens group at the Max Perutz Labs Vienna provided the Doc2B protein; Iva Lucic in the Leonard group supplied the Akt protein. Euripedes Almeida Ribeiro advised on fluorescence anisotropy measurements. Markus Engstler (University of Würzburg) provided the bloodstream form GFP cells as well as lab space and support. Susanne Fenz (University of Würzburg) assisted with the purification of trypanosome lipids. The authors thank the staff of MX and SAXS beamlines at ESRF in Grenoble and EMBL-Hamburg for their excellent support. EM data were recorded at the EM Facility of the Vienna BioCenter Core Facilities GmbH (VBCF), a member of the Vienna BioCenter (VBC), Austria. Proteomics analyses were performed by the Mass Spectrometry Facility at Max Perutz Labs Vienna using the VBCF instrument pool.

References

Adam SA, Marr RS, Gerace L (1990) Nuclear protein import in permeabilized mammalian cells requires soluble cytoplasmic factors. *J Cell Biol* 111: 807-16

Adams PD, Afonine PV, Bunkoczi G, Chen VB, Davis IW, Echols N, Headd JJ, Hung LW, Kapral GJ, Grosse-Kunstleve RW, McCoy AJ, Moriarty NW, Oeffner R, Read RJ, Richardson DC, Richardson JS, Terwilliger TC, Zwart PH (2010) PHENIX: a comprehensive

1409 Python-based system for macromolecular structure solution. *Acta Crystallogr D Biol*
1410 *Crystallogr* 66: 213-21

1411 Adl SM, Bass D, Lane CE, Lukes J, Schoch CL, Smirnov A, Agatha S, Berney C, Brown
1412 MW, Burki F, Cardenas P, Cepicka I, Chistyakova L, Del Campo J, Dunthorn M, Edvardsen
1413 B, Eglit Y, Guillou L, Hampl V, Heiss AA et al. (2019) Revisions to the Classification,
1414 Nomenclature, and Diversity of Eukaryotes. *J Eukaryot Microbiol* 66: 4-119

1415 Allen CL, Goulding D, Field MC (2003) Clathrin-mediated endocytosis is essential in
1416 Trypanosoma brucei. *Embo J* 22: 4991-5002

1417 Andrade MA, Perez-Iratxeta C, Ponting CP (2001) Protein repeats: structures, functions,
1418 and evolution. *J Struct Biol* 134: 117-31

1419 Bangs JD, Uyetake L, Brickman MJ, Balber AE, Boothroyd JC (1993) Molecular cloning and
1420 cellular localization of a BiP homologue in Trypanosoma brucei. Divergent ER retention
1421 signals in a lower eukaryote. *J Cell Sci* 105 (Pt 4): 1101-13

1422 Bastin P, Bagherzadeh Z, Matthews KR, Gull K (1996) A novel epitope tag system to study
1423 protein targeting and organelle biogenesis in Trypanosoma brucei. *Mol Biochem Parasitol*
1424 77: 235-9

1425 Batram C, Jones NG, Janzen CJ, Markert SM, Engstler M (2014) Expression site
1426 attenuation mechanistically links antigenic variation and development in Trypanosoma
1427 brucei. *Elife* 3: e02324

1428 Bennett HJ, Davenport JB, Collins RF, Trafford AW, Pinali C, Kitmitto A (2013) Human
1429 junctophilin-2 undergoes a structural rearrangement upon binding PtdIns(3,4,5)P3 and the
1430 S101R mutation identified in hypertrophic cardiomyopathy obviates this response. *Biochem*
1431 *J* 456: 205-17

1432 Blanchet CE, Spilotros A, Schwemmer F, Graewert MA, Kikhney A, Jeffries CM, Franke D,
1433 Mark D, Zengerle R, Cipriani F, Fiedler S, Roessle M, Svergun DI (2015) Versatile sample
1434 environments and automation for biological solution X-ray scattering experiments at the
1435 P12 beamline (PETRA III, DESY). *J Appl Crystallogr* 48: 431-443

1436 Bligh EG, Dyer WJ (1959) A rapid method of total lipid extraction and purification. *Can J*
1437 *Biochem Physiol* 37: 911-7

1438 Brennich ME, Kieffer J, Bonamis G, Antolinos AD, Hutin S, Pernot P, Round A (2016) Online
1439 data analysis at the ESRF bioSAXS beamline, BM29. *Journal of Applied Crystallography* 49:
1440 203-212

1441 Brennich ME, Round AR, Hutin S (2017) Online Size-exclusion and Ion-exchange
1442 Chromatography on a SAXS Beamline. *J Vis Exp*

1443 Burkard G, Fragoso CM, Roditi I (2007) Highly efficient stable transformation of
1444 bloodstream forms of Trypanosoma brucei. *Mol Biochem Parasitol* 153: 220-3

1445 Camacho L, Smertenko AP, Perez-Gomez J, Hussey PJ, Moore I (2009) Arabidopsis Rab-E
1446 GTPases exhibit a novel interaction with a plasma-membrane phosphatidylinositol-4-
1447 phosphate 5-kinase. *J Cell Sci* 122: 4383-92

1448 Carman PJ, Dominguez R (2018) BAR domain proteins-a linkage between cellular
1449 membranes, signaling pathways, and the actin cytoskeleton. *Biophys Rev* 10: 1587-1604

1450 Chung J, Torta F, Masai K, Lucast L, Czapla H, Tanner LB, Narayanaswamy P, Wenk MR,
1451 Nakatsu F, De Camilli P (2015) INTRACELLULAR TRANSPORT. PI4P/phosphatidylserine
1452 countertransport at ORP5- and ORP8-mediated ER-plasma membrane contacts. *Science*
1453 349: 428-32

1454 Cronan JE (2003) Bacterial membrane lipids: where do we stand? *Annu Rev Microbiol* 57:
1455 203-24

1456 Doyle SA (2005) High-throughput cloning for proteomics research. *Methods Mol Biol* 310:
1457 107-13

1458 El-Gebali S, Mistry J, Bateman A, Eddy SR, Luciani A, Potter SC, Qureshi M, Richardson
1459 LJ, Salazar GA, Smart A, Sonnhammer ELL, Hirsh L, Paladin L, Piovesan D, Tosatto SCE,
1460 Finn RD (2019) The Pfam protein families database in 2019. *Nucleic Acids Res* 47: D427-
1461 D432

1462 Emsley P, Cowtan K (2004) Coot: model-building tools for molecular graphics. *Acta*
1463 *Crystallogr D Biol Crystallogr* 60: 2126-32

1464 Engstler M, Thilo L, Weise F, Grunfelder CG, Schwarz H, Boshart M, Overath P (2004)
1465 Kinetics of endocytosis and recycling of the GPI-anchored variant surface glycoprotein in
1466 Trypanosoma brucei. *Journal of cell science* 117: 1105-15

1467 Epand RM, Epand RF (2009) Lipid domains in bacterial membranes and the action of
1468 antimicrobial agents. *Biochim Biophys Acta* 1788: 289-94

1469 Esson HJ, Morriswood B, Yavuz S, Vidilaseris K, Dong G, Warren G (2012) Morphology of
1470 the trypanosome bilobe, a novel cytoskeletal structure. *Eukaryot Cell* 11: 761-72

1471 Franke D, Svergun DI (2009) DAMMIF, a program for rapid ab-initio shape determination in
1472 small-angle scattering. *J Appl Crystallogr* 42: 342-346

1473 Fyffe SA, Alphey MS, Buetow L, Smith TK, Ferguson MA, Sorensen MD, Bjorkling F, Hunter
1474 WN (2006) Reevaluation of the PPAR-beta/delta ligand binding domain model reveals why it
1475 exhibits the activated form. *Mol Cell* 21: 1-2

1476 Gibson DG, Young L, Chuang RY, Venter JC, Hutchison CA, 3rd, Smith HO (2009)
1477 Enzymatic assembly of DNA molecules up to several hundred kilobases. *Nat Methods* 6:
1478 343-5

1479 Graewert MA, Franke D, Jeffries CM, Blanchet CE, Ruskule D, Kuhle K, Flieger A, Schafer
1480 B, Tartsch B, Meijers R, Svergun DI (2015) Automated pipeline for purification, biophysical
1481 and x-ray analysis of biomacromolecular solutions. *Sci Rep* 5: 10734

1482 Grunfelder CG, Engstler M, Weise F, Schwarz H, Stierhof YD, Morgan GW, Field MC,
1483 Overath P (2003) Endocytosis of a glycosylphosphatidylinositol-anchored protein via
1484 clathrin-coated vesicles, sorting by default in endosomes, and exocytosis via RAB11-
1485 positive carriers. *Mol Biol Cell* 14: 2029-40

1486 Gubbels MJ, Vaishnava S, Boot N, Dubremetz JF, Striepen B (2006) A MORN-repeat
1487 protein is a dynamic component of the Toxoplasma gondii cell division apparatus. *J Cell Sci*
1488 119: 2236-45

1489 Guo A, Wang Y, Chen B, Wang Y, Yuan J, Zhang L, Hall D, Wu J, Shi Y, Zhu Q, Chen C,
1490 Thiel WH, Zhan X, Weiss RM, Zhan F, Musselman CA, Pufall M, Zhu W, Au KF, Hong J et al.
1491 (2018) E-C coupling structural protein junctophilin-2 encodes a stress-adaptive
1492 transcription regulator. *Science* 362

1493 Habicht J, Woehle C, Gould SB (2015) Tetrahymena Expresses More than a Hundred
1494 Proteins with Lipid-binding MORN Motifs that can Differ in their Subcellular Localisations. *J*
1495 *Eukaryot Microbiol* 62: 694-700

1496 Hatzopoulos GN, Erat MC, Cutts E, Rogala KB, Slater LM, Stansfeld PJ, Vakonakis I (2013)
1497 Structural analysis of the G-box domain of the microcephaly protein CPAP suggests a role
1498 in centriole architecture. *Structure* 21: 2069-77

1499 Hemsley A, Arnheim N, Toney MD, Cortopassi G, Galas DJ (1989) A simple method for site-
1500 directed mutagenesis using the polymerase chain reaction. *Nucleic Acids Res* 17: 6545-51

1501 Holm L, Laakso LM (2016) Dali server update. *Nucleic Acids Res* 44: W351-5

1502 Holm L, Rosenstrom P (2010) Dali server: conservation mapping in 3D. *Nucleic Acids Res*
1503 38: W545-9

1504 Hu K (2008) Organizational changes of the daughter basal complex during the parasite
1505 replication of Toxoplasma gondii. *PLoS Pathog* 4: e10

1506 Hu K, Johnson J, Florens L, Fraunholz M, Suravajjala S, DiLullo C, Yates J, Roos DS,
1507 Murray JM (2006) Cytoskeletal components of an invasion machine--the apical complex of
1508 Toxoplasma gondii. *PLoS Pathog* 2: e13

1509 Hutchinson EG, Thornton JM (1994) A revised set of potentials for beta-turn formation in
1510 proteins. *Protein Sci* 3: 2207-16

1511 Im YJ, Davis AJ, Perera IY, Johannes E, Allen NS, Boss WF (2007) The N-terminal
1512 membrane occupation and recognition nexus domain of Arabidopsis phosphatidylinositol
1513 phosphate kinase 1 regulates enzyme activity. *J Biol Chem* 282: 5443-52

1514 Jacobs SA, Harp JM, Devarakonda S, Kim Y, Rastinejad F, Khorasanizadeh S (2002) The
1515 active site of the SET domain is constructed on a knot. *Nat Struct Biol* 9: 833-8

1516 Jayasinghe I, Clowsley AH, Lin R, Lutz T, Harrison C, Green E, Baddeley D, Di Michele L,
1517 Soeller C (2018) True Molecular Scale Visualization of Variable Clustering Properties of
1518 Ryanodine Receptors. *Cell Rep* 22: 557-567

1519 Jiang M, Hu J, White FKH, Williamson J, Klymchenko AS, Murthy A, Workman SW, Tseng
1520 GN (2019) S-Palmitoylation of junctophilin-2 is critical for its role in tethering the
1521 sarcoplasmic reticulum to the plasma membrane. *J Biol Chem* 294: 13487-13501

1522 Joosten RP, Long F, Murshudov GN, Perrakis A (2014) The PDB_REDO server for
1523 macromolecular structure model optimization. *IUCrJ* 1: 213-20

1524 Kabsch W (2010) Xds. *Acta Crystallogr D Biol Crystallogr* 66: 125-32

1525 Kajava AV (2012) Tandem repeats in proteins: from sequence to structure. *J Struct Biol*
1526 179: 279-88

1527 Kelly SM, Jess TJ, Price NC (2005) How to study proteins by circular dichroism. *Biochim*
1528 *Biophys Acta* 1751: 119-39

1529 Kohl L, Sherwin T, Gull K (1999) Assembly of the paraflagellar rod and the flagellum
1530 attachment zone complex during the Trypanosoma brucei cell cycle. *J Eukaryot Microbiol*
1531 46: 105-9

1532 Krissinel E, Henrick K (2007) Inference of macromolecular assemblies from crystalline state.
1533 *J Mol Biol* 372: 774-97

1534 Kunita R, Otomo A, Mizumura H, Suzuki K, Showguchi-Miyata J, Yanagisawa Y, Hadano S,
1535 Ikeda JE (2004) Homo-oligomerization of ALS2 through its unique carboxyl-terminal regions
1536 is essential for the ALS2-associated Rab5 guanine nucleotide exchange activity and its
1537 regulatory function on endosome trafficking. *J Biol Chem* 279: 38626-35

1538 Lacomble S, Vaughan S, Gadelha C, Morphew MK, Shaw MK, McIntosh JR, Gull K (2009)
1539 Three-dimensional cellular architecture of the flagellar pocket and associated cytoskeleton
1540 in trypanosomes revealed by electron microscope tomography. *Journal of cell science* 122:
1541 1081-90

1542 Li J, Liu H, Raval MH, Wan J, Yengo CM, Liu W, Zhang M (2019) Structure of the
1543 MORN4/Myo3a Tail Complex Reveals MORN Repeats as Protein Binding Modules.
1544 *Structure*

1545 Li MZ, Elledge SJ (2012) SLIC: a method for sequence- and ligation-independent cloning.
1546 *Methods Mol Biol* 852: 51-9

1547 Ma H, Lou Y, Lin WH, Xue HW (2006) MORN motifs in plant PIPKs are involved in the
1548 regulation of subcellular localization and phospholipid binding. *Cell Res* 16: 466-78

1549 Maeda K, Anand K, Chiapparino A, Kumar A, Poletto M, Kaksonen M, Gavin AC (2013)
1550 Interactome map uncovers phosphatidylserine transport by oxysterol-binding proteins.
1551 *Nature* 501: 257-61

1552 Marvin RG, Wolford JL, Kidd MJ, Murphy S, Ward J, Que EL, Mayer ML, Penner-Hahn JE,
1553 Haldar K, O'Halloran TV (2012) Fluxes in "free" and total zinc are essential for progression
1554 of intraerythrocytic stages of Plasmodium falciparum. *Chem Biol* 19: 731-41

1555 McCoy AJ, Grosse-Kunstleve RW, Adams PD, Winn MD, Storoni LC, Read RJ (2007)
1556 Phaser crystallographic software. *J Appl Crystallogr* 40: 658-674

1557 Mecklenburg KL (2007) Drosophila retinophilin contains MORN repeats and is conserved in
1558 humans. *Mol Genet Genomics* 277: 481-9

1559 Micsonai A, Wien F, Bulyaki E, Kun J, Moussong E, Lee YH, Goto Y, Refregiers M, Kardos J
1560 (2018) BeStSel: a web server for accurate protein secondary structure prediction and fold
1561 recognition from the circular dichroism spectra. *Nucleic Acids Res* 46: W315-W322

1562 Micsonai A, Wien F, Kernya L, Lee YH, Goto Y, Refregiers M, Kardos J (2015) Accurate
1563 secondary structure prediction and fold recognition for circular dichroism spectroscopy.
1564 *Proc Natl Acad Sci U S A* 112: E3095-103

1565 Mikami K, Saavedra L, Sommarin M (2010) Is membrane occupation and recognition nexus
1566 domain functional in plant phosphatidylinositol phosphate kinases? *Plant Signal Behav* 5:
1567 1241-4

1568 Molla-Herman A, Ghossoub R, Blisnick T, Meunier A, Serres C, Silbermann F, Emmerson C,
1569 Romeo K, Bourdoncle P, Schmitt A, Saunier S, Spassky N, Bastin P, Benmerah A (2010)
1570 The ciliary pocket: an endocytic membrane domain at the base of primary and motile cilia. *J*
1571 *Cell Sci* 123: 1785-95

1572 Morriswood B, Havlicek K, Demmel L, Yavuz S, Sealey-Cardona M, Vidilaseris K, Anrather
1573 D, Kostan J, Djinovic-Carugo K, Roux KJ, Warren G (2013) Novel Bilobe Components in
1574 Trypanosoma brucei Identified Using Proximity-Dependent Biotinylation. *Eukaryot Cell* 12:
1575 356-67

1576 Morriswood B, He CY, Sealey-Cardona M, Yelinek J, Pypaert M, Warren G (2009) The
1577 bilobe structure of Trypanosoma brucei contains a MORN-repeat protein. *Mol Biochem*
1578 *Parasitol* 167: 95-103

1579 Morriswood B, Schmidt K (2015) A MORN-repeat protein facilitates protein entry into the
1580 flagellar pocket of Trypanosoma brucei. *Eukaryot Cell*

1581 Moser von Filseck J, Copic A, Delfosse V, Vanni S, Jackson CL, Bourguet W, Drin G (2015)
1582 INTRACELLULAR TRANSPORT. Phosphatidylserine transport by ORP/Osh proteins is
1583 driven by phosphatidylinositol 4-phosphate. *Science* 349: 432-6

1584 Munro ML, Jayasinghe ID, Wang Q, Quick A, Wang W, Baddeley D, Wehrens XH, Soeller C
1585 (2016) Junctophilin-2 in the nanoscale organisation and functional signalling of ryanodine
1586 receptor clusters in cardiomyocytes. *J Cell Sci* 129: 4388-4398

1587 Murshudov GN, Vagin AA, Dodson EJ (1997) Refinement of macromolecular structures by
1588 the maximum-likelihood method. *Acta Crystallogr D Biol Crystallogr* 53: 240-55

1589 Nakada T, Kashihara T, Komatsu M, Kojima K, Takeshita T, Yamada M (2018) Physical
1590 interaction of junctophilin and the CaV1.1 C terminus is crucial for skeletal muscle
1591 contraction. *Proc Natl Acad Sci U S A* 115: 4507-4512

1592 Otomo A, Hadano S, Okada T, Mizumura H, Kunita R, Nishijima H, Showguchi-Miyata J,
1593 Yanagisawa Y, Kohiki E, Suga E, Yasuda M, Osuga H, Nishimoto T, Narumiya S, Ikeda JE
1594 (2003) ALS2, a novel guanine nucleotide exchange factor for the small GTPase Rab5, is
1595 implicated in endosomal dynamics. *Hum Mol Genet* 12: 1671-87

1596 Panjkovich A, Svergun DI (2018) CHROMIXS: automatic and interactive analysis of
1597 chromatography-coupled small-angle X-ray scattering data. *Bioinformatics* 34: 1944-1946

1598 Pelletier L, Stern CA, Pypaert M, Sheff D, Ngo HM, Roper N, He CY, Hu K, Toomre D,
1599 Coppens I, Roos DS, Joiner KA, Warren G (2002) Golgi biogenesis in Toxoplasma gondii.
1600 *Nature* 418: 548-52

1601 Perni S, Lavorato M, Beam KG (2017) De novo reconstitution reveals the proteins required
1602 for skeletal muscle voltage-induced Ca(2+) release. *Proc Natl Acad Sci U S A* 114: 13822-
1603 13827

1604 Pernot P, Round A, Barrett R, De Maria Antolinos A, Gobbo A, Gordon E, Huet J, Kieffer J,
1605 Lentini M, Mattenet M, Morawe C, Mueller-Dieckmann C, Ohlsson S, Schmid W, Surr J,
1606 Theveneau P, Zerrad L, McSweeney S (2013) Upgraded ESRF BM29 beamline for SAXS on
1607 macromolecules in solution. *J Synchrotron Radiat* 20: 660-4

1608 Pettersen EF, Goddard TD, Huang CC, Couch GS, Greenblatt DM, Meng EC, Ferrin TE
1609 (2004) UCSF Chimera--a visualization system for exploratory research and analysis. *J*
1610 *Comput Chem* 25: 1605-12

1611 Porod G (1951) Die Rontgenkleinwinkelstreuung Von Dichtgepackten Kolloiden Systemen
1612 .1. *Kolloid Z Z Polym* 124: 83-114

1613 Pramanik J, Keasling JD (1997) Stoichiometric model of Escherichia coli metabolism:
1614 incorporation of growth-rate dependent biomass composition and mechanistic energy
1615 requirements. *Biotechnol Bioeng* 56: 398-421

1616 Rao VD, Misra S, Boronenkov IV, Anderson RA, Hurley JH (1998) Structure of type IIbeta
1617 phosphatidylinositol phosphate kinase: a protein kinase fold flattened for interfacial
1618 phosphorylation. *Cell* 94: 829-39

1619 Rappsilber J, Mann M, Ishihama Y (2007) Protocol for micro-purification, enrichment, pre-
1620 fractionation and storage of peptides for proteomics using StageTips. *Nat Protoc* 2: 1896-
1621 906

1622 Receveur-Brechot V, Durand D (2012) How random are intrinsically disordered proteins? A
1623 small angle scattering perspective. *Curr Protein Pept Sci* 13: 55-75

1624 Richmond GS, Gibellini F, Young SA, Major L, Denton H, Lilley A, Smith TK (2010)
1625 Lipidomic analysis of bloodstream and procyclic form Trypanosoma brucei. *Parasitology*
1626 137: 1357-92

1627 Rossi D, Scarcella AM, Liguori E, Lorenzini S, Pierantozzi E, Kutchukian C, Jacquemond V,
1628 Messa M, De Camilli P, Sorrentino V (2019) Molecular determinants of homo- and
1629 heteromeric interactions of Junctophilin-1 at triads in adult skeletal muscle fibers. *Proc Natl*
1630 *Acad Sci U S A* 116: 15716-15724

1631 Saliba AE, Vonkova I, Ceschia S, Findlay GM, Maeda K, Tischer C, Deghou S, van Noort V,
1632 Bork P, Pawson T, Ellenberg J, Gavin AC (2014) A quantitative liposome microarray to
1633 systematically characterize protein-lipid interactions. *Nat Methods* 11: 47-50

1634 Saliba AE, Vonkova I, Deghou S, Ceschia S, Tischer C, Kugler KG, Bork P, Ellenberg J,
1635 Gavin AC (2016) A protocol for the systematic and quantitative measurement of protein-
1636 lipid interactions using the liposome-microarray-based assay. *Nat Protoc* 11: 1021-38

1637 Salzer U, Kostan J, Djinovic-Carugo K (2017) Deciphering the BAR code of membrane
1638 modulators. *Cell Mol Life Sci* 74: 2413-2438

1639 Scholz J, Besir H, Strasser C, Suppmann S (2013) A new method to customize protein
1640 expression vectors for fast, efficient and background free parallel cloning. *BMC Biotechnol*
1641 13: 12

1642 Schumann Burkard G, Jutzi P, Roditi I (2011) Genome-wide RNAi screens in bloodstream
1643 form trypanosomes identify drug transporters. *Mol Biochem Parasitol* 175: 91-4

1644 Studier FW (2005) Protein production by auto-induction in high density shaking cultures.
1645 *Protein Expr Purif* 41: 207-34

1646 Svergun D, Barberato C, Koch MHJ (1995) CRYSOL - A program to evaluate x-ray solution
1647 scattering of biological macromolecules from atomic coordinates. *Journal of Applied*
1648 *Crystallography* 28: 768-773

1649 Svergun DI (1992) Determination of the Regularization Parameter in Indirect-Transform
1650 Methods Using Perceptual Criteria. *Journal of Applied Crystallography* 25: 495-503

1651 Svergun DI (1999) Restoring low resolution structure of biological macromolecules from
1652 solution scattering using simulated annealing. *Biophys J* 76: 2879-86

1653 Szklarczyk R, Heringa J (2004) Tracking repeats using significance and transitivity.
1654 *Bioinformatics* 20 Suppl 1: i311-7

1655 Takeshima H, Komazaki S, Nishi M, Iino M, Kangawa K (2000) Junctophilins: a novel family
1656 of junctional membrane complex proteins. *Mol Cell* 6: 11-22

1657 Tsuchida J, Nishina Y, Wakabayashi N, Nozaki M, Sakai Y, Nishimune Y (1998) Molecular
1658 cloning and characterization of meichroacidin (male meiotic metaphase chromosome-
1659 associated acidic protein). *Dev Biol* 197: 67-76

1660 Tyanova S, Temu T, Cox J (2016) The MaxQuant computational platform for mass
1661 spectrometry-based shotgun proteomics. *Nat Protoc* 11: 2301-2319

1662 Valentini E, Kikhney AG, Previtali G, Jeffries CM, Svergun DI (2015) SASBDB, a repository
1663 for biological small-angle scattering data. *Nucleic Acids Res* 43: D357-63

1664 Volkov VV, Svergun DI (2003) Uniqueness of ab initio shape determination in small-angle
1665 scattering. *Journal of Applied Crystallography* 36: 860-864

1666 Wilson JR, Jing C, Walker PA, Martin SR, Howell SA, Blackburn GM, Gamblin SJ, Xiao B
1667 (2002) Crystal structure and functional analysis of the histone methyltransferase SET7/9.
1668 *Cell* 111: 105-15

1669 Winn MD, Ballard CC, Cowtan KD, Dodson EJ, Emsley P, Evans PR, Keegan RM, Krissinel
1670 EB, Leslie AG, McCoy A, McNicholas SJ, Murshudov GN, Pannu NS, Potterton EA, Powell
1671 HR, Read RJ, Vagin A, Wilson KS (2011) Overview of the CCP4 suite and current
1672 developments. *Acta Crystallogr D Biol Crystallogr* 67: 235-42

1673 Wirtz E, Leal S, Ochatt C, Cross GA (1999) A tightly regulated inducible expression system
1674 for conditional gene knock-outs and dominant-negative genetics in Trypanosoma brucei.
1675 *Mol Biochem Parasitol* 99: 89-101

1676 Woo JS, Srikanth S, Nishi M, Ping P, Takeshima H, Gwack Y (2016) Junctophilin-4, a
1677 component of the endoplasmic reticulum-plasma membrane junctions, regulates Ca2+
1678 dynamics in T cells. *Proc Natl Acad Sci U S A* 113: 2762-7

1679 Xiao B, Jing C, Wilson JR, Walker PA, Vasisht N, Kelly G, Howell S, Taylor IA, Blackburn
1680 GM, Gamblin SJ (2003) Structure and catalytic mechanism of the human histone
1681 methyltransferase SET7/9. *Nature* 421: 652-6

1682 Yuan ZF, Liu C, Wang HP, Sun RX, Fu Y, Zhang JF, Wang LH, Chi H, Li Y, Xiu LY, Wang
1683 WP, He SM (2012) pParse: a method for accurate determination of monoisotopic peaks in
1684 high-resolution mass spectra. *Proteomics* 12: 226-35

1685 Zens B, Sawa-Makarska J, Martens S (2015) In vitro systems for Atg8 lipidation. *Methods*
1686 75: 37-43
1687

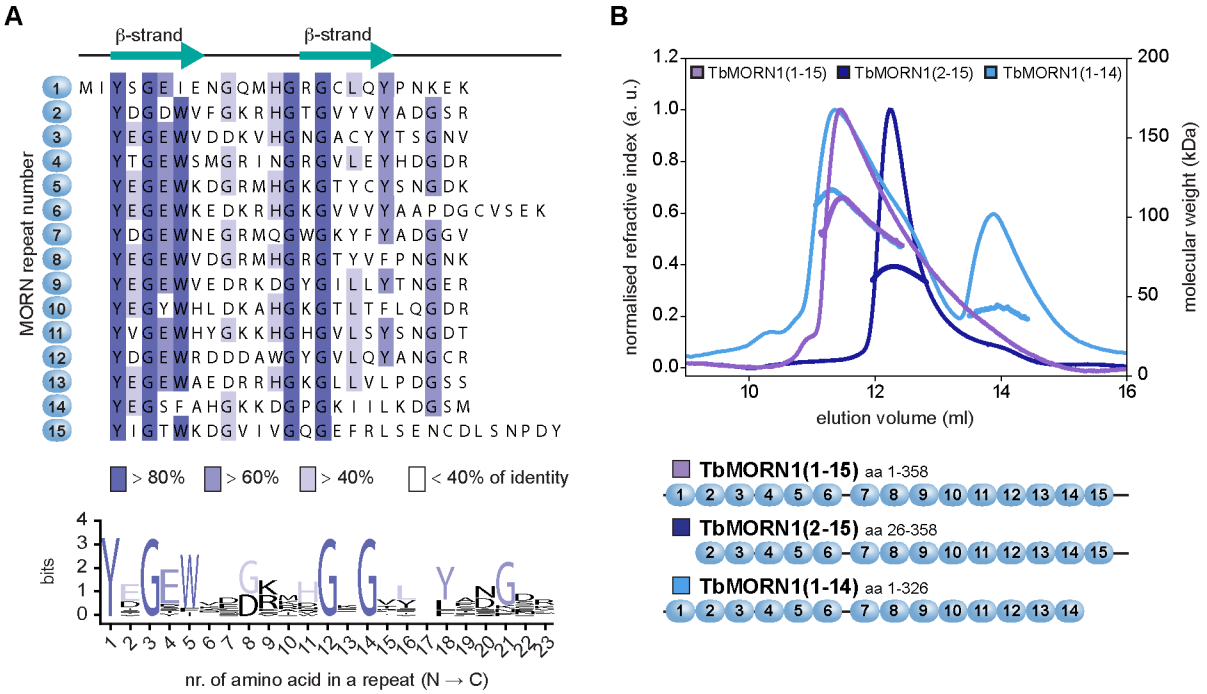

Figure 1. TbMORN1 primary structure and dimerisation. (A) Primary structure of TbMORN1, with individual MORN repeats shown in alignment, and coloured according to amino acid conservation. A schematic of the predicted secondary structure of each repeat is shown above the alignment. A consensus amino acid sequence of the individual MORN repeats from TbMORN1 based on the alignment is shown in the sequence logo below. **(B)** TbMORN1 dimerises via its C-terminus. SEC-MALS profiles of TbMORN1(1-15), TbMORN1(2-15), and TbMORN1(1-14). Schematics are shown underneath. TbMORN1(1-15) tended to form high-order assemblies, whereas removal of the first MORN repeat resulted in a monodisperse dimer. Removal of the last MORN repeat in TbMORN1(1-14) resulted in a polydisperse mixture of monomers, dimers, and other species. Chromatographic separation was done using a Superdex 200 Increase 10/300 GL column, void volume 7.2 ml.

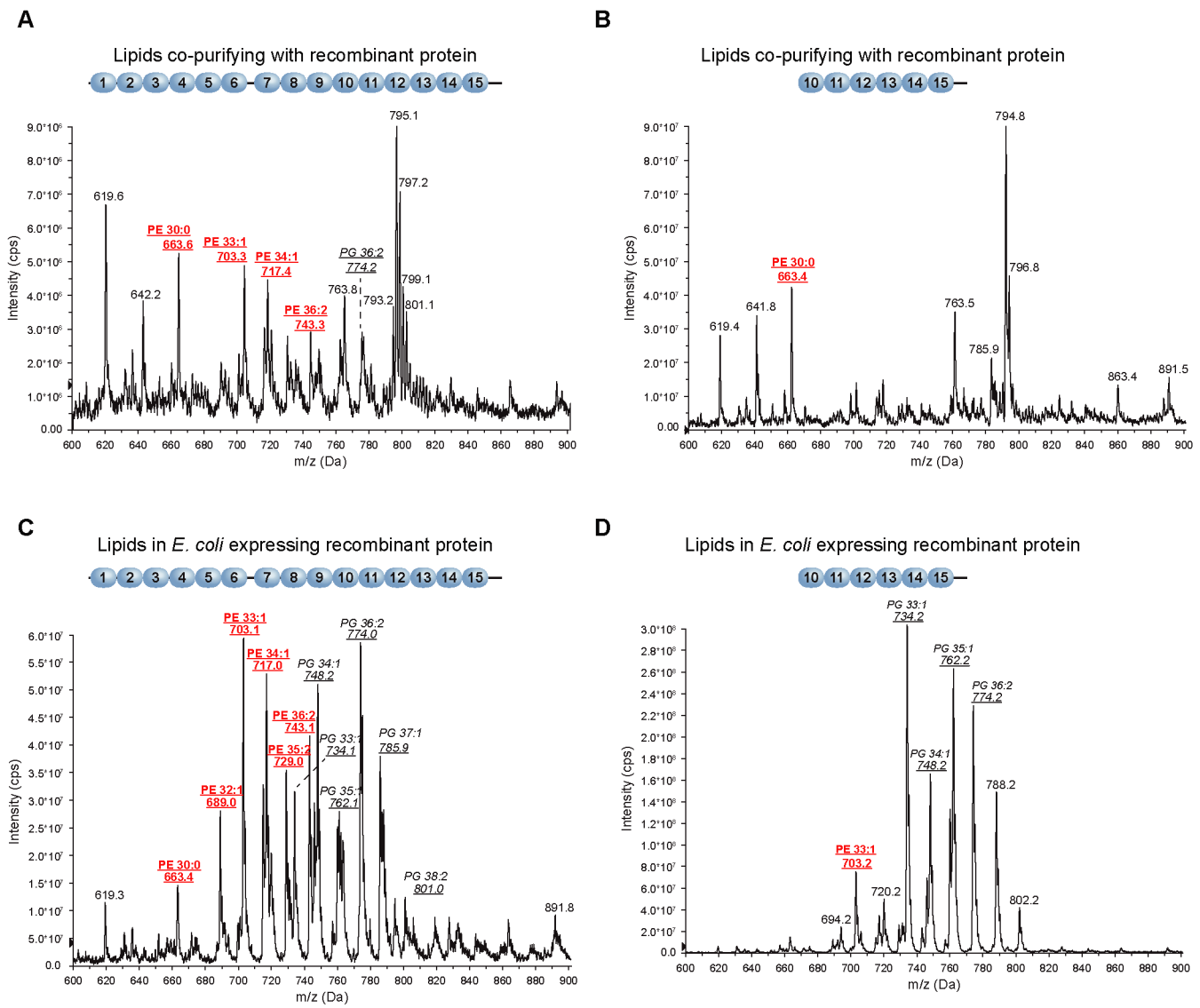

Figure 2. Recombinant TbMORN1 co-purifies with PE and increases *E. coli* PE levels. Negative ion mode survey scan (600-900 m/z) of lipid extracts from the indicated conditions. **(A,B)** Lipid extracts from purified recombinant TbMORN1(1-15) **(A)** and TbMORN1(10-15) **(B)**. A large amount of PE co-purified with TbMORN1(1-15) but very little was associated with TbMORN1(10-15). **(C,D)** Lipid extracts from *E. coli* cells expressing the indicated constructs. **(C)** Cells expressing TbMORN1(1-15) had elevated PE levels. **(D)** Cells expressing TbMORN1(10-15) showed no changes to cellular lipid ratios compared to wild-type (empty vector control). In all cases, phospholipid identity was confirmed by daughter fragmentation and reported here. Schematics of the recombinant TbMORN1 constructs are shown above the traces.

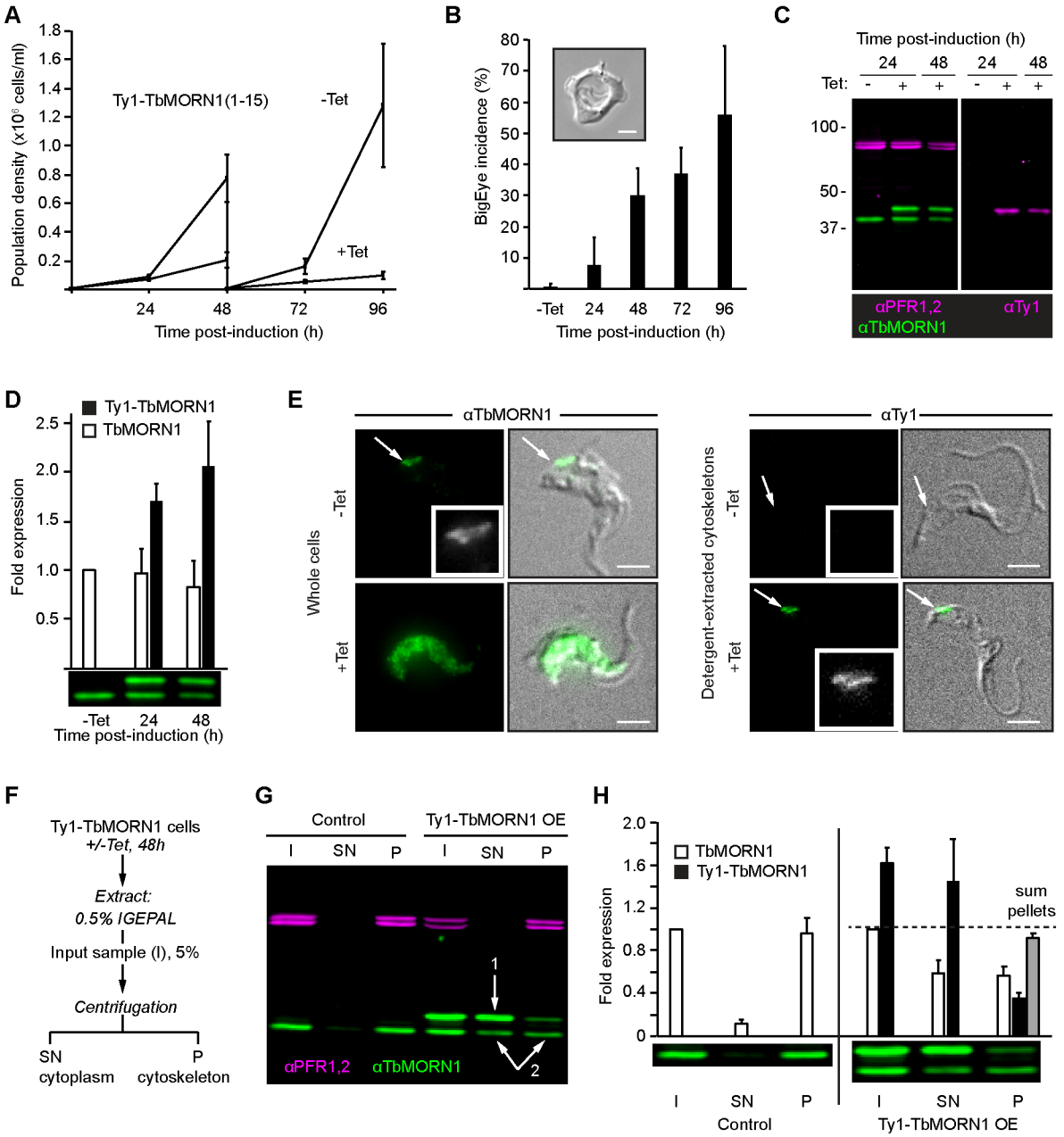

Figure 3. Overexpression of Ty1-tagged TbMORN1 causes a dominant negative phenotype. (A) Overexpression of Ty1-TbMORN1 is deleterious. Growth curves of control (-Tet) cells, and cells inducibly expressing Ty1-TbMORN1(1-15) (+Tet). Population density was measured every 24h, and the cultures split and reseeded at 48h. Data were compiled from 3 separate clones, each induced in 3 independent experiments; bars show mean +/- SD. **(B)** Overexpression of Ty1-TbMORN1 produces a BigEye phenotype. The incidence of BigEye cells was counted in control (-Tet) and Ty1-TbMORN1-expressing cells at the indicated timepoints. Data were compiled from 3 separate clones, each induced in 3 independent experiments; bars show mean + SD. The inset shows an example BigEye cell. Scale bar, 2 µm. **(C)** Tight induction of Ty1-TbMORN1 expression. Whole-cell lysates were harvested from control (-Tet) and Ty1-TbMORN1-expressing cells (+Tet) at the indicated timepoints and probed with anti-TbMORN1 and anti-Ty1 antibodies. PFR1,2 were used as a loading control. At least three independent inductions were carried out for each clone; an exemplary blot is shown. **(D)** Quantification of overexpression. The levels of endogenous TbMORN1 and ectopic Ty1-TbMORN1 in immunoblots were normalised relative to the PFR1,2 signal. Data were compiled using 3 separate clones, each induced in at least two independent experiments; bars show mean + SD. **(E)** Ty1-TbMORN1 can localise correctly to the cytoskeleton. Whole cells or detergent-extracted cytoskeletons were fixed and labelled with anti-TbMORN1 or anti-Ty1 antibodies. The fluorescence signal is shown with the transmitted light image of the cell overlaid; inset shows the fluorescence signal from the antibody in greyscale. Results confirmed for 3 separate clones, exemplary images are shown. Scale bars, 2 µm. **(F)** Schematic of the fractionation protocol. **(G)** Overexpression of Ty1-TbMORN1 displaces the endogenous protein from the cytoskeleton. Control and Ty1-TbMORN1-expressing cells were fractionated as shown in panel F and the I, SN, and P fractions were blotted. PFR1,2 was used as a marker for the cytoskeleton. Expression of Ty1-TbMORN1 was accompanied by a displacement of endogenous TbMORN1 from the insoluble (P) fraction into the soluble (SN) fraction (arrows 1,2). Equal fractions (5%) were loaded in each lane. 3 independent experiments using 3 separate clones were carried out; an exemplary blot is shown. **(H)** Quantification of the fractionation data. Bars show mean + SD.

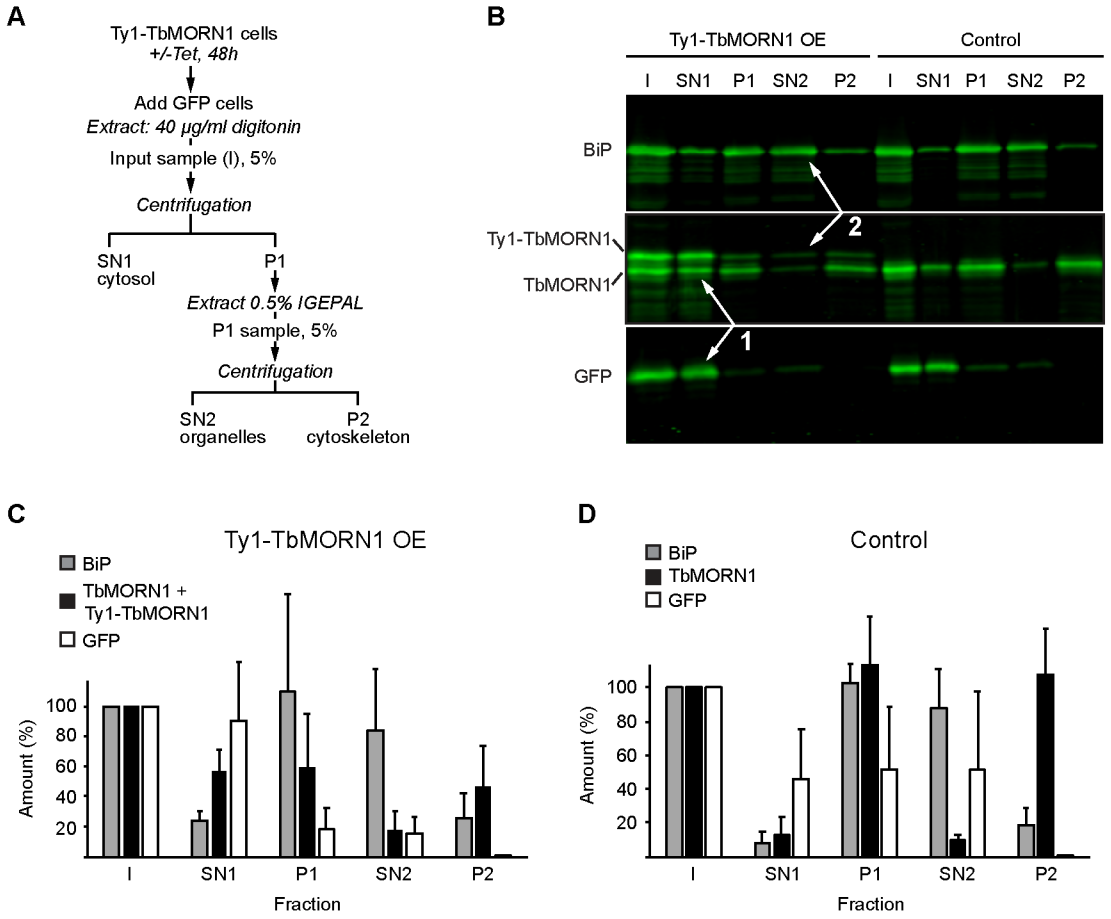

Figure 4. Overexpressed Ty1-TbMORN1 is predominantly cytosolic. (A) Schematic of the two-step fractionation scheme. **(B)** Immunoblots of fractions taken from control and Ty1-TbMORN1 overexpressing cells, using anti-BiP, anti-TbMORN1 and anti-GFP antibodies. Note that the membrane was cut into three strips for the immunoblot. Equal fractions (5%) were loaded in each lane. The overexpressed Ty1-TbMORN1 was predominantly extracted by digitonin and partitioned with the cytosolic GFP into the SN1 fraction (arrows 1). Very little of the remainder was subsequently extracted with non-ionic detergent into the SN2 fraction (arrows 2), with most partitioning into the cytoskeleton-associated P2 fraction. Three independent experiments were carried out using cells from three clones pooled together; an exemplary blot is shown. **(C,D)** Quantification of the immunoblots of the two-step fractionation. Data were compiled from three independent experiments, each using cells pooled from three separate clones. Bars show mean values + SD.

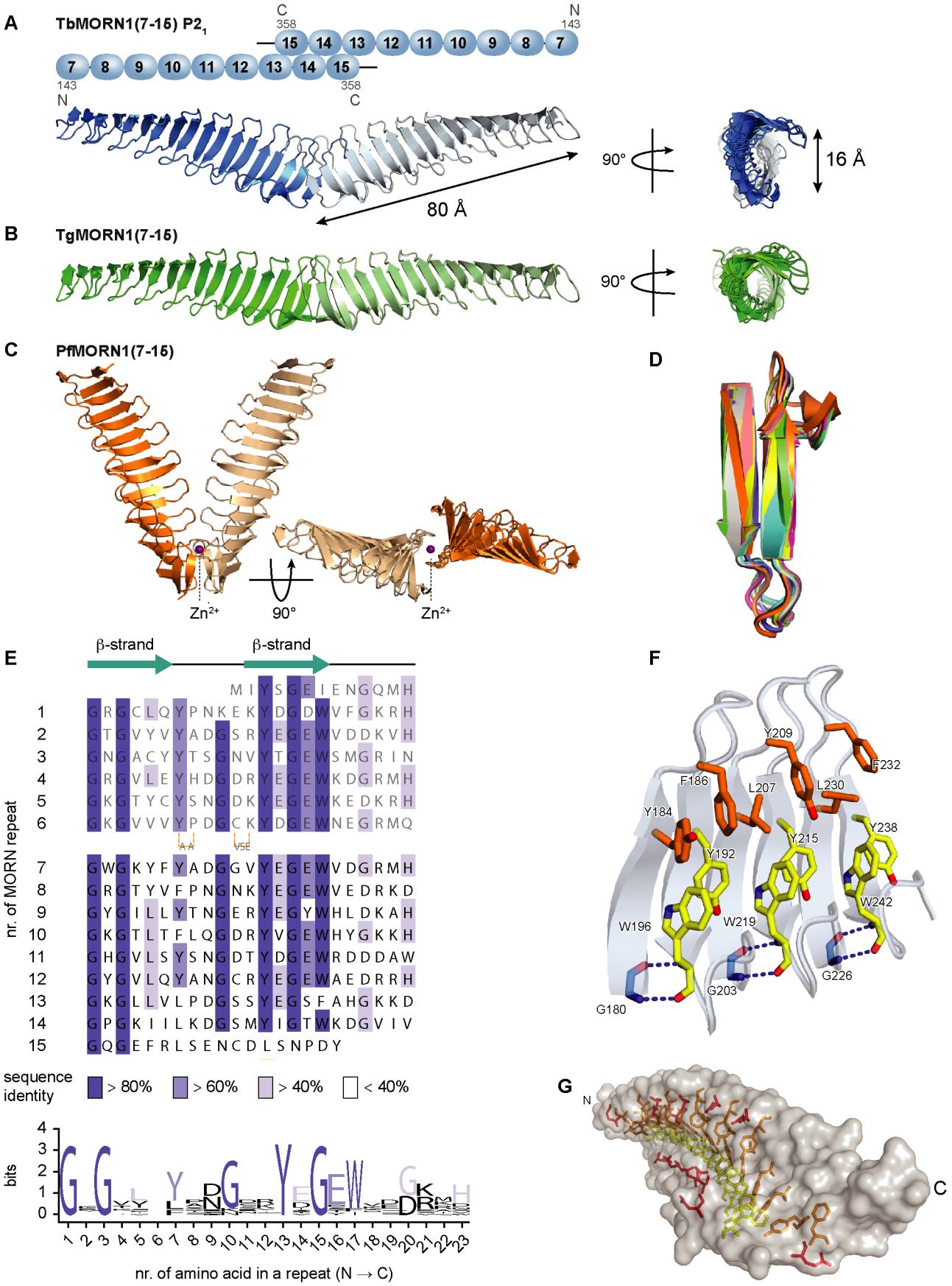
A
TbMORN1(7-15) P2₁
C
358
N
143
15 14 13 12 11 10 9 8 7
7 8 9 10 11 12 13 14 15
143
N
358
C
90°
16 Å
80 Å
B
TgMORN1(7-15)
90°
C
PfMORN1(7-15)
Zn2+
90°
Zn2+
D
E
β-strand
β-strand
nr. of MORN repeat
sequence identity
> 80%
> 60%
> 40%
< 40%
bits
nr. of amino acid in a repeat (N → C)
F
Y209
F232
F186
L207
L230
Y184
Y238
Y215
Y192
W242
W196
W219
G226
G203
G180
G
N
C

Figure 5. High-resolution structures of MORN repeat proteins and a structural redefinition of the MORN repeat. (A) Schematic depiction and crystal structure of the TbMORN1(7-15) dimer in its $P2_1$ crystal form. Amino acid numbers and N- and C-termini are indicated in the schematic. The crystal structure is shown in two orientations, with main dimensions indicated in Å. The structure contains 2 x 9 MORN repeats, and is an antiparallel homodimer with the subunits arranged in a splayed tail-to-tail configuration. The secondary structure consists of exclusively antiparallel beta-strands and peripherally positioned loops, which together form a longitudinal groove through the middle of the protein. **(B)** Crystal structure of TgMORN1(7-15) shown in two orientations. The number of MORN repeats and the configuration is the same as for TbMORN1(7-15) in panel A. **(C)** Crystal structure of PfMORN1(7-15) shown in two orientations. The bound Zn^{2+} ion is labelled. The structure contains 2 x 9 MORN repeats, again in tail-to-tail configuration but with an overall V-shaped arrangement. **(D)** Alignment of all 9 TbMORN1(7-15) MORN repeats in the crystal structure reveals a high level of structural conservation. **(E)** A revised consensus MORN repeat sequence, based on the crystal structures. A new alignment of the MORN repeats in TbMORN1 is shown. Repeats 7-15 are present in the crystal structure; repeats 1-6 are inferred. Conservation of sequence identity is indicated by colour intensity. Each MORN repeat consists of a β-hairpin, built up of two 6-residue β-strands connected by a 5-residue loop. The β-hairpin is followed by a 6-residue loop that connects to the next MORN repeat. The new 23-residues long consensus MORN repeat starts with the GxG motif. **(F)** The tertiary structure of individual MORN repeats is stabilised by hydrogen bonds between the first G of the GxG motif and the W from the YEGEW motif. MORN repeat arrays are further stabilised by aromatic stacking between the highly conserved aromatic residues in the YEGEW and LxY motifs, and by T-shaped π-stacking interactions of the highly conserved Y of the YEGEW motif, which is sandwiched between the W residue of its own motif, and the W residue in the next YEGEW motif. **(G)** A single TbMORN1(7-15) subunit viewed at an oblique angle. The residues of the YEGEW and LxY motifs involved in aromatic stacking line the surface of the longitudinal groove running through the middle of the protein.

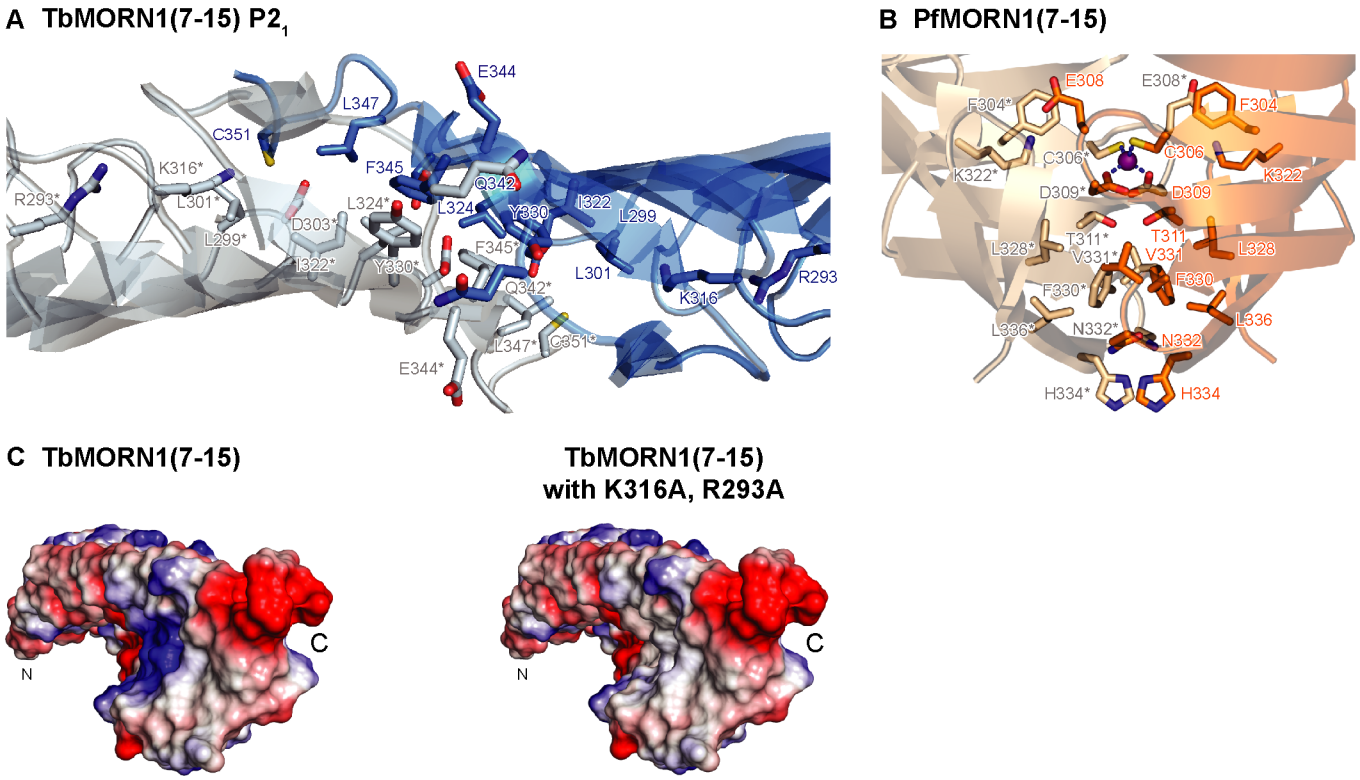

Figure 6. Dimerisation interfaces of TbMORN1(7-15) and PfMORN1(7-15). (A) The dimerisation interface of TbMORN1(7-15) P2$_1$ involves residues from MORN repeats 12-15, which stabilise the dimer interface via aromatic π-stacking (Tyr330 and Phe345 from the respective subunits), hydrophobic interactions (Leu301, Leu347, Ile339, Ile322, Leu324), and additionally via hydrogen bonding interactions at the edges of the dimer interface. In comparison to the TbMORN1(7-15) C2 crystal structure, there are no disulphide bridges stabilising the dimerisation interface of TbMORN1(7-15) P2$_1$. **(B)** The dimerisation interface of the V-shaped PfMORN1(7-15) dimer is smaller and is additionally stabilised by the incorporation of a structural Zn^{2+} ion, which is tetrahedrally coordinated by Cys306 and Asp309 residues from each respective subunit. Thr311 holds the side chain of Asp309 in the appropriate orientation. The dimer interface is additionally stabilised by symmetric hydrogen bonding between the Thr311 pair, aromatic stacking between the Phe330 pair, a hydrophobic cluster formed by Leu328, Val331 and Leu336, two salt bridges between Lys322 and Glu308 from the respective subunits, anion-π interaction of a side chain of Glu308 with Phe304, and a combination of aromatic stacking (His334 pair) and polar interactions (His334, Asn332) at the vertex of the dimer. **(C)** An electrostatic map calculated for a single subunit of TbMORN1(7-15). Vacuum electrostatics were calculated in Pymol, where red denotes -65.7 kT and blue denotes +65.7 kT. The structure on the right shows the predicted effect of two point mutations, R293A from MORN repeat 13, and K316A from MORN repeat 14. The mutations are expected to result in the loss of a postively-charged patch close to the dimer interface, and consequently disrupt the dimerisation of the TbMORN1(2-15) constructs.

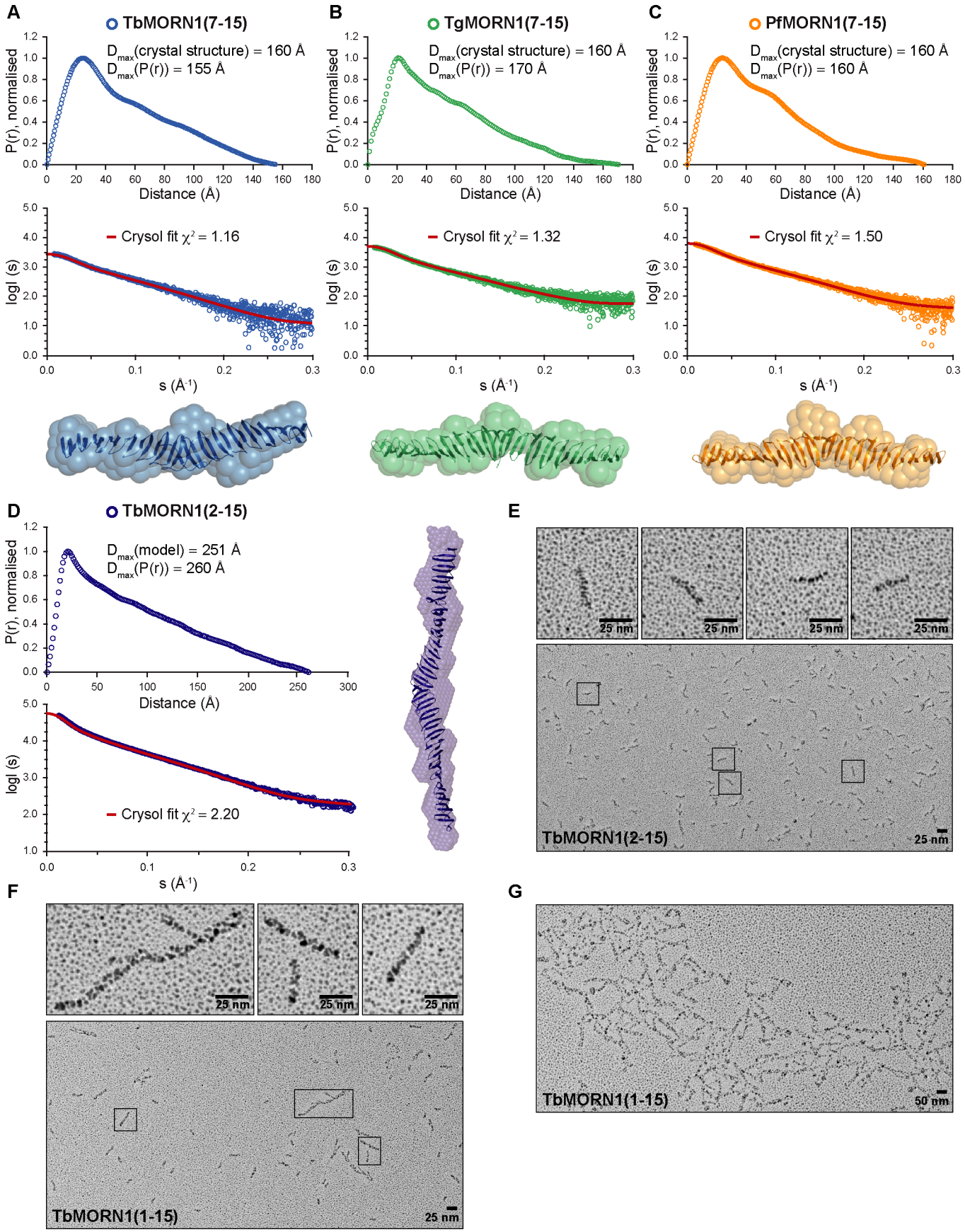
A
TbMORN1(7-15)
Dmax(crystal structure) = 160 Å
Dmax(P(r)) = 155 Å
P(r), normalised
Distance (Å)
Crysol fit χ2 = 1.16
logI (s)
s (Å-1)
B
TgMORN1(7-15)
Dmax(crystal structure) = 160 Å
Dmax(P(r)) = 170 Å
Crysol fit χ2 = 1.32
C
PfMORN1(7-15)
Dmax(crystal structure) = 160 Å
Dmax(P(r)) = 160 Å
Crysol fit χ2 = 1.50
D
TbMORN1(2-15)
Dmax(model) = 251 Å
Dmax(P(r)) = 260 Å
Crysol fit χ2 = 2.20
E
25 nm
TbMORN1(2-15)
F
TbMORN1(1-15)
G
50 nm
TbMORN1(1-15)

Figure 7. MORN1 proteins form extended dimers in solution as assessed by SAXS and EM experiments. **(A-D)** SAXS experiments on: **(A)** TbMORN1(7-15), **(B)** TgMORN1(7-15), **(C)** PfMORN1(7-15), and **(D)** TbMORN1(2-15). For each respective protein, the results include a P(r) plot with derived experimental D_{max} value compared with a D_{max} value derived from the structure, an experimental SAXS scattering data with a fit calculated by the Crysol programme, and a SAXS-based ab initio molecular envelope. In the case of TbMORN1(2-15), the theoretical D_{max} value was derived from a structural model, which was generated by spiking the TbMORN1(7-15) structure with additional structures of individual TbMORN1(7-15) subunits. **(E-G)** EM with rotary shadowing of TbMORN1(2-15) and full-length TbMORN1. **(E)** TbMORN1(2-15) forms a homogenous population of extended dimers of approximately 25 nm in length (see insets for individual examples). **(F)** Full-length TbMORN1 is heterogeneous and includes rare filaments of 175-200 nm in length (first inset) and individual dimers (second and third inset). **(G)** Higher-order assemblies of full-length TbMORN1 assembled in a mesh-like structure. Magnification, 71,000x; scale bars, 25 nm, 50 nm as indicated. n (independent replicates) = 2, n (biological replicates) = 2.

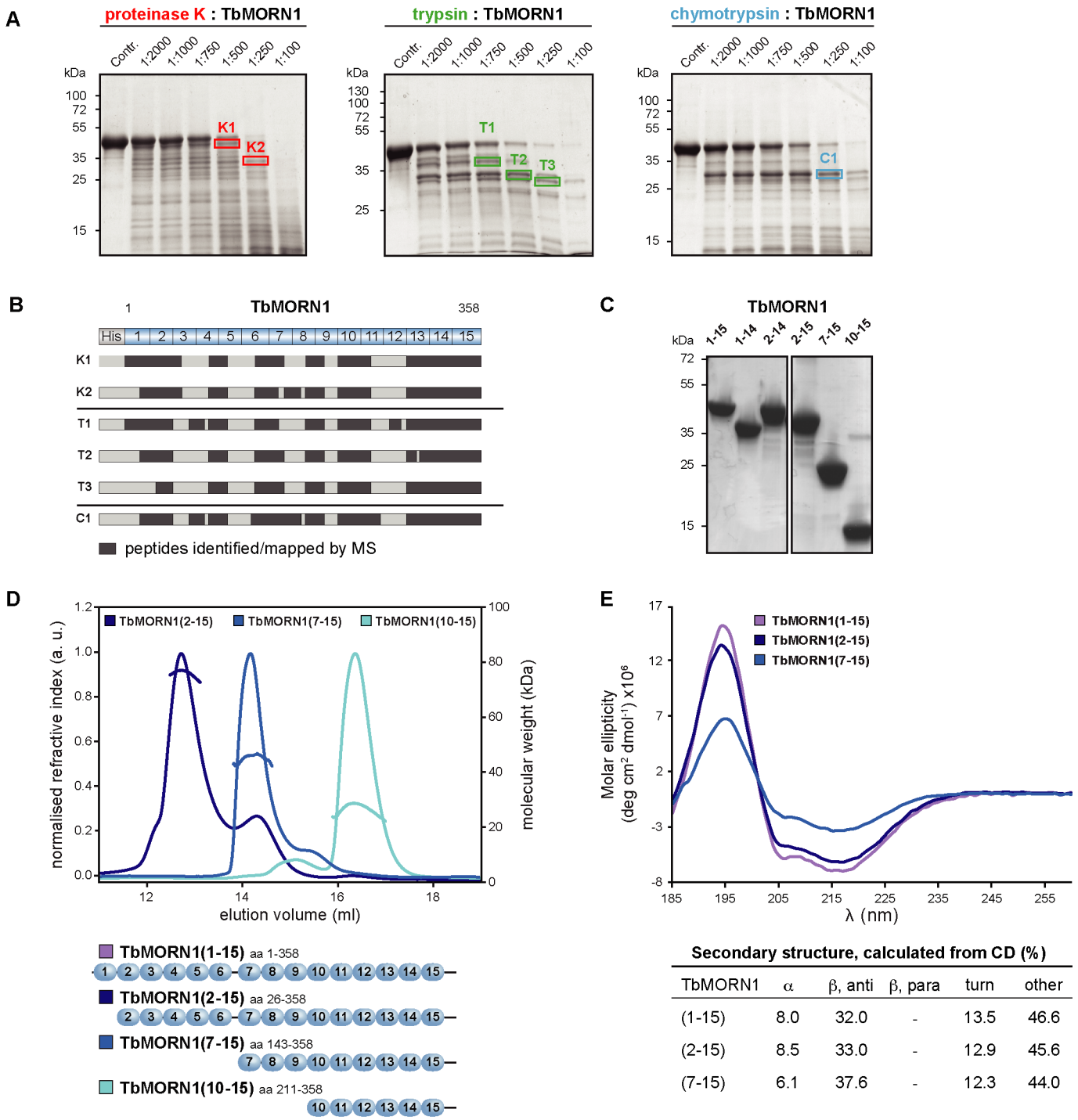

Secondary structure, calculated from CD (%)

TbMORN1	α	β, anti	β, para	turn	other
(1-15)	8.0	32.0	-	13.5	46.6
(2-15)	8.5	33.0	-	12.9	45.6
(7-15)	6.1	37.6	-	12.3	44.0

Figure S1. Low-resolution structural analysis of TbMORN1. **(A)** Full-length TbMORN1 with an N-terminal HisTag was subjected to limited proteolysis using proteinase K (red), trypsin (green), and chymotrypsin (cyan) at protease:protein ratios (w/w) as indicated on each panel. Samples were resolved by SDS-PAGE and selected bands (labelled boxes) corresponding to proteolytic products were excised and analysed by mass spectrometry. Control (Contr.) corresponds to protein without protease treatment. **(B)** Mass spectrometry analysis of the excised proteolytic products indicated in panel A. Peptides identified and mapped by mass spectrometry are shown as dark grey boxes; a schematic of the full-length construct is shown above, with individual MORN repeats labelled. Note that the proteolytic products show progressive degradation from their N-termini, while the C-terminal part is stable. **(C)** Coomassie-stained SDS-PAGE gel showing purified recombinant TbMORN1 truncations. **(D)** SEC-MALS traces of TbMORN1(2-15), (7-15), and (10-15). Chromatographic separation was done using a Superdex 200 Increase 10/300 GL column, void volume 7.2 ml. The three proteins all eluted as dimers. Schematics are shown underneath. **(E)** Far-UV CD profiles of TbMORN1, TbMORN1(2-15) and (10-15). A positive peak at 195 nm and a negative one at 218 nm demonstrated that the constructs are all β-proteins. The secondary structure content predictions for each construct were calculated in BeStSel and are shown below the CD graph.

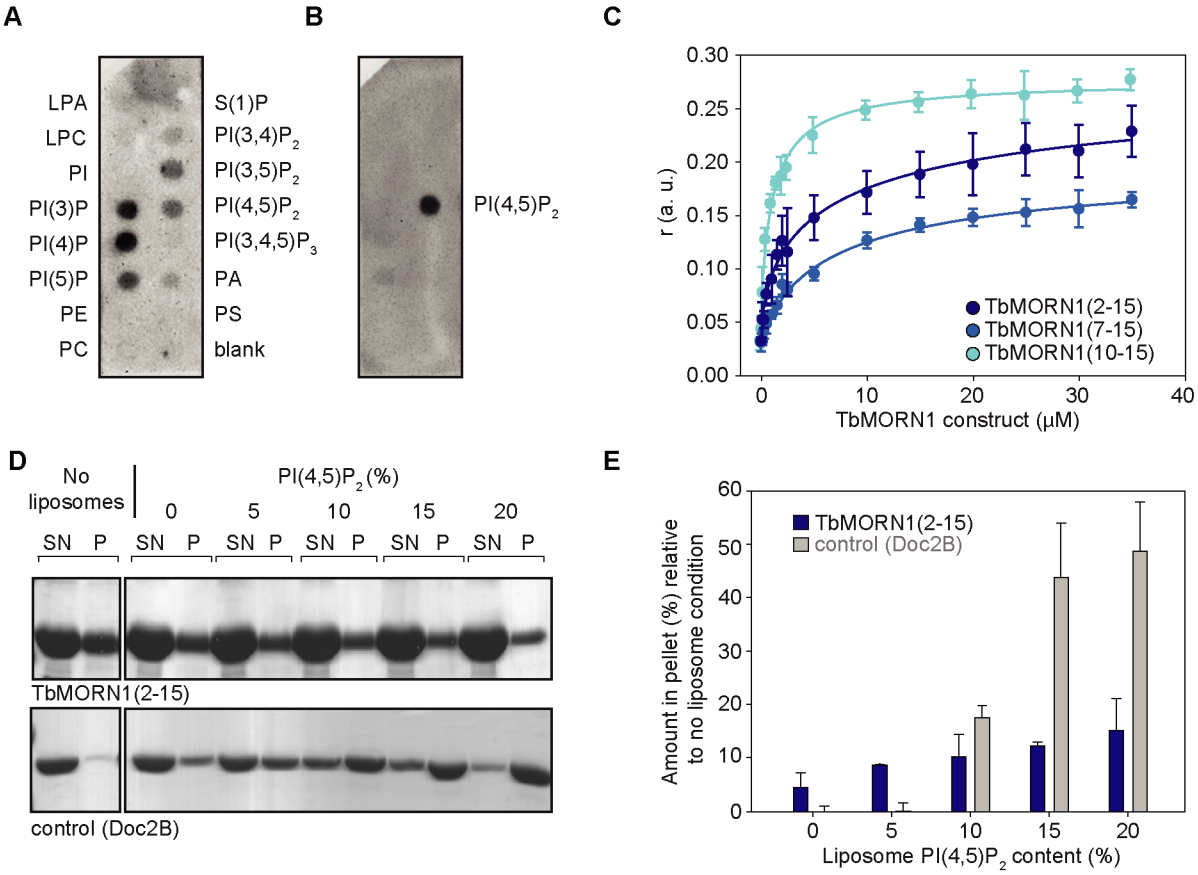

Figure S2. TbMORN1 interacts with phospholipids but not liposomes. (A) Purified recombinant TbMORN1 binds to multiple phospholipid species in protein-lipid overlay assays. PIP strips were incubated with purified recombinant TbMORN1(1-15) protein, and bound proteins were detected by immunoblotting with anti-strep antibodies. Abbreviations: PI(n)P, phosphatidylinositol (n) phosphate; PA, phosphatidic acid; LPA, lysophosphatidic acid; LPC, lysophosphatidylcholine; PI, phosphatidylinositol; PE, phosphatidylethanolamine; PC, phosphatidylcholine; S(1)P, sphingosine-1-phosphate; PS, phosphatidylserine. Data were obtained from 3 independent experiments using 2 biological replicates; an exemplary blot is shown. **(B)** PIP strip overlaid with the PH domain of PLCδ, a positive control for PI(4,5)P_2 binding. Data were obtained from 3 independent experiments using 3 biological replicates; an exemplary blot is shown. The PIP strips presented here were exposed to the light source for the same time. **(C)** Fluorescence anisotropy measurements of 0.1 μM BODIPY TMR-PI(4,5)P_2-C16 in the presence of TbMORN1(2-15), (7-15) and (10-15). All three truncations of TbMORN1 interacted with the 16-carbon PI(4,5)P_2 with binding affinities in the low micromolar range. Data obtained from 3 independent experiments using 3 biological replicates, with 10 technical replicates for each experiment. Traces show mean values, bars are s.e.m. **(D)** Liposome co-sedimentation assay. POPC liposomes containing 0, 5, 10, 15 and 20% of porcine brain PI(4,5)P_2 were incubated with 10 μM TbMORN1(2-15). TbMORN1(2-15) was found in both pellet (P) and supernatant (SN) fractions but did not increase proportionally to PI(4,5)P_2 concentration. The positive control, Doc2B, bound PI(4,5)P_2 in a concentration-dependent manner, with a shift from SN to P fractions proportional to the increase in % of PI(4,5)P_2 present in the liposomes. Data were obtained from 2 independent experiments using 2 biological replicates; an exemplary blot is shown. **(E)** Quantification of the liposome pelleting assays. The amount of protein in the pellet fraction is presented relative to the amount present in the pellet fraction of the no liposome condition.

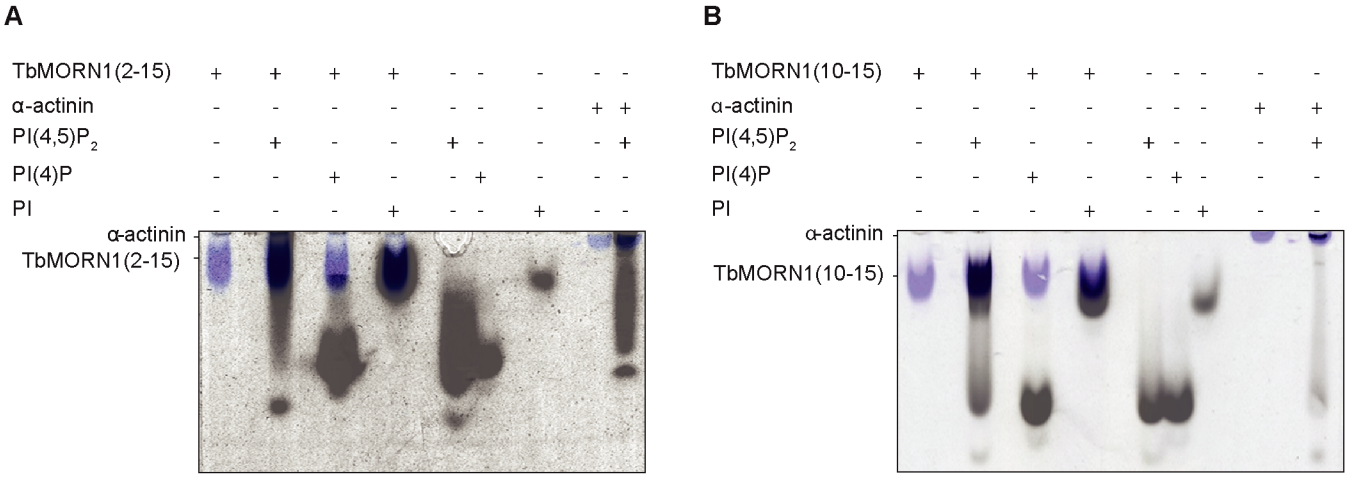

Figure S3. TbMORN1 constructs interact with PI(4,5)P_2 in native gel bandshift assays. (A) Native gel electrophoresis of TbMORN1(2-15) and **(B)** TbMORN1(10-15) in the presence and absence of PI(4,5)P_2, PI(4)P and PI, all labelled with Bodipy TMR fluorescent dye. α-actinin served as a positive control of PI(4,5)P_2 binding. Data obtained from two independent experiments, each using a different biological replicates.

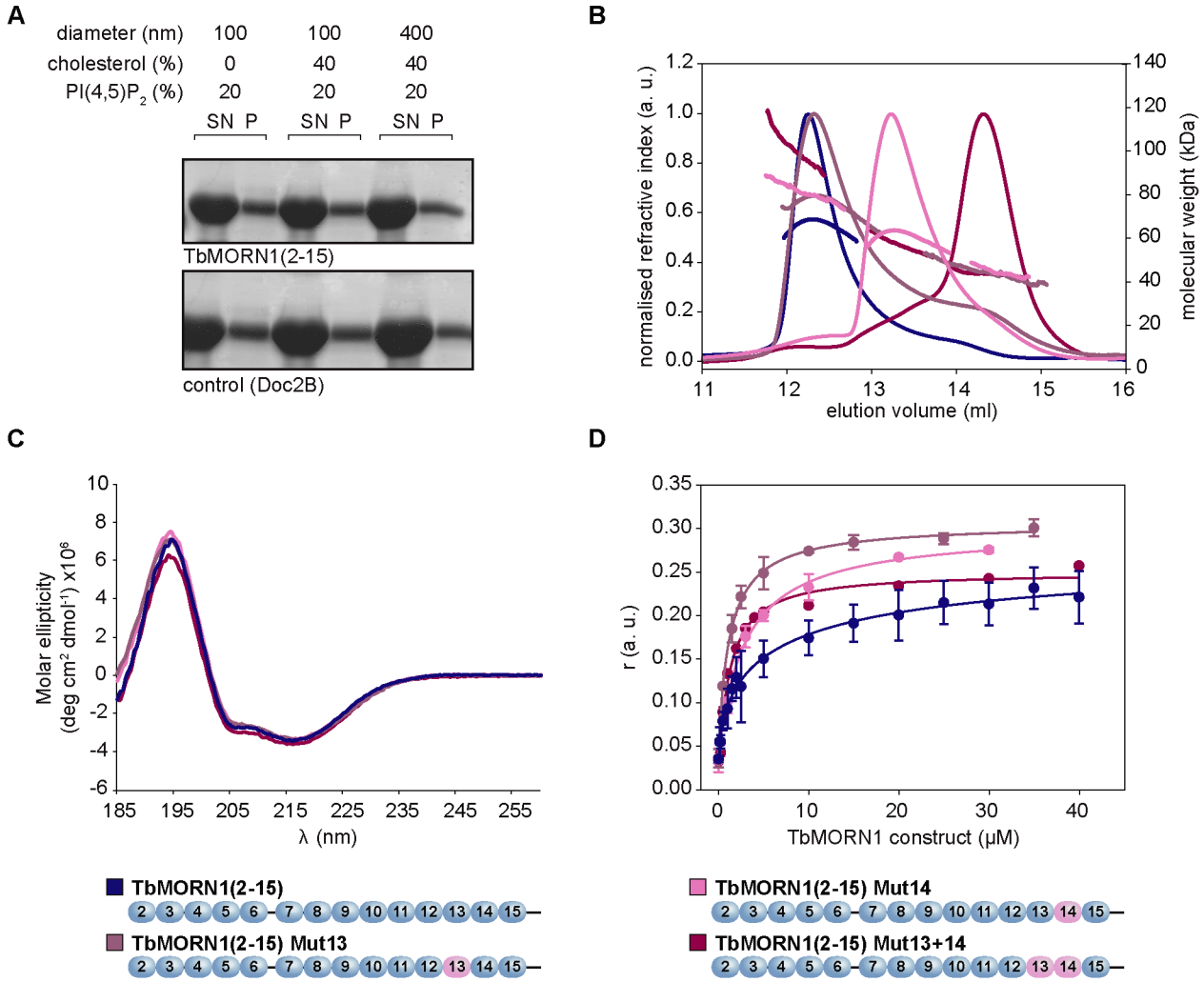

Figure S4. Mutagenesis of putative PI(4,5)P_2 binding sites in TbMORN1(2-15) has no effect on binding. (A) Liposome co-sedimentation assay performed on TbMORN1(2-15) in the presence of POPC liposomes containing 20% of porcine brain PI(4,5)P_2 and 0 or 40% cholesterol. The excess cholesterol was expected to promote local high concentrations of PI(4,5)P_2 on the surface of the liposomes. To assay for the effect of curvature, two batches of liposomes containing 20% PI(4,5)P_2 and 40% of cholesterol were tested, with the diameter of the liposomes being either 100 or 400 nm. No significant co-sedimentation of TbMORN1(2-15) and PI(4,5)P_2-containing liposomes was observed. The positive control, 10 μM Doc2B was predominantly found in the pellet (P) fractions. **(B)** SEC-MALS profiles of TbMORN1(2-15) and its mutagenised variants. Residues comprising the putative PI(4,5)P_2-binding sites in MORN repeats 13 and 14 were mutated to alanines. Mutagenesis of repeat 13 (Mut13) did not result in any change to the dimeric status of the protein. However, mutagenesis of repeat 14 (Mut14) resulted in a mixture of monomers and dimers being eluted, while mutagenesis of both repeats (Mut13+14) resulted in monomeric protein. Chromatographic separation was done using a Superdex 200 Increase 10/300 GL column, void volume 7.2 ml. **(C)** Far-UV CD profiles of TbMORN1(2-15) and its putative PI(4,5)P_2-binding mutants. The constructs remained β-proteins despite the site-directed mutagenesis. **(D)** Fluorescence anisotropy measurements of TbMORN1(2-15) and its putative PI(4,5)P_2-binding mutants, measured in the presence of 0.1 μM BODIPY TMR-PI(4,5)P_2. All constructs showed good interaction with the fluorophore-conjugated PI(4,5)P_2.

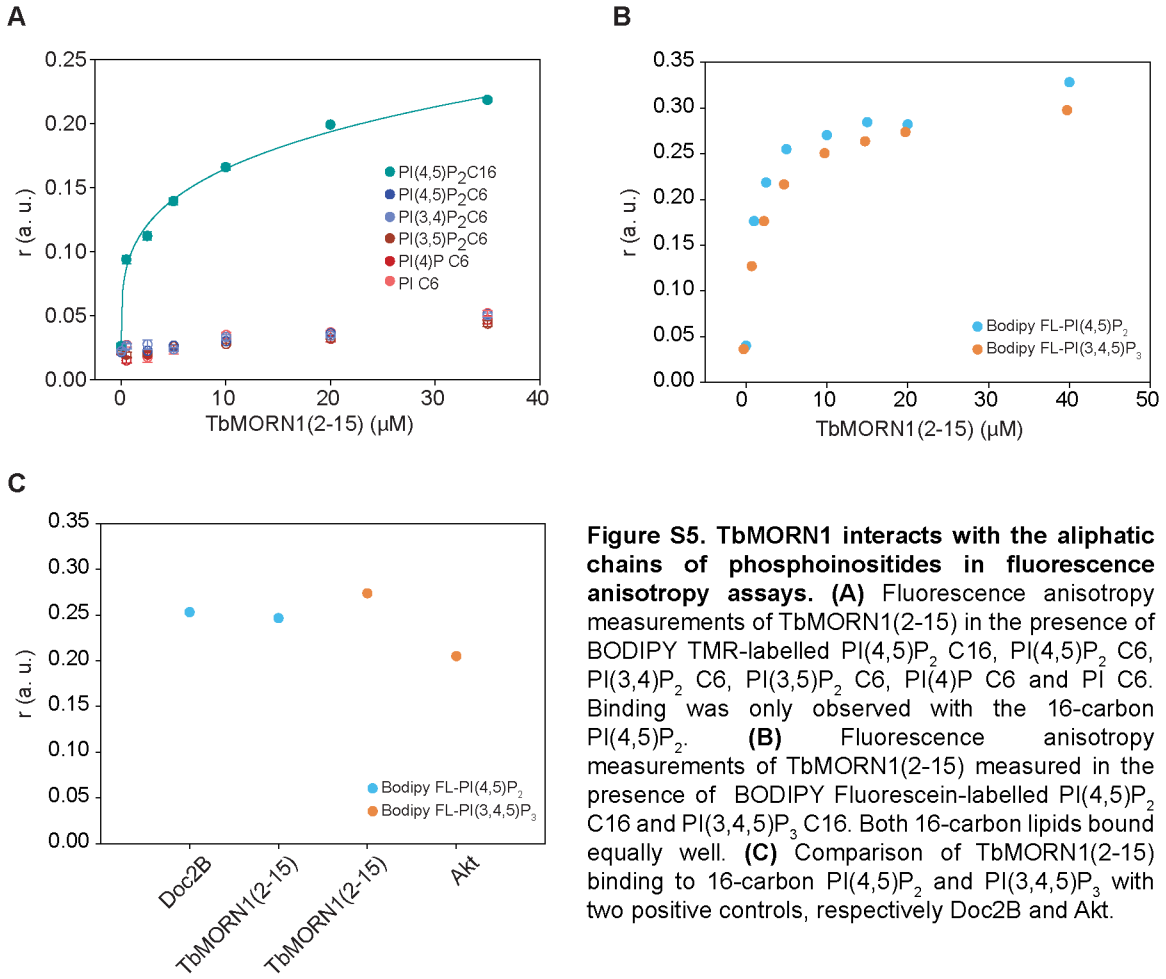

Figure S5. TbMORN1 interacts with the aliphatic chains of phosphoinositides in fluorescence anisotropy assays. (A) Fluorescence anisotropy measurements of TbMORN1(2-15) in the presence of BODIPY TMR-labelled PI(4,5)P_2 C16, PI(4,5)P_2 C6, PI(3,4)P_2 C6, PI(3,5)P_2 C6, PI(4)P C6 and PI C6. Binding was only observed with the 16-carbon PI(4,5)P_2. **(B)** Fluorescence anisotropy measurements of TbMORN1(2-15) measured in the presence of BODIPY Fluorescein-labelled PI(4,5)P_2 C16 and PI(3,4,5)P_3 C16. Both 16-carbon lipids bound equally well. **(C)** Comparison of TbMORN1(2-15) binding to 16-carbon PI(4,5)P_2 and PI(3,4,5)P_3 with two positive controls, respectively Doc2B and Akt.

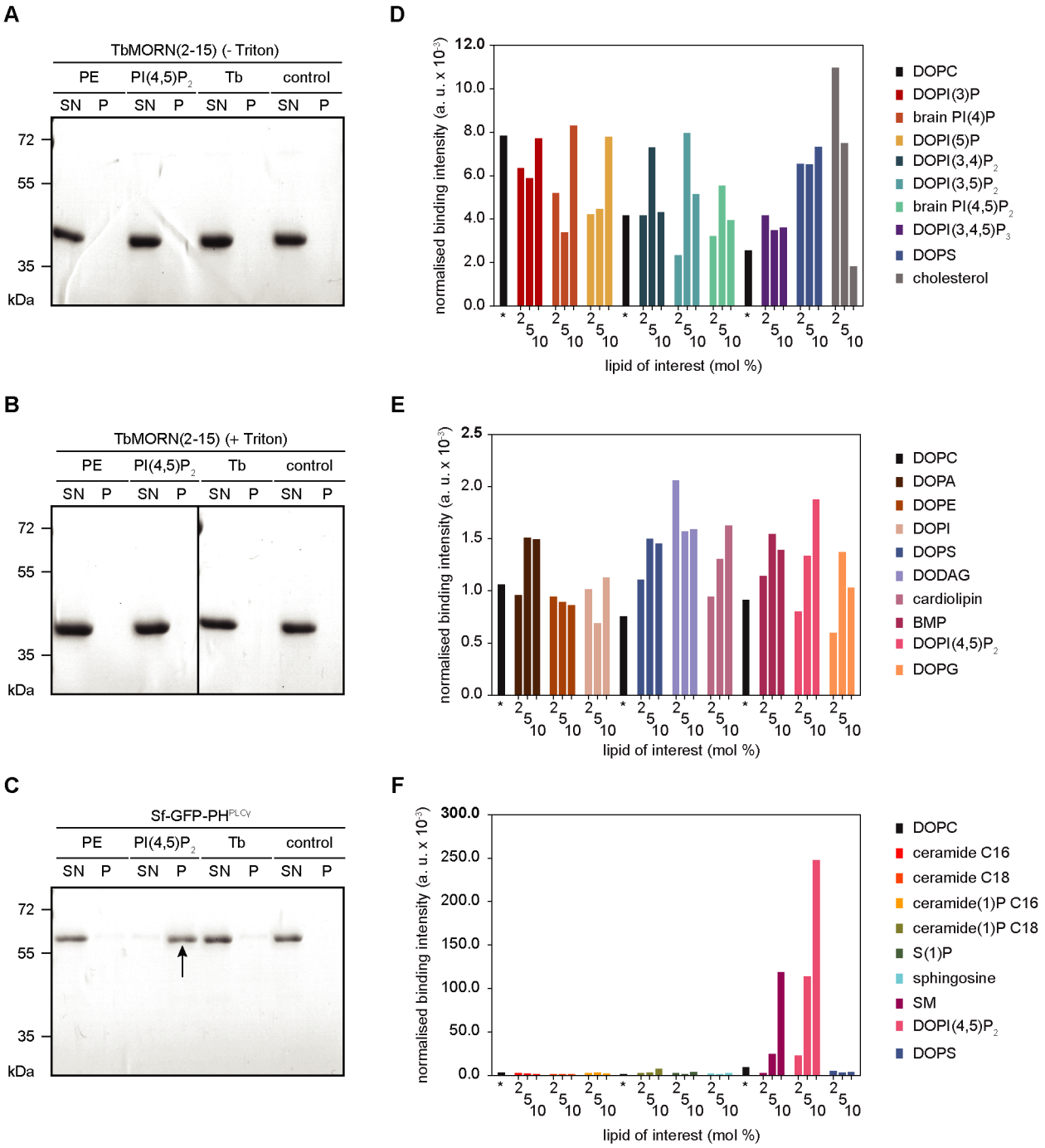

Figure S6. TbMORN1(2-15) does not bind to liposomes in vitro. (A-C) Liposome pelleting assays using sucrose-loaded vesicles (SLVs). TbMORN1(2-15) was purified in the absence **(A)** or presence **(B)** of Triton X-100 in the lysis buffer. The purified proteins were incubated with SLVs, which were then pelleted by centrifugation. Supernatant (SN) and pellet (P) fractions were analysed by SDS-PAGE using Coomassie staining. The SLVs were made from commercial lipids with an excess of either PE or PI(4,5)P_2, and also reconstituted from purified whole-cell trypanosome lipids (Tb). A no-SLV condition was included as an additional negative control. **(C)** The PH domains of PLCγ was used as a positive control for PI(4,5)P_2 binding. As expected, the PLCγ PH domain co-sedimented with PI(4,5)P_2-containing SLVs and was entirely present in the P fraction in this condition (arrow). The recombinant TbMORN1 proteins remained in the SN fraction in all conditions. **(D-F)** Liposome microarray analysis. Microchips carrying giant unilamellar vesicles (GUVs) with lipids of interest at three different concentrations (2, 5 and 10 mol %) were incubated with purified recombinant EGFP-TbMORN1(2-15). No significant binding was observed to either phosphoinositide lipids or PE. **(D)** n (independent replicates) = 7; **(E)** n (independent replicates) = 3. **(F)** Microchip incubated with PLC-δ1 PH domain as a positive control. A specific and concentration-dependent binding between the PLC-δ1 PH domain and DOPI(4,5)P_2 and SM was observed. DOPC, a carrier lipid, was used as an internal negative control of binding, as well as a marker for tracking positions of liposomes on a given microarray. n (independent replicates) = 1. Note the different scales on the y-axes of the three charts.

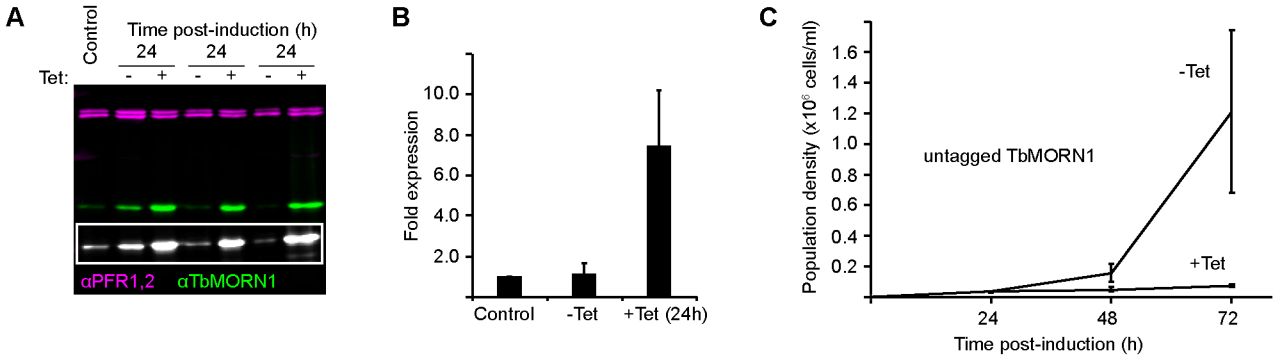

Figure S7. Overexpression of untagged TbMORN1 causes a dominant negative phenotype. (A) Inducible overexpression of untagged TbMORN1. Immunoblot of whole-cell lysates from three separate clones overexpressing untagged TbMORN1 from an ectopic locus. TbMORN1 was detected using anti-TbMORN1 antibodies; PFR1,2 were used as a loading control and detected using anti-PFR1,2 antibodies. Inset shows a greyscale image of the TbMORN1 channel with enhanced levels so that the endogenous protein is visible. Three separate clones were assayed, each in three independent experiments; an exemplary blot is shown. One of the three clones appeared to have slightly leaky expression, with TbMORN1 levels in the -Tet condition being higher than controls. **(B)** Quantification of overexpression. TbMORN1 levels in control, uninduced (-Tet) and induced (+Tet) were normalised relative to the loading control and expressed relative to the control cells. Approximately 7-fold overexpression was achieved relative to control cells. Data were obtained from blots using 3 separate clones, each induced in 3 independent experiments. Bars show mean + SD. **(C)** Overexpression of untagged TbMORN1 is deleterious. Uninduced (-Tet) and TbMORN1 overexpressing (+Tet) cells were assayed at 24 h intervals in a 3-day timecourse. Data were obtained from blots using 3 separate clones, each induced in 3 independent experiments. Mean +/- SD.

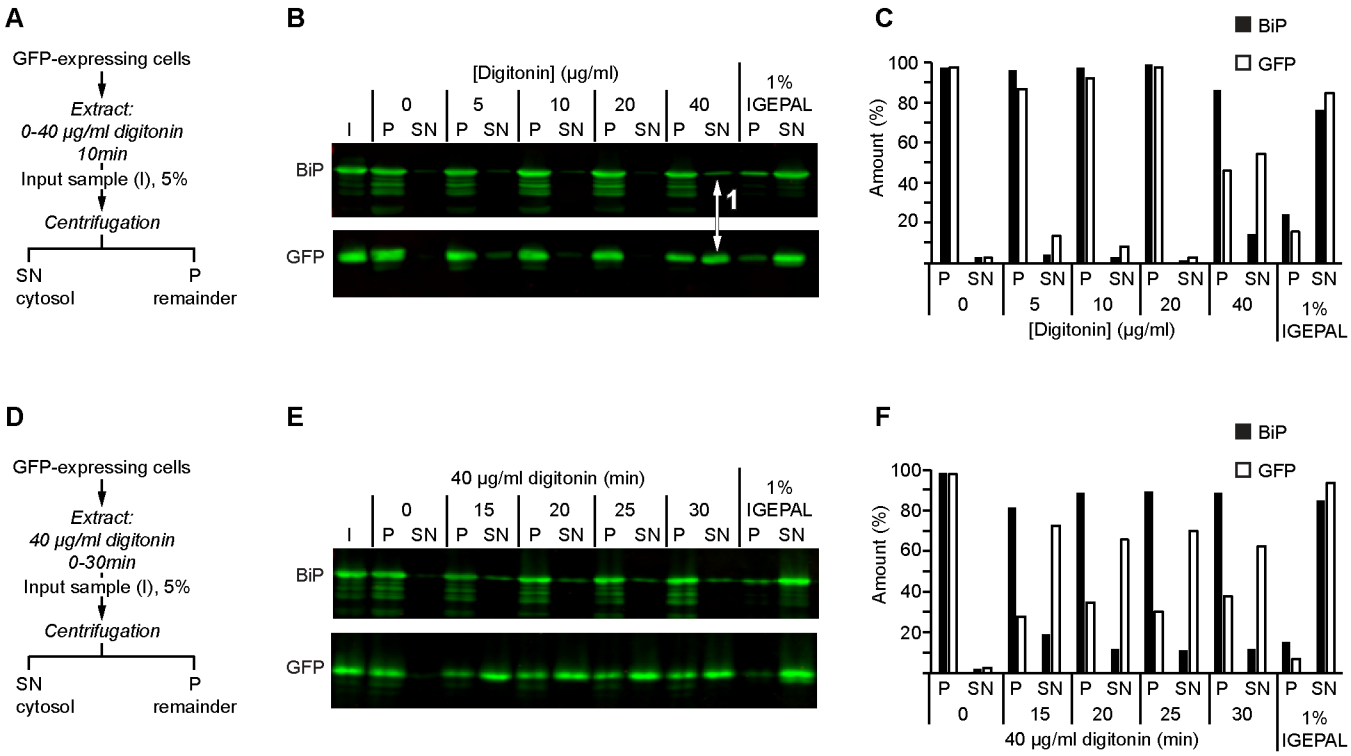

Figure S8. Optimisation of digitonin fractionation. (A) Schematic of the one-step fractionation scheme. Cells expressing cytosolic GFP (Batram et al., 2014) were incubated for 10 min with increasing concentrations (0-40 µg/ml) of digitonin, using 1% IGEPAL as a positive control for full extraction. At the end of the incubation, the soluble and insoluble fractions were separated by centrifugation. **(B)** Equal fractions (5%) of the supernatant (SN) and pellet (P) were probed with antibodies specific for GFP and the endoplasmic reticulum chaperone BiP. At 40 µg/ml digitonin, good solubilisation of GFP was achieved with only negligible solubilisation of BiP (arrow 1). Both proteins were efficiently solubilised using 1% IGEPAL as a positive control. Multiple independent experiments were carried out; an exemplary blot is shown. Note that the membrane was cut into strips prior to blotting, but the samples shown are from the same experiment. **(C)** Quantification of the immunoblot shown in B. **(D, E, F)** As per panels A-C, but with constant 40 µg/ml digitonin concentration and varying incubation time (0-30 min). Increasing the incubation time over a range of 15-30 min did not appear to notably increase the amount of GFP extraction. As a result, a 25 min incubation time was used in the subsequent experiments.

A

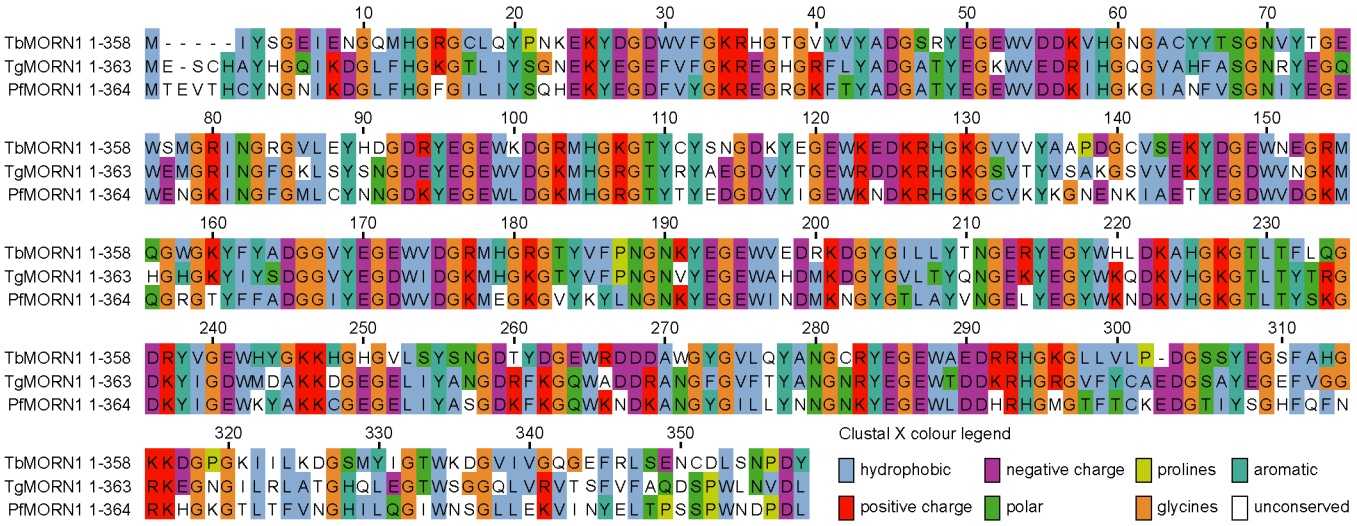

B

Comparison of MORN1 proteins and % of their sequence identity	
T. brucei / P. falciparum	54
T. brucei / T. gondii	57
P. falciparum / T. gondii	65

C

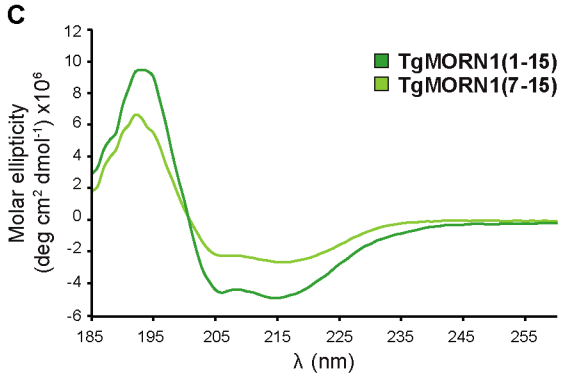

Secondary structure, calculated from CD (%)

TgMORN1	α	β, anti	β, para	turn	other
(1-15)	5.3	30.8	0.8	13.0	50.1
(7-15)	4.8	42.3	-	11.8	41.1

D

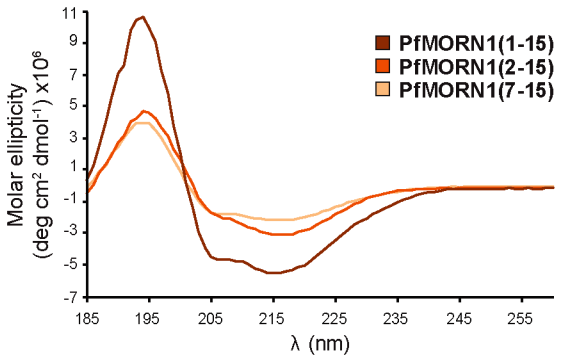

Secondary structure, calculated from CD (%)

PfMORN1	α	β, anti	β, para	turn	other
(1-15)	6.4	29.8	1.9	13.8	48.1
(2-15)	6.2	35.7	-	13.4	44.7
(7-15)	6.6	32.6	1.0	12.0	47.8

Figure S9. Comparison of MORN1 proteins, and secondary structure analysis of apicomplexan MORN1s. (A) Amino acid sequence alignment of MORN1 proteins from *Trypanosoma brucei, Toxoplasma gondii* and *Plasmodium falciparum*. The number of amino acids in each protein is indicated, amino acid numbers in the alignment are those for TbMORN1. The alignment is coloured according to the amino acid properties. **(B)** Pairwise comparison of percentage sequence identity between the three proteins. **(C)** Far-UV CD measurements obtained for TgMORN1(1-15) and TgMORN1(7-15). The secondary structure content predictions for each of the measured proteins were calculated in BeStSel and are shown below the CD graph. **(D)** As (C), but PfMORN1(1-15), (2-15) and (7-15). Like TbMORN1, TgMORN1 and PfMORN1 are also all-β proteins.

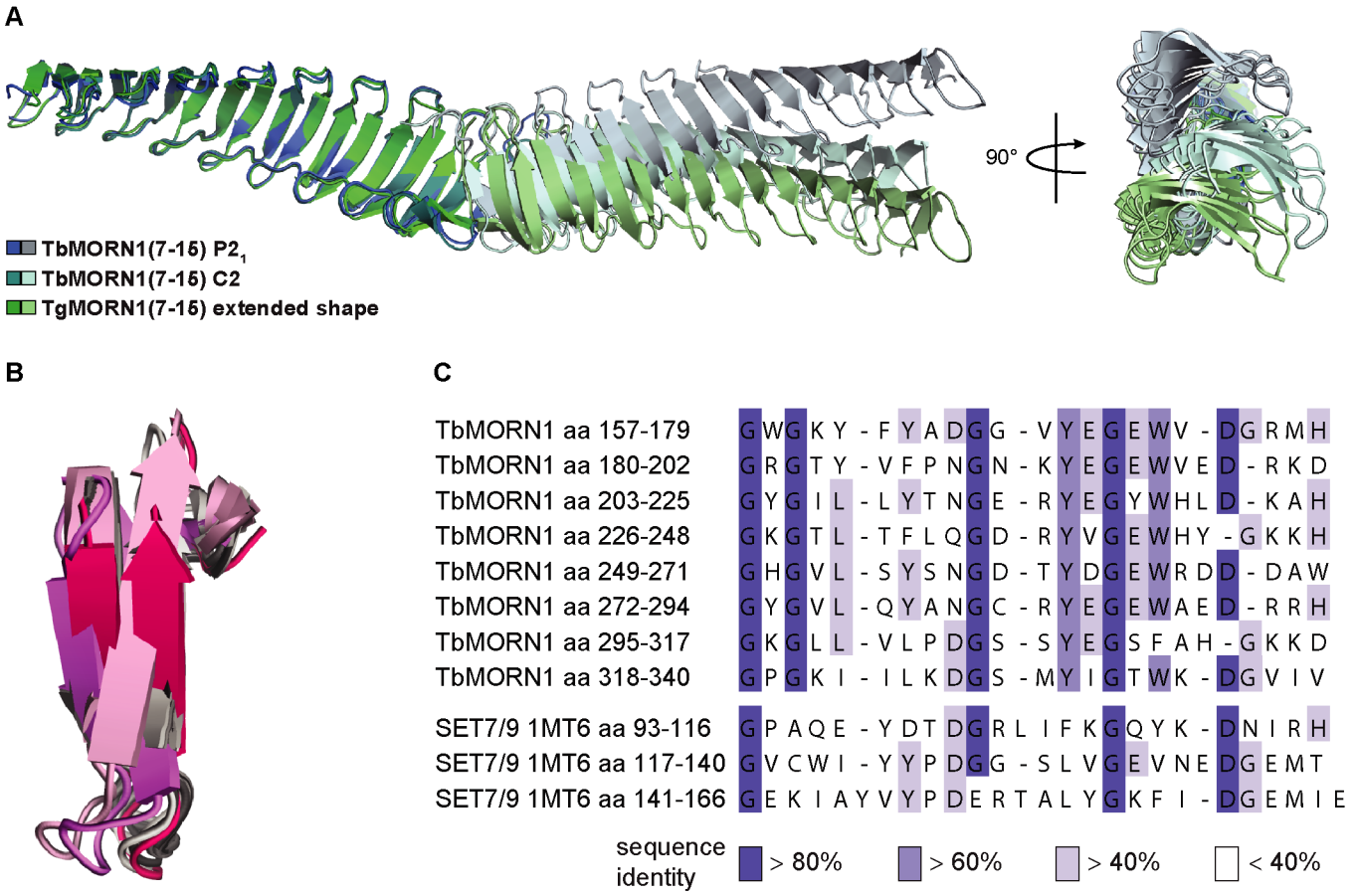

Figure S10. Comparision of MORN1 extended dimers, and with SETD7 (SET7/9). (A) TbMORN1(7-15) P2$_1$, TbMORN1(7-15) C2, and TgMORN1(7-15) extended dimers superimposed on each other, and displayed in two orientations. In contrast to the other two proteins, the P2$_1$ crystal structure of TbMORN1(7-15) displays a bend of approximately 30° among the subunits. **(B)** TbMORN1(7-15) MORN repeats superimposed on three MORN repeats from SETD7 (SET7/9). Alignment of the three MORN repeats from SETD7 with MORN repeat 7 from the TbMORN1(7-15) crystal structure over 22-23 aligned C-atoms yielded rmsd values of 2.3, 1.5 and 1.9 Å respectively. **(C)** Sequence alignment of MORN repeats from the TbMORN1(7-15) crystal structure with three MORN repeats from SETD7. The first Gly residue is conserved in all MORN repeats of TbMORN1(7-15) and SETD7 structures.

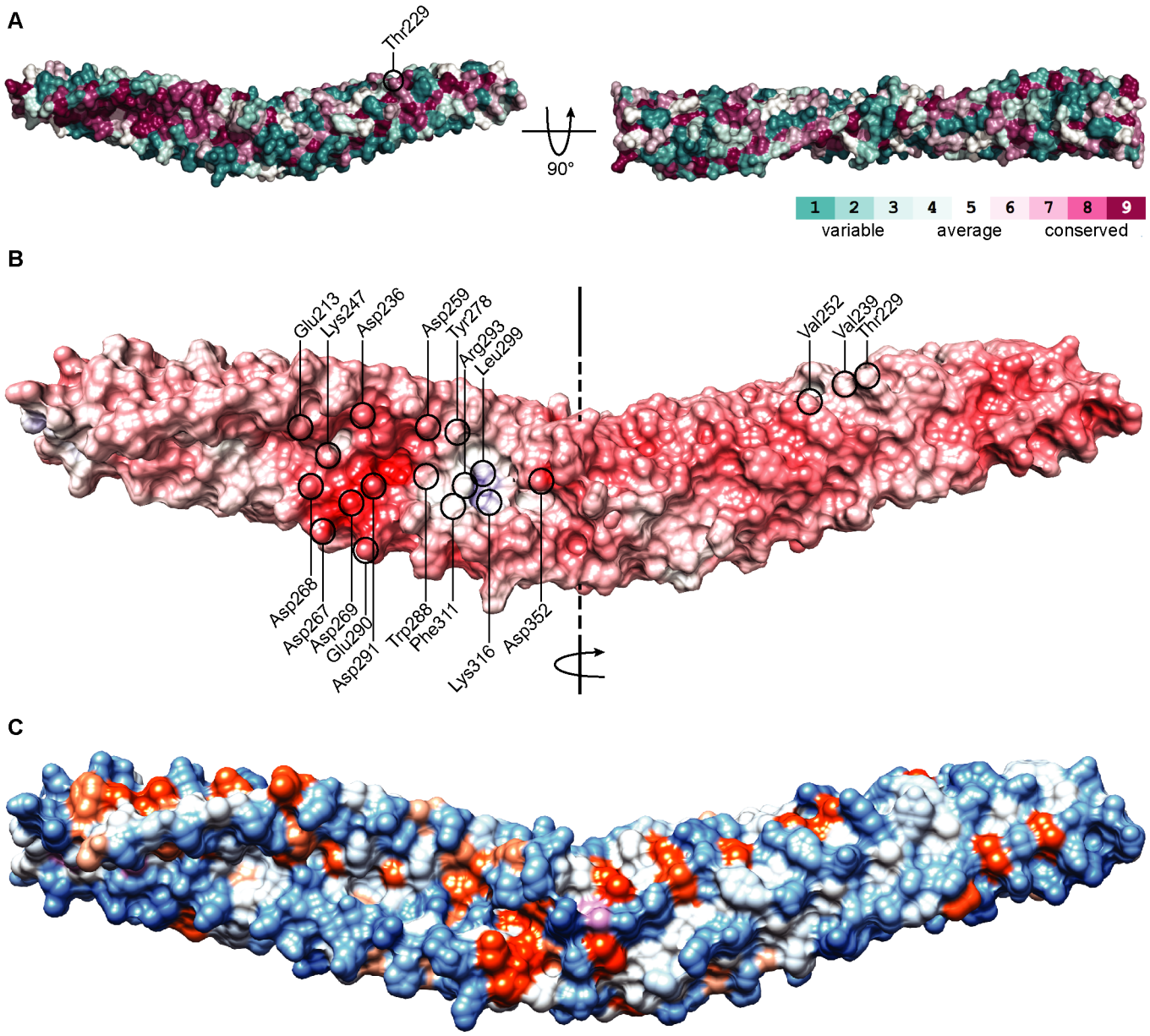

Figure S11. Conservation and properties of residues in TbMORN1(7-15). (A) Conservation map of the TbMORN1(7-15) $P2_1$ crystal structure reveals a highly conserved stretch of residues along the groove. The structure is shown in two orientations, with residues colour-coded according to the level of conservation. **(B)** An electrostatic map of TbMORN1(7-15) $P2_1$. Calculations were performed using APBS suite, displayed by Chimera. Colour scale: red = -13 kT; blue = +13 kT. Individual residues contributing to its surface electrostatics are labelled, namely those of the two negatively-charged loops building up a negative patch inside the groove, and the residues contributing to a small positively-charged region close to the dimer interface. **(C)** Hydrophobic map of TbMORN1(7-15) $P2_1$. Colour scale: blue = hydrophilic; orange = hydrophobic, pink = methionine residues.

A TbMORN1(7-15) C2

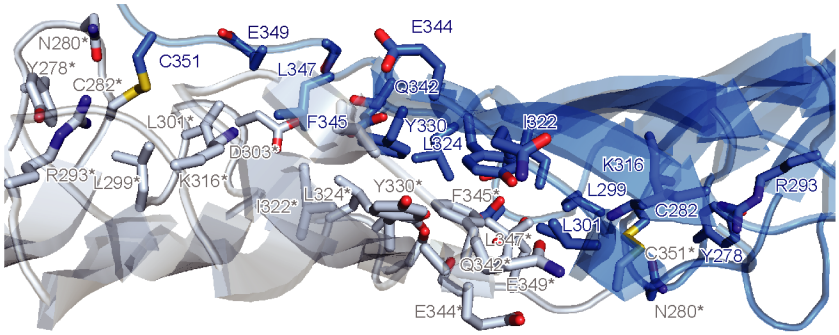

B TgMORN1(7-15)

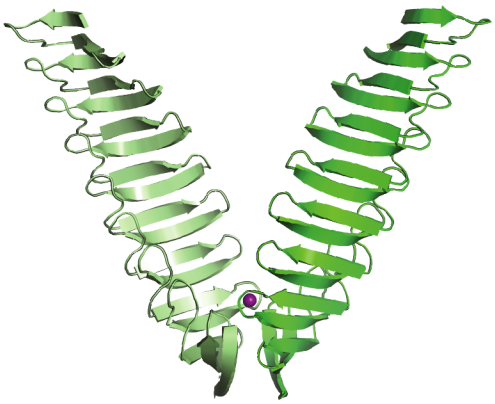

C TgMORN1(7-15) extended dimer

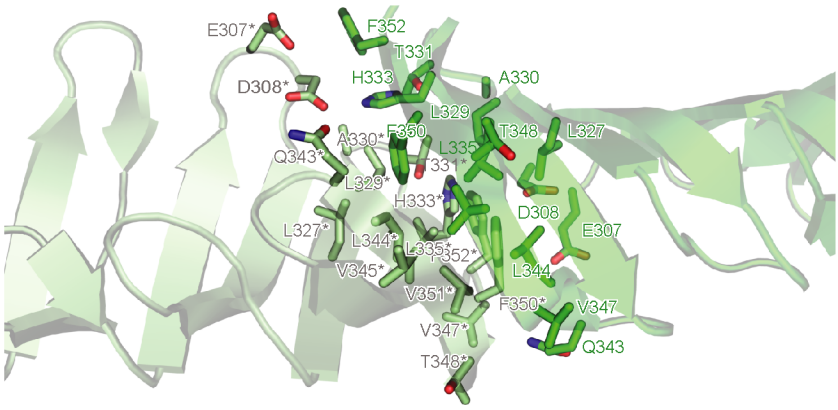

D TgMORN1(7-15) V-shaped dimer

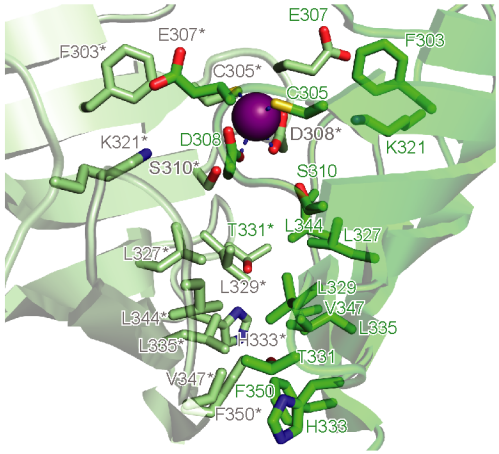

E SAXS - Kratky plots

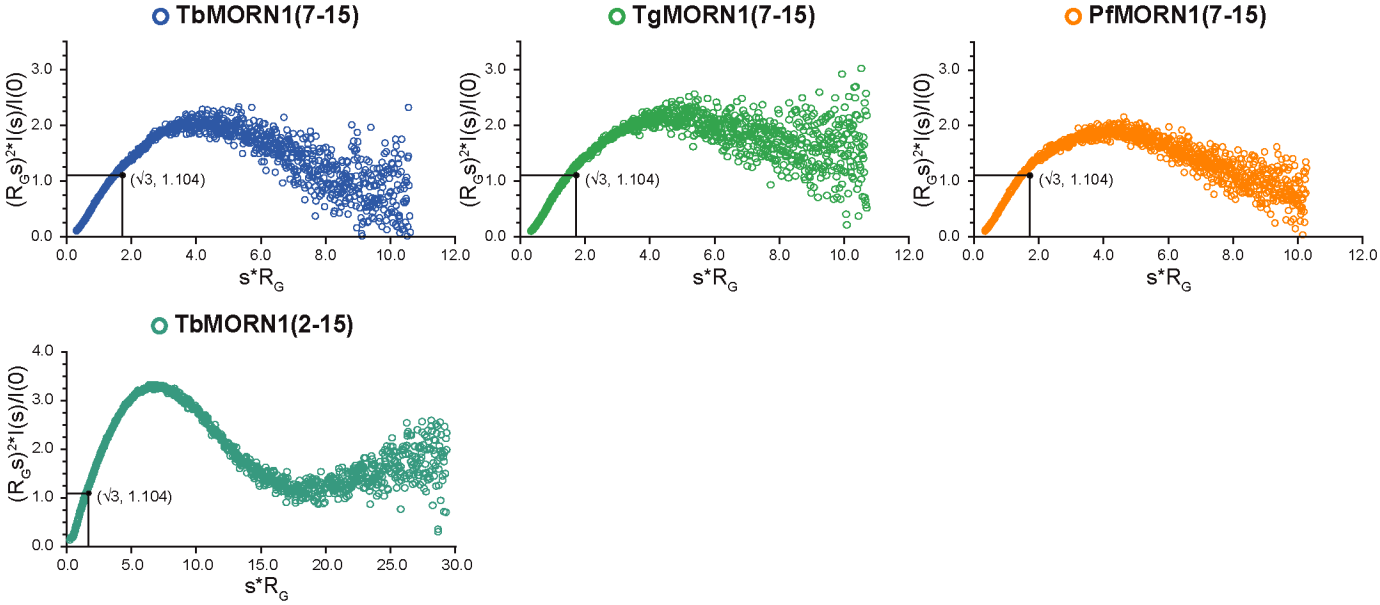

Figure S12. MORN dimer interfaces and SAXS analysis of proteins in solution. (A) Dimer interface of TbMORN1(7-15) C2 crystal form. In comparison to the $P2_1$ form, the dimer interface of C2 structure is broader, and is additionally stabilised by two disulphide bridges formed between Cys351 at the C-terminus of repeat 15 and Cys282 from the β-hairpin loop of repeat 12. **(B)** Crystal structure of the TgMORN1(7-15) V-shaped dimer, incorporating Zn^{2+} in its dimerisation interface. **(C)** Dimer interface of the TgMORN1(7-15) extended dimer, which utilises residues from MORN repeats 13-15. In contrast to TbMORN1(7-15), where the dimerisation interface is centred around aromatic stacking, a hydrophobic core plays a crucial role in the dimer interface of extended TgMORN1(7-15). Leu327, Leu329, Leu335, Leu344, Val345, Val347, Phe350 and Phe352 are part of this hydrophobic core. The dimer is stabilised by a single salt bridge formed between the Asp308 of one subunit and the His333 of the other subunit. This salt bridge is further stabilised by two hydrogen bonds between the main-chain nitrogen of Val345 and a carbonyl oxygen of Val347 of respective subunits. **(D)** Dimer interface of the TgMORN1(7-15) V-shaped dimer. Cys305 and Asp308 incorporate a structural Zn^{2+} ion, which stabilises the somewhat smaller dimerisation interface of this protein. Although its dimerisation interface is very similar to that of PfMORN1(7-15), it lacks the aromatic core of PfMORN1(7-15). The latter is replaced by a series of unique aromatic stacking interactions at the protein´s vertex, these being contributed by a pair of Phe350 residues, sandwiched between a pair of His333 residues. **(E)** Kratky plots derived from SAXS analysis of TbMORN1(7-15), TgMORN1(7-15), PfMORN1(7-15), and TbMORN1(2-15). The shape of the plots suggests an elongated shape of the dimers in solution.

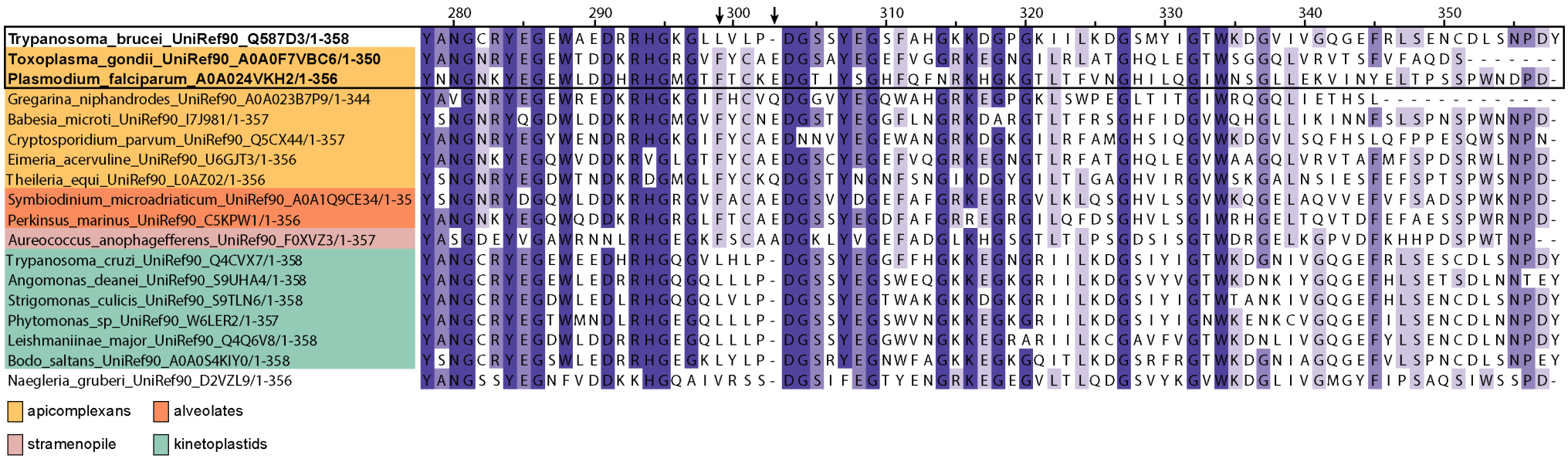

Figure S13. Conservation of residues for formation of V-shaped dimers in Apicomplexa and related clades. Amino acid sequence alignment of the C-termini of TbMORN1, TgMORN1, PfMORN1, and fifteen other MORN repeat-containing proteins from related taxa. Amino acid numbers are given according to the TbMORN1 protein, and the three proteins with experimentally-determined high-resolution structures are shown in bold within the black box. Essential for formation of a V-shaped dimer are a coordinating Cys residues and an anion-π interaction pair. In TbMORN1, the coordinating Cys residue has been substituted for Leu (Leu 301). Similarly the Phe and Glu residues of the anion-π interaction pair (indicated with black arrows) have been substituted for Leu (Leu299) and are not present (deletion after Pro302) respectively. This supports the conclusion that TbMORN1 exists only in the extended form, while the apicomplexan proteins and those from related clades are probably capable of adopting both extended and V-shaped conformations.

Table 1. X-ray data collection statistics.

	PfMORN (SMet)	**PfMORN**	**TbMORN**	**TbMORN**	**TgMORN**	**TgMORN (V-shape)**
Source	ID29	ID29	ESRF ID23-1	ESRF ID23-1	ESRF ID30B	ESRF ID30B
Wavelength (Å)	0.979	0.976	0.979	1.89	0.967	1.0
Resolution (Å)	47.47-2.5 (2.59-2.5)	46.3-2.14 (2.2-2.14)	48.28-2.35 (2.43-2.35)	48.14-2.53 (2.65-2.53)	48.92-2.90 (3.08-2.90)	49.45-2.50 (2.60-2.50)
Space group	*C222₁*	*C222₁*	$P2_1$	*C2*	$P4_32_12$	$P6_222$
Unit cell (Å, º)	a=57.33, b= 79.18, c= 94.42	a=57.33, b= 79.18, c= 94.42	a=69.04, b=27.63, c=114.54; β=101.83	a=192.88, b=49.74, c=41.98	a=b=53.92, c=348.85	a=b=205.86, c=40.58
Molecules (a.u.)	1	1	2	2	2	1
Unique reflections	7832(762)	12148 (974)	17460 (1247)	12419(975)	12331 (1819)	18162 (1960)
Completeness (%)	99.5(98.3)	99.6(98.1)	95.4 (71.5)	93.1(60.0)	99.1 (95.4)	99.7 (97.9)
R_{merge}[b]	0.059(0.301)	0.037 (1.283)	0.092 (0.466)	0.116 (1.365)	0.140 (2.252)	0.198 (2.116)
R_{meas}[c]	0.062(0.314)	0.042 (1.510)	0.100 (0.532)	0.146 (1.893)	0.158 (2.536)	0.204 (2.177)
CC(1/2)	0.999(0.983)	1.000 (0.467)	0.998 (0.897)	0.995 (0.303)	0.999 (0.772)	0.999 (0.426)
Multiplicity	13.0 (12.9)	4.2 (3.2)	6.1 (4.1)	6.2 (3.7)	8.4 (8.0)	17.9 (18.1)
I/sig(I)	30.3 (8.1)	17.5 (0.8)	13.4 (2.8)	9.3 (0.9)	11.8 (0.5)	14.6 (1.6)
B_{Wilson} (Å^2)	57.3	58.0	18.74	36.7	22.97	42.3
R_{work}[e]/R_{free}[f]		23.0/26.4	23.2/25.6	22.5/28.2	31.8/33.8	20.1/23.9
r.m.s.d. bonds (Å)		0.003	0.004	0.011	0.0084	0.007
r.m.s.d. angles (°)		0.6	1.24	1.612	1.417	0.811

[a] Values in parentheses are for the highest resolution shell.

[b] $$R_{merge} = \frac{\sum_{hkl}\sum_{i=1}^{N}\left|I_{i(hkl)} - \bar{I}_{(hkl)}\right|}{\sum_{hkl}\sum_{i=1}^{N} I_{i(hkl)}}$$

[c] $$R_{meas} = \frac{\sum_{hkl}\sqrt{N/(N-1)}\sum_{i=1}^{N}\left|I_{i(hkl)} - \bar{I}_{(hkl)}\right|}{\sum_{hkl}\sum_{i=1}^{N} I_{i(hkl)}}$$

where $\bar{I}_{(hkl)}$ is the mean intensity of multiple $I_{i(hkl)}$ observations of the symmetry-related reflections, N is the redundancy

[e] $$R_{work} = \frac{\sum\left||F_{obs}| - |F_{calc}|\right|}{\sum|F_{obs}|}$$

[f] R_{free} is the cross-validation R_{factor} computed for the test set of reflections (5%) which are omitted in the refinement process.

Intermolecular cross-links in TbMORN1

chemical cross-linking agent	cross-linked amino acids and respective MORN repeats	best e-value	number of PSMs in the dimer
BS^3 (spacer arm length 11.4 Å)	aa 100 x aa 123 (repeat 5 x repeat 6)	7.5×10^{-13}	4
	aa 223 x aa 246 (repeat 10 x repeat 11)	5.7×10^{-22}	7
	aa 296 x aa 321 (repeat 13 x repeat 14)	1.8×10^{-11}	56
	aa 321 x aa 321 (repeat 14 x repeat 14)	6.4×10^{-5}	1
EDC (spacer arm length 0 Å)	aa 308 x aa 321 (repeat 14 x repeat 14)	1.1×10^{-8}	5
	aa 321 x aa 326 (repeat 14 x repeat 15)	1.9×10^{-9}	3

Table S1. Intermolecular contacts in TbMORN1. A summary of intermolecular cross-links in the TbMORN1 dimer as a result of chemical cross-linking with either BS^3 or EDC followed by mass spectrometry analysis. To remove low quality peptide-spectrum matches (PSMs), an additional e-Value cutoff of < 0.001 was applied. In order to distinguish intra- from inter-molecular chemical cross-links, results from monomers and dimers were compared. Cross-links were scored as intermolecular when there were: (1) minimally 3 peptide PSMs in dimer and (2) minimally 3-times more PSMs in dimer than in monomer. Results compiled from two independent experiments.

TbMORN1 construct	Thermostability T_m (°C) (DSF)
2-15	44.2 ± 0.3
$2\text{-}15^{Mut13}$	43.8 ± 0.3
$2\text{-}15^{Mut14}$	41.4 ± 0.5
$2\text{-}15^{Mut13+14}$	41.7 ± 0.3

Table S2. Analysis of TbMORN1(2-15) mutagenesis constructs. Thermostability of TbMORN1(2-15) and its mutagenised derivatives with mutations in MORN repeats 13 and 14 was measured by differential scanning fluorimetry (DSF), given here as melting temperature (T_m) values (°C).

Data collection parameters				
Radiation source	Petra III (DESY, Hamburg, Germany)			ESRF (Grenoble, France)
Beamline	EMBL P12			BM29
Detector	Pilatus 2M			Pilatus 1M
Beam geometry (mm, FWHM)	0.12 x 0.20			0.10 x 0.20
Wavelength (nm)	0.12			0.099
Sample-detector distance (m)	3.1			2.867
Momentum transfer *s* range (nm^{-1})	0.01 – 4.0			0.04 – 5.0
Exposure time (s)	1 sec (SEC-SAXS mode) 0.05 sec (Batch mode)			1 sec (SEC-SAXS mode)
Overall Parameters				
	TbMORN1 (7-15)	**TgMORN1 (7-15)**	**PfMORN1 (7-15)**	**TbMORN1 (2-15)**
Buffer	Buffer 1*	Buffer 2**	Buffer 2**	Buffer 2**
Temperature (°C)	20	20	10	20
Working concentration (mg/ml) Concentration range measured	n.a.	n.a.	1 1-8	n.a.
R_g from Guinier approximation (nm)	4.1±0.04	4.0±0.03	3.8±0.1	6.5±0.6
R_g from PDDF (nm)	4.4±0.02	4.3±0.04	4.2±0.03	7.2±0.05
D_{max} (nm)	155	17.0	16.0	260
Molecular weight, I(0) (kDa)	n.a.	n.a.	52 ±5	n.a.
Molecular weight, offline RALS (kDa)	46±5	50±5	32±5	74±5
Molecular weight from DATMOV, (kDa)	60±5	58±5	46±5	71±5
Molecular weight from sequence (dimer, kDa)	52	49	46	70
Software employed				
Primary data reduction	SASFLOW			ESRF EDNA pipeline
Data processing	PRIMUS/Chromixs			
Calculation of theoretical data	Crysol			
Ab initio modelling	DAMMIN		DAMMIF	
SASBDB accession code	SASDGA7	SASDGB7	SASDGC7	SASDG97

Buffer 1* 20 mM Tris, 200 mM NaCl, 2% glycerol, 0.5 mM DTT
Buffer 2** 20 mM Tris-HCl pH 7.5, 100 mM NaCl

Table S3. SAXS data collection summary.